Solid-phase arsenic speciation in glacial aquifer sediments of west-central Minnesota, USA:
a micro-X-ray absorption spectroscopy approach for quantifying trace-level speciation

A Dissertation
SUBMITTED TO THE FACULTY OF
UNIVERSITY OF MINNESOTA
BY

Sarah Luella Nicholas

IN PARTIAL FULFILLMENT OF THE REQUIREMENTS
FOR THE DEGREE OF
DOCTOR OF PHILOSOPHY

Brandy M. Toner, Adviser, Edward Nater, Co-adviser

June 2017

Acknowledgements

Funding for my research came from a grant to Professor Toner from the Center for Urban and Regional Affairs, a grant to Professor Toner from the Office of the Vice President for Research, and a USGS Water Research Grant to Professor Toner (jointly funded by the USGS's Water Resources Research Initiative Program and the Minnesota Agricultural Experiment Station's Center for Agricultural Impacts on Water Quality).

Further support came from a Science Fellowship from the UMN Graduate School, the Allmaras Memorial Fellowship from the Department of Soil, Water, and Climate, and a Doctoral Dissertation Fellowship from the University of Minnesota – Twin-Cities (UMN) Graduate School.

Sarah Baldvins and Reba Van Beusekom assisted me in my research when they were undergraduates. They were funded by the UMN Undergraduate Research Opportunities Program (UROP).

I would like to thank Alan Knaeble, Gary Meyer, Angela Gowan, Barb Lusardi, and Harvey Thorleifson at the Minnesota Geological Survey.

I would like to thank synchrotron scientists Matthew Marcus, Sirine Fakra and Josep Roque-Rosell (Advanced Light Source, ALS, BL10.3.2). The ALS is supported by the

Director, Office of Science, Office of Basic Energy Sciences, of the U.S. DOE under Contract No. DE-AC02-05CH11231.

I would also like to thank beamline scientists Mahaling Balasubramanian and Steve Heald (Advanced Photon Source, APS, PNC/XSD, 20-BM), and Matthew Newville (APS, 13-BM) for their support of this project. PNC/XSD facilities at the APS, and research at these facilities, are supported by the U. S. Department of Energy (DOE) - Basic Energy Sciences, a Major Resources Support grant from NSERC, the University of Washington, Simon Fraser University, and the APS. Use of the APS is also supported by the U. S. DOE, Office of Basic Energy Sciences, under Contract DE-AC02-06CH11357.

I would like to thank Sara Baldvins, Lindsey Briscoe, Shahida Quazi, and Ryan Lesneiwiski (UMN) and Sofia Oufqir (University of Mohamed V-Agdal, Morocco) for assistance with sample preparation of the archived tills.

Prof. Bernhardt Saini-Eidukat and the department Geological Sciences at North Dakota State University lent me lab space for the night work on the Clay County samples and NDSU undergraduate student Lane Folkers assisted me in the field.

I would like to thank Brandi Cron Kammermans, Michael Ottman, Rebecca Sims, Reba Van Beusekom, and Olga Furmann for their help with the Meeker County enrichment experiment.

I would like to thank Brandi Cron Kammermans, Jill Coleman Wasik, Colleen Hoffman, and Jeff Sorensen for co-staffing the beamline at 10.3.2 with me, and Brandi for taking me along to 13 ID E in Chicago.

I would like to thank Karl Wirth at Macalester College for his guidance and patience.

I would like to thank my committee: Mindy Erickson, Carrie Jennings, Paul Bloom, and Edward Nater for their advice, support, and patience.

I would like to thank Professor Peter Croot my post-doctoral advisor at the National University of Ireland, Galway for allowing me to continue to work on arsenic papers during the first six months of my post-doctoral work.

I would like to thank Soil, Water, and Climate staff Kari Jarcho, Marjorie Bonse, Joel Nelson, Thor Sellie, Andy Scobbie, and Dave Ruschy for making the wheels go around.

I would like to thank my parents Kathleen Hall and David Nicholas, my husband Joshua Lynch and my daughters Maura Nicholas Lynch and Brigid Nicholas Lynch.

Brandy Toner took me on in 2010 when I wanted to come back to science but didn't know how. I have her to thank not only for teaching me spectroscopy and low-T

geochemistry but for sending me to sea in 2013. None of us could have predicted how that would turn out but it's been a wonderful experience. I am truly grateful for my time on team Toner.

Dedication

For Joshua Lynch

Abstract

Arsenic (As) is a geogenic contaminant affecting groundwater in geologically diverse systems. The footprint of the Des Moines Lobe glacial advance in west-central Minnesota, is a regional nexus of drinking-water wells that exceed the US EPA maximum contaminant level for arsenic ($As>10 \mu g L^{-1}$). Arsenic release from aquifer sediments to groundwater is favored when biogeochemical conditions in aquifers fluctuate.

The specific objective of this research was to identify the solid-phase sources and geochemical mechanisms of release of As in aquifers of the Des Moines Lobe glacial advance. The overarching hypothesis is that gradients in hydrologic conductivity and redox conditions found at aquifer-aquitard interfaces promote a suite of geochemical reactions leading to mineral alteration and release of As to groundwater. A microprobe X-ray absorption spectroscopy (μXAS) approach was developed and applied to rotosonic drill core samples to identify the solid-phase speciation of As in aquifer, aquitard, and aquifer-aquitard interface sediments. This approach addressed the low solid-phase As concentrations, as well as the fine-scale physical and chemical heterogeneity of the sediments. The solid-phase Fe and As speciation was interpreted using sediment and well-water chemical data to propose solid-phase As reservoirs and release mechanisms. The results are consistent with three different As release mechanisms: (1) desorption from Fe oxyhydroxides, (2) reductive dissolution of Fe oxyhydroxides, and (3) oxidative dissolution of Fe sulfides. The findings confirm that glacial sediments at the interface

between aquifer and aquitard are geochemically active zones for As. The diversity of As release mechanisms is consistent with the geographic heterogeneity observed in the distribution of elevated-As wells.

Supplementary file "*Nicholas dissertation supplementary files 1 to 5.xlsx"* was submitted to the UMN digital conservancy with this thesis. It is an excel workbook with five tables. Tables 1 and 2 are the complete provenance and citation information for all As and Fe reference spectra used. Tables 3, 4, and 5 are the reference spectra fits, fractions, and scores for the sampled spectra from cores OTT3, TG3, and UMRB2.

Table of Contents

List of Tables

List of Figures

CHAPTER 1. INTRODUCTION – GEOGENIC ARSENIC CONTAMINATION OF WELL WATER

Previous work on arsenic in Minnesota well water

West-central Minnesota is a geographic nexus of drinking-water wells with arsenic (As) concentrations above the United States Environmental Protection Agency maximum contaminant level (MCL) of 10μgL^{-1}(Welch 2000). The affected wells are constructed in glacial aquifers in the footprint of the Des Moines lobe glacial advance. Distribution of As-affected wells is heterogeneous with respect to location and well depth (Erickson and Barnes 2005a). A summary of previous work on well and groundwater As in western Minnesota by Welch (2000), Kavinetsky (2000), and the Minnesota Department of Health (2001) can be found in Melinda Erickson's dissertation (Erickson 2005). The most prolific investigator of arsenic in Minnesota groundwater is Erickson herself (Erickson and Barnes 2004; Erickson and Barnes 2005a,b,; Erickson and Barnes 2006). This dissertation is predicated on the paradigm articulated by McMahon (2001) that hydrogeochemical gradients found at interfaces between different sediment types create active biogeochemical reaction zones. Earlier work on As in western Minnesota aquifers (Erickson and Barnes 2005 a, b) suggested that (bio)geochemical processes active at the interface between an aquifer and contact till were the probable source of As to the aquifers. From these previous results we hypothesized that if a geochemical process at the till-aquifer interface were releasing As from the till to waters, then As speciation in altered till in contact with aquifer sediments will be measurably different from As speciation in till distal to the aquifer. Evidence to support this hypothesis would include

reduced As and Fe in sulfide minerals in unaltered tills and oxidized As and Fe in altered till near-aquifer sediments.

Geogenic arsenic contamination of drinking water worldwide

The primary path of human exposure to As is through drinking water (IPCS 2001, WHO 2010). Prolonged consumption of drinking water at >50 μg As L^{-1} is associated with an increased risk of skin, kidney, bladder and lung cancers (Smith et al. 1992). The US EPA maximum contaminant level (MCL) for arsenic is 10ugL^{-1}. Between 150,000 and 200,000 Minnesotans get their drinking water from wells with arsenic concentrations exceeding this limit (Erickson 2005).

Most drinking-water As is geogenic, meaning that the arsenic sources are naturally-occurring geological materials (Hem 1985; Smedley and Kinniburgh 2002). Human exposure to arsenic through drinking water is found in local areas worldwide. The problem is most severe and most well studied in Bangladesh, West Bengal, Vietnam and Cambodia. The geologic setting of these areas is recently eroded Himalayan sediments that were deposited rapidly with very little weathering into fluvial deposits of the Mekong, Red, and Ganges rivers (Smedley and Kinnebourgh 2002). These areas are very close to sea level, local water tables are near the surface and the groundwater tends to be in a chemically reduced state. There is general agreement that the solid-phase sources of the arsenic in these areas are oxidized As species associated with iron (oxyhydr)oxides, and that this As is liberated under reducing conditions (Islam et al. 2005; Cummings et al. 1999). Disagreement persists among different research groups about the exact

mechanism releasing As to waters from the solids (Benner et al. 2008, Neumann et al. 2010, and Burgess et al. 2010).

Geogenic arsenic contamination of drinking water in North America

Geogenic As contamination of groundwater in the United States tends to be local rather than widespread and occurs in diverse geologic settings: metamorphosed bedrock in Maine (Ayotte et al. 2003), sulfide deposits in the Michigan basin (Kolker et al. 2003) and in the Fox River Valley of Wisconsin (Schrieber et al. 2000), glacial tills in Minnesota and South Dakota (Erickson 2005a,b), hydrothermal waters in Idaho and California, and evaporate deposits in the Central Valley of California (Welch et al. 2000). The upper aquifers in west-central Minnesota are porous and permeable glacial materials deposited by the Des Moines lobe (Figure 1). Radiocarbon dates indicate that the Des Moines Lobe advanced rapidly, and probably included sections of very fast moving ice called ice-streams, similar to those active in Antarctica today (Patterson 1998). The Des Moines lobe ice streams would have originated from what is now central Canada at the end of the last glaciation (Jennings 2006). The ice streams had different points of origin and traveled different paths, so they entrained and deposited diverse geologic materials (Slatt and Eyles 1981). Des Moines Lobe ice-stream sediments are underlain by older aquifer-bearing sediments from previous glacial periods (Harris and Berg 2006; Harris et al. 1999; Patterson et al. 1999, Wright 1972). Because Des Moines lobe deposits are widespread and complex, identification of these glacial deposits as a probable source of As to well water leaves a wide range of possible geologic sources of As.

Glacial *aquifers* typically form in glacial-stream sediments composed of sand and gravel deposited by glacial meltwater (Figure 2) (Prothero and Schwab, 1996), but may also form in sandy lake sediment. The sediment layers confining these aquifers are commonly *tills* made of materials transported and deposited by the glacier. Tills are poorly sorted sediments with a matrix of finely-ground clay and silt size material. The fine-grained matrix of till creates low-permeability conditions which allows tills to function as confining layers, or *aquitards,* in glacial aquifer systems (Berg 2006, 2008). Aquitards limit the movement of groundwater to the more conductive sands and gravels of the aquifers. Glacial aquifers tend to be laterally discontinuous (Ojakangas and Matsch 1982), which likely contributes to the geographic heterogeneity observed in groundwater properties, including As concentrations.

Well construction

Wells in Minnesota are typically constructed by driving a solid-walled steel pipe through the confining layer (clay-rich glacial till), and then installing perforated section of pipe called the screen into the aquifer materials (glacial stream sands and gravels). Erickson and Barnes (2005b) found that wells constructed in the As-affected area of Minnesota with shorter screens, closer to the confining layer (glacial till) were more likely to have elevated As than wells with longer screens set farther from the confining layer. This suggests that the geologic contact between the glacial till (confining layers) and glacial stream sediments (aquifer materials) is a possible source of the As to groundwater, and

that oxidation-reduction (redox) changes caused by movement of the water table across this stratigraphic contact could liberate As to waters.

None of the suspect glacial materials in western Minnesota is particularly high in arsenic; the concentration range is from 3-10 $mgkg^{-1}$. Estimated averages for the concentration of arsenic in the continental crust range from 1.5 to 5.1 $mgkg^{-1}$ (*1.5 mg kg^{-1}* Taylor and McLennan 1985, 1995; *2 mg kg^{-1}* Wedepohl 1995;.*4 mg kg^{-1}* Gao et al 1988; *4.8 mg kg^{-1}* Rudnick and Gao 2003; *5.1 mg kg^{-1}* Sims et al. 1990). Clearly the crustal average is a hard thing to estimate, but we can see from these numbers that that values measured in western Minnesota sediments are close to average crustal As concentrations. The paradox of unexceptional concentration in the host solids and high aqueous concentrations is the hallmark of geogenic arsenic contamination worldwide (Smedley and Kinniburgh, 2002). Moderate arsenic concentrations in the solids and heterogenous distribution of high arsenic wells within wells with similar aqueous chemistry suggest that speciation of arsenic in the solid phase plays an important role in the liberation of arsenic to groundwater.

Solid-phases sources of arsenic to waters and the importance of speciation

Arsenic in aquifer sediments is associated with iron (Fe) minerals. Some reduced solid-phase sources of As to waters are As-bearing Fe sulfides (such as arsenopyrite, FeAsS, or As-rich pyrite $FeS_{2-x}As_x$) (Schreiber and Rimstidt 2013). Frequent oxidized solid-phase sources of As to waters are As species co-precipitated with Fe(oxyhydr)oxides and

aqueous As species sorbed to Fe(oxyhydr)oxides (Smedley and Kinniburgh 2002) such as goethite, or ferrihydrite). From the perspective of As sequestration and release to groundwater, these minerals are oxidation-reduction (redox) end-members. Each is a solid-phase reservoir with strong potential for As release when (bio)geochemical conditions, especially redox, in aquifers change.

Arsenic-bearing sulfides are typically a stable As reservoir under chemically reduced, anoxic conditions. An increase in oxidation state, as from the introduction of oxygen, would tend to dissolve As-bearing sulfides and liberate As to waters. Sulfide minerals in shale fragments are frequently proposed as the parent-material source of As in glacial deposits in the upper Midwest (Welch et al. 2000). Shales are fine-grained sedimentary rocks, and black shales are those having > 1 % carbon by weight, which form in reduced environments and frequently contain sulfide minerals (Prothero and Schwab 1996). Some of the Upper Cretaceous shales of the Manitoba escarpment (Grosz et al. 2004; Jennings et al. 2015) are likely sources of sediments to glaciers that deposited till in western Minnesota during the last ice age. In particular, the Boyne member of the Carlile Formation, and the Pembina member of the Pierre Shale Formation are black shales with high concentrations of As in sulfides (Bamburak 2008). In these shale units As may substitute for sulfur (S) in the mineral pyrite (FeS_2; As substituted for S in pyrite, $FeAs_xS_{2-x}$) (Bamburak 2008).

In contrast to As-rich pyrite, Fe-(oxyhydr)oxide minerals are stable under *oxic* conditions. They can sequester As in the solid phase by sorption reactions or by co-preciptiation, in which aqueous As species ($As(OH)_3$, $H_2AsO_4^-$, $HAsO_4^{2-}$) get trapped

within clusters of Fe(oxyhydr)oxides during precipitation and are occluded from the solution (Townshend and Jackwerth, 1989; Romero et al. 2013). In the presence of oxygen and dissolved As, Fe(oxyhydr)oxides tend to co-precipitate As. A drop in redox state, as with the consumption of oxygen by microbial activity, can lead to dissolution of Fe(oxyhydr)oxides, which also reduces and liberates As (Schreiber et al. 2000). Iron (oxyhydr)oxides can also retain As through adsorption reactions at the mineral surface in weak, labile associations. Poorly ordered Fe(oxyhydr)oxides have been reported to provide more sorption sites than well-ordered phases because of their greater surface area (Borgaard 1983). Increases in pH and anion competition are known to cause As-desorption (Banerjee et al. 2008). In most systems where adsorbed and co-precipitated As in Fe (oxyhydr)oxides are implicated in As release to groundwater the co-precipitation or sorption mechanism is believed to be authigenic, meaning that the mineral formed from solution in its current location (Smedley and Kinniburgh 2002). Recent work by Jennings et al. (2015) suggests that some oxidized As may have been sourced from the Gammon Ferruginous member of the Pierre Shale Formation (Bamburak 2008) as arsenate co-precipitated with siderite ($FeCO_3$).

Speciation has long been seen as key to understanding the mobilization of arsenic from solids to groundwaters. Earlier work on speciation began with extractions (Keon et al. 2001, Huerta-Dias and Morse 1990) and column or reactor experiments (Cummings et al. 1999, Islam et al. 2005).

X-ray absorption spectroscopy **(**XAS) opened up the possibility of making direct measurements on environmental concentrations of As in the solid phase. Much of the early XAS on arsenic came from the Gordon Brown Group (MIT) the Scott Fendorf Group (Idaho and later Stanford) and the arsenic XAS literature is still dominated by these groups and their former students and postdocs. An excellent summary of previous synchrotron-based work on As can be found in Foster and Kim (2014).

CHAPTER 2: SOLID-PHASE ARSENIC SPECIATION IN AQUIFER SEDIMENTS: A MICRO-X-RAY ABSORPTION SPECTROSCOPY APPROACH FOR QUANTIFYING TRACE-LEVEL SPECIATION

Sarah L. Nicholas[1,2], Melinda L. Erickson[3], Laurel G. Woodruff[3], Alan R. Knaeble[4], Matthew A. Marcus[5], Joshua K. Lynch[6,7], Brandy M. Toner[1]*

[1] *Department of Soil, Water, and Climate, University of Minnesota-Twin Cities, Saint Paul, MN, USA*

[2] *Department of Earth and Ocean Sciences, National University of Ireland, Galway, Ireland*

[3] *United States Geological Survey, Minnesota Water Science Center, Mounds View, MN, USA*

[4] *Minnesota Geological Survey, Saint Paul, MN, USA*

[5] *Advanced Light Source, Lawrence Berkeley National Laboratory, Berkeley, CA, USA*

[6] *Department of Biomedical Informatics and Computational Biology, University of Minnesota-Twin Cities, Saint Paul, MN, USA*

[8] *Department of Agricultural and BioSystems Engineering, University of Arizona, Tucson AZ, USA*

*Corresponding author: toner@umn.edu

Abstract – Arsenic (As) is a geogenic contaminant affecting groundwater in geologically diverse systems globally. Arsenic release from aquifer sediments to groundwater is favored when biogeochemical conditions, especially oxidation-reduction (redox) potential, in aquifers fluctuate. The specific objective of this research is to identify the solid-phase sources and geochemical mechanisms of release of As in aquifers of the Des Moines Lobe glacial advance. The overarching hypothesis is that gradients in hydrologic conductivity and redox conditions found at aquifer-aquitard interfaces promote a suite of geochemical reactions leading to mineral alteration and release of As to groundwater. A microprobe X-ray absorption spectroscopy (μXAS) approach is developed and applied to rotosonic drill core samples to identify the solid-phase speciation of As in aquifer, aquitard, and aquifer-aquitard interface sediments. This approach addresses the low solid-phase As concentrations, as well as the fine-scale physical and chemical heterogeneity of the sediments. The spectroscopy data is analyzed using novel cosine-distance and correlation-distance hierarchical clustering for Fe 1s and As 1s μXAS datasets. The solid-phase Fe and As speciation is then interpreted using sediment and well-water chemical data to propose solid-phase As reservoirs and release mechanisms. The results confirm that in two of the three locations studied, the glacial sediment forming the aquitard is the source of As to the aquifer sediments. The results are consistent with three different As release mechanisms: (1) desorption from Fe oxyhydroxides, (2) reductive dissolution of Fe oxyhydroxides, and (3) oxidative dissolution of Fe sulfides. The findings confirm that glacial sediments at the interface

between aquifer and aquitard are geochemically active zones for As. The diversity of As release mechanisms is consistent with the geographic heterogeneity observed in the distribution of elevated-As wells.

2.1. INTRODUCTION

Arsenic (As) is a naturally-occurring (geogenic) contaminant affecting groundwater in geologically diverse systems in Asia, Europe, Africa, and North and South America. In many cases, As contamination is localized within specific aquifer sediments due to a confluence of hydrological, geochemical, and biological conditions (Stuckey et al. 2015). Despite the localized aspect of As contamination of groundwater, the conditions needed to produce contamination are found in many locations worldwide (Smedley and Kinneborough 2002).

Arsenic in aquifer sediments is often associated with iron (Fe) and sulfur (S) minerals, primarily oxyhydroxides and sulfides of Fe. Arsenic-bearing Fe sulfides such as arsenopyrite, FeAsS, or As-rich pyrite $FeS_{2-x}As_x$, are minerals that are favored under chemically reducing conditions (Schreiber and Rimstidt 2013). Under chemically oxidizing conditions As is associated with Fe(oxyhydr)oxides such as goethite, α-FeOOH, through sorption and co-precipitation reactions. From the perspective of As removal from and release to groundwater, these mineral types represent oxidation-reduction (redox) end-members. Each is a solid-phase reservoir with strong potential for As release when (bio)geochemical conditions, especially redox, in aquifers change. A

good understanding of As speciation in the solid phase is necessary to identify the processes liberating As to waters (Kocar et al. 2008, Haque et al. 2008, Quicksall et al. 2008, Saalfield and Bostick 2009).

The hydrogeochemical gradients found at interfaces between different sediment types, for example aquifer and aquitard sediments, are thought to create active biogeochemical reaction zones (McMahon 2001). For As in glacial aquifers, this principle has been demonstrated through a comparison of As concentrations in wells with screened intervals with varying proximity to an aquitard. Wells that were screened near the aquitard were more likely to have elevated well-water As concentrations than wells with screens farther from the aquitard (Erickson and Barnes 2005a). These findings suggest that the original solid-phase source of the As is in the aquitard (Erickson and Barnes 2005b).

The objective of the present research is to identify the solid-phase sources of As in the complex glacial aquifer system of the Des Moines Lobe glacial advance, and to explain the geographic heterogeneity of As affected wells within this aquifer system. Our hypothesis is that gradients in hydrologic conductivity and oxidation-reduction (redox) conditions present at the aquifer-aquitard contact can cause oxidative (e.g. As-bearing pyrite) or reductive (e.g. As-sorbed ferrihydrite) alteration of minerals and release of As to groundwater.

In this contribution we use an As 1s and Fe 1s (K-edge) microprobe X-ray absorption spectroscopy (XAS) approach to identify the solid-phase speciation of As in aquifer sediments collected from an As-affected region of the Des Moines Lobe glacial advance.

We describe and quantify differences in As speciation among: 1) aquifer sediments, 2) mid-aquitard sediments, and 3) aquitard sediments at the aquifer-aquitard contact. Our analytical approach follows a quantitative track and a descriptive track. For the quantitative track, we use sediment chemistry and a novel As speciation mapping approach to measure the total As concentration as well as relative abundance of four As species types:

1) mineral-bound arsenate — As(V),

2) mineral-bound arsenite —As(III),

3) As(III)-sulfide — orpiment-type sulfide in which As is the metal bound to reduced S, and

4) As(-I) sulfide — arsenopyrite and arsenian-pyrite type sulfides, in which As substitutes for sulfur in the disulfide and is bound to both Fe and S.

For the descriptive track, we use linear combination fitting and hierarchical clustering of X-ray absorption near-edge structure (XANES) spectra to describe As and Fe speciation in detail at discrete points in each sample. The spectroscopic data are interpreted in the context of existing databases of well water chemistry.

2.1.1 Arsenic Release Mechanisms in Glacial Aquifers

Three specific As release mechanisms are relevant for glacial aquifers and aquitards: desorption, reductive dissolution of Fe(III)(oxyhydr)oxides, and oxidative dissolution of sulfide minerals (Harvey and Beckie 2005).

2.1.1.1 Adsorption and Desorption

Adsorption is a process by which molecules and ions in one phase attach to the surface of another phase via weak electrostatic bonds. In the case of As, sorbing species are often arsenate (e.g. H_3AsO_4, $H_2AsO_4^-$, $HAsO_4^{-2}$, AsO_4^{-3}) or an arsenite aqueous species (e.g. H_3AsO_3, $H_2AsO_3^-$, $HAsO_3^{-2}$, AsO_3^{-3}) (Cullen and Reimer 1989). The arsenate species $H_2AsO_4^-$ and $HAsO_4^{-2}$ and the arsenite species H_3AsO_3 are the most relevant for the circumneutral suboxic aquifer conditions. Arsenate is typically bound to Fe(oxyhydr)oxides via inner-sphere complexes while arsenite species tend to sorb to Fe(oxyhydr)oxides via both inner and outer sphere complexes (Goldberg and Johnston 2001).

Adsorbed species return to solution through desorption processes. In reductive desorption the chemical reduction of a sorbed species results in its release to solution (e.g. sorbed arsenate reduced to arsenite). Reductive desorption is often attributed to microbial activity but could be caused by any process that lowers the redox potential. The overall effect of frequent changes in redox state from oxic to reduced on As-affected systems is a greater concentration of dissolved As (O'Day et al. 2004). Competitive ions, especially anions such as ortho-phosphate (e.g. ligand exchange with ortho-

phosphate) are known to increase desorption of As (Banerjee et al. 2008; Gao et al. 2011). Sorption processes are thought to be important in controlling As concentrations in groundwater in the Red River of Vietnam (Mai et al. 2014) and in Bangladesh (Harvey et al. 2002; Polizzotto et al. 2006; Itai et al. 2010; van Geen et al. 2013). Desorption tends to liberate As without changes to speciation of Fe or S and should have little impact on Fe and S concentrations in groundwater. Well waters in which desorption is a primary factor in liberating As would have little difference in dissolved Fe and S concentrations between high As and low As wells. If As were released to waters via desorption, then the solid phase would include arsenate and/or arsenite co-located with Fe(III) secondary minerals, such as clays and (oxyhydr)oxides.

2.1.1.2 Reductive Dissolution

Reductive dissolution occurs when the chemical reduction of atoms in a crystal leads to higher solubility reaction products and dissolution of the mineral. In oxic systems, where Fe and As are present, As is often associated with Fe (oxyhyr)oxides through sorption and co-precipitation reactions. Dissolution of Fe(oxyhydr)oxide releases As and Fe from these minerals to solution (Smedley and Kinneborough 2002).

(Equation 1)

$$HAsO_4^{2-} \cdots FeOOH\ (s) + 3H^+(aq) + \ e^- \rightarrow Fe^{2+}(aq) + 2H_2O\ (l) + \ HAsO_4^{2-}$$

When sorbed arsenate is present, reductive desorption may accompany reductive dissolution (Erbs et al. 2010). Reductive dissolution of As-bearing Fe(oxyhydr)oxides

has been identified as an important process releasing As from industrially contaminated sediments (Weber et al. 2010), mine wastes (Langmuir et al. 2006), natural soils (Bennett and Dudas 2003), and sediments (Chow and Taillefert 2009; Rowland et al. 2007; Akai et al. 2004; McArthur et al. 2004).

Reductive dissolution of As-bearing Fe(oxyhydr)oxides would be expected to be preceded by sulfate reduction, and would tend to liberate As and Fe to solution without an increase in sulfate concentration (Borch et al. 2010, Hansel et al. 2015). Well waters in which reductive dissolution is a primary factor in liberating As should have higher Fe concentrations without an increase in sulfate in sulfate between high As and low As wells. If As were released to waters via reductive dissolution, then arsenate and arsenite would be co-located with Fe(III) bearing secondary minerals, such as clays and (oxyhydr)oxides.

2.1.1.3. Oxidative Dissolution

Oxidative dissolution is the process by which minerals dissolve due to chemical oxidation of one or more elements in the mineral crystal, and it may be congruent (all elements in the mineral dissolve) or incongruent (some elements dissolve and others transform into another mineral). An example of congruent oxidative dissolution would be the oxidation of arsenopyrite (AsFeS) or As-pyrite ($FeS_{2-x}As_x$) to form Fe^{2+}, arsenite, and sulfate aqueous reaction products. Under low pH conditions (e.g. acid waste) this reaction produces $Fe^{2+}_{(aq)}$ (Walker et al. 2006; Schreiber and Rimstidt 2013; Corkhill and Vaughan 2009).

(Equation 2)

$$4FeAsS_{(s)} + 11O_{2(g)} + 6H_2O_{(l)} \rightarrow 4Fe^{2+}_{(aq)} + 4H_3AsO_{3(aq)} + 4SO^{2-}_{4(aq)}$$

In circumneutral and basic pH environments, $Fe^{2+}_{(aq)}$ oxidizes to Fe(III) and precipitates as an Fe(oxyhydr)oxide. The precipitated (oxyhydr)oxide may form a weathering rind that slows further oxidation (Schreiber and Rimstidt 2013), and the freshly formed (oxyhydr)oxide presents favorable binding sites for the dissolved As (Yu et al. 2007; James and Bartlett 1999).

(Equation 3) $$Fe^{2+}_{(aq)} + 2H_2O_{(l)} \rightarrow FeOOH_{(s)} + 3H^{+}_{(aq)} + e^{-}$$

Depending on redox and pH, arsenite could stay in solution, sorb to the newly formed Fe(oxyhydr)oxide mineral, or oxidize to arsenate and subsequently sorb to the Fe(oxyhydr)oxide mineral. It is the balance between solid and aqueous phase As that will determine the amount of As in the groundwater.

Oxidative dissolution of As sulfides has been identified as a source of As to groundwater in mine wastes (Yu et al. 2007; Nesbitt et al. 1995) and in bedrock aquifers that contain sulfide minerals (West et al. 2012; Kolker et al. 2003; Schreiber et al. 2000). For As to be liberated to waters from sulfides, As-bearing sulfide minerals must be present in the sediments, and an oxidant available in solution.

If oxidative dissolution of As-bearing sulfides were occurring, then wells with elevated As would also have higher concentrations of dissolved Fe and sulfate than in the nearby wells without elevated As. If incongruent dissolution, or very rapid oxidation and re-

precipitation of Fe as (oxyhydr)oxides, were occurring, then particles with As sulfides and Fe(oxyhydr)oxides would be co-located in the aquifer solids.

2.2. MATERIALS AND METHODS

2.2.1 Regional Setting

Samples for analysis were collected from rotary-sonic cores of glacial deposits within the footprint of the Des Moines Lobe Glacial advance in west-central Minnesota, USA (Fig.1) (Welch 2000). This region is a nexus of drinking-water wells that exceed the US EPA maximum contaminant level (MCL) As>10μgL^{-1}. The upper aquifers are glacial materials deposited by different ice-streams within the Des Moines Lobe. These fast-moving glaciers were similar to those active in Antarctica today and originated from an ice dome in what is now central Canada at the end of the last glaciation (Patterson 1998; Jennings 2006). The ice-streams had different points of origin and traveled different paths and therefore entrained and deposited diverse geologic materials (Slatt and Eyles 1981). The geographic extent of the sediments is controlled by bedrock and pre-Des Moines-lobe glacial deposit topographic highs to the east and west. Des Moines Lobe ice-stream sediments are underlain by older aquifer sediments from previous glacial periods (Harris and Berg 2006; Harris et al. 1999; Patterson et al. 1999) that are constrained by the same bedrock topography (Wright 1972). Because Des Moines Lobe deposits are widespread and complex, identification of these glacial deposits as a

probable source of As to well water leaves a wide range of possible geologic sources of As. No single formation has been identified as the source of arsenic to well waters.

Glacial aquifers typically form in glacial-outwash sediments composed of sands and gravels deposited by fast-moving glacial meltwater (Fig.2) (Prothero and Schwab, 1996), but may also form in sandy lake sediment. The sediments confining these aquifers are glacial tills composed of poorly sorted sediments in a matrix of finely-ground clay-sized material (Ojakangas and Matsch 1982). The clay-sized matrix of till creates low-permeability conditions which allow them to function as confining layers, or aquitards, in glacial aquifer systems (Berg 2006, 2008). Aquitards limit the movement of groundwater to the more conductive sands and gravels of the aquifers. Glacial aquifers tend to be laterally discontinuous (Ojakangas and Matsch 1982), which likely contributes to the geographic heterogeneity observed in groundwater properties, including As concentrations (Toner et al. 2011).

Sediments in this region are not unusually elevated in As. The crustal average is about 5.1 $mgkg^{-1}$ (Rudnick and Gao 2003). The highest As concentration found in any of the sediments measured for this study is 12.1 $mgkg^{-1}$, the lowest concentration was 2.6 $mgkg^{-1}$, the average concentration was 6.6 $mgkg^{-1}$and the median concentration was 6.8 $mgkg^{-1}$. The distribution of the elevated-As wells is strongly heterogeneous with respect to geography and well depth and previous research based on well-water chemistry and well-construction records suggested that the aquitard/aquifer interface was the likely source of As from solids to waters (Erickson and Barnes, 2005a). Wells with screened intervals

close to an aquitard are more likely to have elevated well-water As concentrations than wells with screens farther from the aquitard (Fig. 3; Erickson and Barnes 2005b). These findings suggest that the original solid-phase source of the As is in the till, and that hydrological and biogeochemical processes at the aquitard-aquifer interface could be liberating As to groundwater.

2.2.2 Sample Selection

Samples for analysis were selected from archived rotasonic cores drilled by the Minnesota Geological Survey, and archived at the Lands and Minerals Drill Core Library, Minnesota Department of Natural Resources, Hibbing, Minnesota, USA. Cores in the sample archive are stored in wooden core-boxes in ambient air.

Sets of samples were analyzed from three cores (Fig.1). The cores and the depths analyzed were chosen based on their proximity to high As drinking water wells, and the depths of the wells (Minnesota Department of Health [MDH], 2001, 2002; Minnesota Pollution Control Agency [MPCA] 1999; Toner et al 2011). Core OTT3 (Grant County, Minnesota, 46.06°N, 95.998°W) was collected and described by the Minnesota Geological Survey in 1997 (Harris et al. 1999). Fifteen subsamples of the different strata from core OTT3 were analyzed for sediment chemistry and three samples of these strata were also examined via XAS. Core TG3 (Stevens County, Minnesota,45.39°N, 99.055°W) was collected by the Minnesota Geological Survey in 2000 (Harris and Berg 2006). Eleven subsamples of the different strata from core TG3 were analyzed for sediment chemistry and four samples of the sampled strata were also examined via XAS.

Core UMRB2 was collected by the Minnesota Geological Survey in 1997 (Patterson et al 1999). Nineteen subsamples from the different strata of core UMRB2 were analyzed for sediment chemistry and four samples of those strata were also examined via XAS. A single sample from a fourth core (TG4 sample 28, Pope County, Minnesota, 45.74°N, 95.623°W, collected in 2000) (Harris and Berg 2006) was also analyzed and these data are included in the supplementary materials. No further samples from TG4 were analyzed so this sample cannot be compared with other materials from the same core. Samples were selected using published stratigraphic descriptions (Harris et al, 1999; Harris and Berg, 2006; Patterson et al. 1999). Sample sets for these aquifer deposits include: (1) a sample from within the aquifer deposit that we will call "aquifer," (2) a sample of aquitard material in close contact with the aquifer that we will call the "aquitard-aquifer contact" or "contact", and (3) a sample of the aquitard material not in contact with the aquifer that we will call "aquitard." The aquitard sample was chosen from the same material as the contact till at a distance at least 5 meters above the contact. In addition to these three types, the UMRB2 set of samples contains a second below-aquifer contact sample. The TG3 set contains an additional sample of a thin silt horizon at the aquifer/aquitard boundary.

2.2.3 Well-Water Chemistry Near the Cores

Well-water chemistry data: pH, Eh, and As, Fe, and sulfate concentrations used in this study (Table 1) came from previous statewide and regional groundwater chemistry studies conducted in 1998 and 1999 (MPCA 1999; MDH 2001, 2002; MGS and MDH 2004). The reported water chemistry comes from single sampling events (each well was

sampled once) so temporal variability and seasonal effects cannot be evaluated from these data. We limited our comparison between the solids and the well water to wells within 10km of each core. We divided the wells near the three cores into two groups, "high" and "low" As concentrations. The high As group has arsenic concentrations that exceed the US EPA MCL of $10\mu gL^{-1}$ and low As group has arsenic concentrations below $10\mu gL^{-1}$. The 10km buffer distance was chosen arbitrarily. Within the 10km buffer of the three cores there were 50 wells, however 19 of these wells had some kind of water treatment in place (either water softeners or Fe removers); these wells were not included in any analysis.

Initial aqueous species activities for the predominance diagram in the discussion were generated with Geochemist's Workbench REACT sub-program (Bethke 2008) using the average Eh, pH, As, Fe, sulfate, and Cl- concentrations of the untreated wells within 10km of the cores (MPCA 1999, MDH 2001). Only 29 of the wells had a reported sulfate measurement. Redox and dissociation constants used to delineate the predominance fields were generated using published constants (James and Bartlett 1999; Wagman 1982; Eary 1992) and enthalpies (Rossini et al. 1952; Stull and Prophet 1971; Bryndzia and Kleppa 1988). These were adjusted to the average measured well-water temperature of 10ºC using the van't Hoff equation (van't Hoff 1874).

2.2.4 Sample Processing

Core sections of interest were photographed in place and then approximately half of each section was removed for processing. The remaining halves are under curation at the MN-

DNR core archive. Outer parts of the core that had been in contact with the core barrel and drilling water were removed from the core and retained separately. In the case of aquifer materials that did not retain a regular shape we collected the aliquot from the innermost part in the core bag. The remaining inner portion of the core was disaggregated in a ceramic mortar and pestle, and sieved to remove pebbles greater than 2 mm. The >2mm pebble fraction was retained separately. The <2mm fraction was then split and an aliquot of the sample (~50g) was ground to <150 μm using a corundum mortar and pestle. The remaining split of the <2mm fraction was retained separately and subsequent splits of this fraction were subjected to dissolution and sediment chemistry. The <150 μm fraction was split into aliquots for sediment chemistry and X-ray absorption spectroscopy.

2.2.5 Unconsolidated Sediment Chemistry

Sediment chemistry was completed by the United States Geological Survey (USGS) contract laboratory using methods detailed in Taggart (2002). For all sediments, the <2mm fractions were digested in a four-acid decomposition (nitric, hydrochloric, perchloric, and hydrofluoric acids) that dissolves most minerals. Forty-two major and trace elements were then measured via a combined inductively coupled plasma atomic emission spectrometry/mass spectrometry (ICP-AES/MS) method. Arsenic and selenium (Se) were measured separately by continuous flow hydride generation-atomic absorption spectrometry, and mercury (Hg) was analyzed by cold-vapor atomic absorption. In addition to the 4-acid near-total extraction, sediment was also subjected to a weak

peroxide leach and analyzed by ICP-MS. This method extracts loosely-bound metals, including As, that are sorbed to sediment.

2.2.6 X-ray Absorption Spectroscopy

2.2.6.1 Bulk X-ray Absorption Spectroscopy

Most of the As 1s X-ray absorption near-edge structure (XANES) reference spectra were collected from reference materials at the Advanced Photon Source (APS), Argonne National Laboratory beamlines 20-BM and 13-BM. At 20-BM, the monochromator was calibrated with gold foil using an assumed value for the XANES inflection point of 11,919.7 eV. After monochromator calibration, a sodium arsenate (main peak maximum set to 11,875 eV at other beamlines) standard was measured to allow for a unified calibration scheme among beamlines. The reference materials were: (1) orpiment, As_2S_3 ; (2) arsenopyrite, FeAsS; (3) arsenate sorbed goethite α-FeOOH; (4) arsenate sorbed 2-line ferrihydrite ; (5) arsenate sorbed diopside $MgCaSi_2O_6$; (6) arsenate sorbed anorthite $CaAl_2Si_2O_8$; (7) arsenate sorbed ramsdellite $Mn(IV)O_4$; (8) arsenate sorbed calcite $CaCO_3$; (9) arsenate sorbed opal $SiO_2 \cdot nH_2O$; (10) arsenite sorbed 2-line ferrihydrite ; (11) aqueous sodium arsenate $NaH_2AsO_4 \cdot H_2O$; (12) aqueous sodium arsenite $Na_3AsO_3 \cdot H_2O$; (13) sodium arsenate NaH_2AsO_4; and (14) sodium arsenite Na_3AsO_3. The goethite (micro-crystalline) and ferrihydrite were synthesized using published methods (Schwertmann and Cornell 1991) and the sorption experiments yielded ~ 800 mg As kg^{-1} oxide at pH 7 and pH 8. The orpiment, arsenopyrite, anorthite, ramsdellite, calcite, and opal were type specimens from the Department of Earth Science, University of

Minnesota. (A complete list and references for all As and Fe reference spectra used are described in the Electronic Annex: EA Table 1 and EA Table 2).

The valence state of As in bulk glacial sediments was also measured using As 1s XANES spectroscopy at the APS beamline 20-BM. Air-dry sediments were packed into Teflon® holders with Kapton® film and nylon screws. The samples were then mounted in a cryogenic holder cooled to 20 K (Janis Research Co., Inc.) for fluorescence mode measurements using a 13-element solid state detector (Canberra). No evidence for photon-induced damage to As speciation was observed under these conditions. The beam spot size on the sample was ~ 400 × 800 μm: this is much smaller than the sample area (~ 5 × 15 mm) so the sample was mapped using X-ray fluorescence (XRF). In these maps, spatial heterogeneity in the As signal was observed despite physical homogenization of the sample (see *Section 3.4 Sample Processing*). Sample locations with relative uniformity of As XRF signal in contiguous pixels were chosen for data collection. Arsenic spectra collected in this way yielded non-uniform chemical signatures within the homogenized samples. A single representative As XANES spectrum could not be measured for an individual sample. Therefore, a microprobe speciation-mapping approach to describe and quantify As speciation in the samples was developed for, and applied to, these sediments.

2.2.6.2 Micro-probe X-ray Absorption Spectroscopy

Microprobe X-ray fluorescence (μXRF) maps, As and Fe 1s XANES spectroscopy, and As "speciation maps" were measured at the X-ray micro-probe beamline 10.3.2,

Advanced Light Source, Lawrence Berkeley National Laboratory (Marcus et al. 2004). For As, the monochromator was calibrated by setting the main resonance of the As XANES spectrum of sodium arsenate to 11,875 eV. For Fe measurements, the monochromator was calibrated using Fe foil with the inflection point of the XANES spectrum set to 7110.75 eV. Powdered samples were adhered to Kapton® film (stabilized underneath by plastic cover-slips; Rinzel®). Fluorescence mode measurements were made with a Canberra 7-element Ge detector, or with Vortex or Amp-Tek silicon drift diode detectors. Measurements were conducted at room temperature in ambient atmosphere. Photon-induced oxidation of As(III) was observed in some samples, so all As XANES data were collected in "quick" mode with a full sweep of the monochromator in 30 s. The number of sweeps per point varied depending on the quality of the spectra, for most points 30-45 sweeps were collected while more diffuse spots required more than 60 sweeps to resolve the spectra sufficiently for fitting.

The speciation of As in the samples was described in two steps:

1) The spatial distributions of total As, Fe, and other elements (calcium, titanium, chromium, manganese, and nickel) were mapped via XRF with a resolution of 5-10 μm^2 pixels (beam size 6μm in the vertical and between 6.2 and 11.6 μm in the horizontal). 2) Point As XANES data were collected in the area of the XRF map. These As spectra were compared with a set of 25 As reference species spectra using linear least-squares combination fitting (LCF) in order to understand the range and combination of As species present. The best-fitting As species were used to inform choices of energies in making

the speciation maps (described below). Linear least-squares combination fitting is described in greater detail in Section *3.9.3 As and Fe XANES Linear Combination Fitting*.

Reference spectra on arsenopyrite (Julcani, Peru) and lollingite (Lölling, Austria) were collected via grazing-exit fluorescence on polished sections by using the Amp-Tek silicon drift diode detector. (A complete list and references for all As and Fe reference spectra used are described in Tables EA1 and EA2).

2.2.7 Analytical Challenges and Approach

Measuring the speciation of As in glacial sediments presents diverse analytical challenges. The overall concentration of As in the samples is very low (3-12 mg kg^{-1}). In addition, As in the samples is physically and chemically heterogeneous and contained within a matrix with high Fe concentrations, which increases the difficulty of X-ray measurements of As. These samples have many particles with dilute As and rare particles with concentrated As, set in a matrix of particles with no detectable As. To test our hypothesis, we needed to know what species were present, and we needed to quantify them at the sample level. To overcome these challenges, we used whole-rock chemistry for total As concentration, and two complementary XAS techniques to describe and quantify the species of As present. An annotated process diagram illustrating the entire μXAS data collection and analysis method for point XANES analysis and speciation mapping is available in the Electronic Annex (EA Fig.1).

We measured solid-phase As speciation with micro-probe XAS in two modes: point-XANES and speciation mapping. Speciation mapping provides quantitative but very general As speciation (valence state) over a large number of particles and aggregates. The point XANES give detailed speciation at representative points within the samples.

For our study this dual approach—point XANES and speciation mapping—was required. A point XANES approach alone failed because the samples are both dilute and heterogeneous with respect to As. It was not possible to collect spectra on a sufficiency of random points to draw statistically supportable conclusions about relative abundance. The point XANES were collected with the goal of illustrating the variety of As species present in the sample, and the speciation mapping was used to determine relative abundance of As species.

All As in these samples is co-located with Fe. For this reason, a good understanding of speciation of Fe is valuable to our interpretation of As release to waters. Arsenic is present in the samples at very low concentrations, while Fe is a major element in the samples. Excluding Fe that is not chemically bound to As presented an analytical challenge, and Fe XANES were collected only on the points that had As XANES collected. To limit our Fe XANES collection to the As XANES points, we calibrated for Fe and collected Fe XANES points after the As mapping and As XANES were complete. To return faithfully to these points, after calibrating on Fe foil we returned to the location of each As XANES point, optimized the beam position for As, and then collected the Fe

XANES at that point. Where we had collected As XANES on diffuse As regions we centered the beam at the middle of the diffuse As region and collected the Fe XANES.

2.2.8 Arsenic Speciation Mapping

An As "speciation mapping" protocol was developed for glacial sediments (Toner et al. 2014) (EA Fig.1 "Quantitative Track"). The method has the same components as chemical/speciation/multi-energy mapping methods developed for S (Zeng et al. 2013, Pickering et al. 2009) and Fe (Lam et al. 2012, Mayhew et al. 2011, Toner et al. 2012, Marcus et al. 2010). Multiple XRF maps were collected from sample areas with energies spanning the As 1s absorption edge. The number of XRF maps and the incident energy for each were chosen based on: 1) the observed As species present (point XANES observations); and 2) the degree to which the absorbance at specific energies could distinguish among the species present. This selection process was aided by a custom beamline program (Electronic Annex Appendix 1: *Mathematical basis of chem map error estimator software*). The XRF maps were deadtime corrected, registered, and compiled into a single file that will be referred to as a "speciation map".

For the glacial sediments, the *chem map error estimator* calculations indicated that six incident energies for XRF maps were needed to describe the As species with a speciation mapping approach: 11830eV (pre-edge), 11868 eV (arsenopyrite), 11869 eV (orpiment), 11871.5 eV (arsenite), 11875 eV (arsenate), and 11979 eV (post-edge). The species listed for each energy are those for which mapping at that energy provides the greatest sensitivity, but all species contribute to the signals at all energies. The speciation map

data sets were composed of six XRF maps that yield a six-point absorption profile at each pixel in the aligned composite map, with an error estimate for the calculated species in a speciation map of less than 10 mol % for each species type. The first three As speciation maps collected (OTT3_55, OTT3_73 and OTT3_74) were collected using 5 single energy maps: the 11868 eV map was not collected. In subsequent As speciation mapping, both 11868eV and 11869eV maps were used to distinguish As(-I) -sulfide (arsenopyrite- type sulfide in which As substitutes for sulfur in the disulfide and is bound to both Fe and reduced S) and As(III)-sulfide (orpiment-type sulfide in which As is the metal bound to reduced S). For the OTT3 series, the estimated error between As(V), As(III), and either As(III)-sulfide or As(-I)-sulfide is 10% but the estimated error in distinguishing between As(-I)-sulfide and As(III)-sulfide is ~30%. For this reason we report a single As-sulfide fraction in the results and discussion of OTT3 samples, rather than As(III)-sulfide and As(-I)-sulfide as for the other samples.

The speciation maps were fit pixel-by-pixel by LCF with reference spectra and a material blank with custom beamline software (Marcus 2010). We used four reference spectra to fit to the map (one each of: sorbed As(V), sorbed As(III), orpiment, and arsenopyrite). This set of reference spectra was identified during the initial As XANES survey as representative of the sample composition. The quality of the speciation map fits was evaluated with the whole-map mean squared error. The agreement between the speciation map fits and point XANES data was evaluated by comparing the species fraction from the maps with the species fraction from the point XANES using the same 4-species reference set as the map, and allowing 4-member fits. This procedure differs

from the point XANES for LCF that were fit with a 25-member reference set that allows up to three members *(3.6.2 Micro-Probe X-ray Absorption Spectroscopy*). Beam size was wider and shorter (12μm × 4μm) for the point XANES collection than for the individual energy maps (6μm × 6μm), so the three pixel locations on the speciation map covered by the point XANES were averaged for comparison (Electronic Annex Figure EA Fig.2). The mole fraction of each As species was calculated by summing the mole fraction from all pixels in the speciation map and normalizing by the number of pixels).

Additional point As XANES spectra were collected within the area of the speciation map to ensure that the pixel-by-pixel fits and a point XANES collected on the same spot were in agreement (EA Fig.1 "Descriptive Track"). Co-located Fe XANES spectra were collected on the same locations as the As XANES to describe As-bearing or associated minerals in greater detail. Co-located As and Fe XANES for the mid-aquitard till (UMRB2_159) were collected from a multichannel XRF map rather than an As speciation map. Arsenic spectra without co-located Fe spectra were collected on the UMRB2 speciation map.

2.2.9 Arsenic and Fe XAS Data Analysis

2.2.9.1 Novel Application of Established Statistical Approaches

To gauge the similarity of the As and Fe spectra from each core we adapted some statistical tools commonly used in genomics and data mining to the spectroscopic data sets. We used correlation-distance hierarchical clustering to compare the normalized sample spectra to each other. Unlike Euclidean fitting methods (e.g. LCF), correlation-

distance fitting is relatively insensitive to scaling (D'haeseleer 2005). This makes it useful for pattern matching and comparing the raw spectra among themselves (database independent) but not very good for evaluating composition (Friedman and Alm 2012). Using correlation-distance we were able to quantify the similarities among the spectra themselves to identify stratum-specific populations.

To complement the database-independent correlation-distance hierarchical clustering, we used cosine-distance clustering on our LCF results (database dependent) for both As and Fe speciation. Cosine-distance hierarchical clustering is frequently used to analyze similarity in compositional data because it can accommodate a large number of components without introducing scaling artifacts (Friedman and Alm 2012). Cosine-distance hierarchical clustering is a popular method used to illustrate patterns of gene expression within a group of organisms (Eisen et al. 1998). It is also a common method used in data mining to evaluate document similarity and for name disambiguation in search engines. We took the results of LCF and assigned each reference spectrum to a broader species category (e.g. goethite, α-Fe(III)OOH, was assigned to Fe(III)(oxyhydr)oxides), based on general chemical properties of the reference materials. Arsenic categories and Fe categories were each normalized to 100% and the resulting vectors traced out a pattern of three basic particle types that were found in all three cores: (1) As and Fe sulfides, (2) oxidized As and Fe, and (3) As sulfide with oxidized Fe.

2.2.9. 2 Arsenic and Fe XANES Correlation Distance

The As and Fe XANES spectra were compared with each other and suites of As and Fe reference spectra (Electronic Annex Tables EA Table 1 and EA Table 2) according to correlation distance in order to compare spectra in a way that is not sensitive to scaling and differences in mean values (D'haesseleer 2005). Correlation distance D_{xy} was calculated between all pairs, where x_μ^i is normalized fluorescence of the sample spectrum at incident energy i, $\bar{x}_\mu$ is the mean of the normalized fluorescence for the first spectrum, y_μ^i is the normalized fluorescence of the second spectrum at incident energy i, and $\bar{y}_\mu$ is the mean of the normalized fluorescence of the second spectrum:

(Equation 4)
$$D_{x,y} = 1 - \frac{\sum_{i=1}^{n} (x_\mu^i - \bar{x}_\mu)(y_\mu^i - \bar{y}_\mu)}{\sqrt{\sum_{i=1}^{n} (x_\mu^i - \bar{x}_\mu)^2} \sqrt{\sum_{i=1}^{n} (y_\mu^i - \bar{y}_\mu)^2}}$$

Sample spectra and selected reference spectra were organized into dendrograms (trees) according to correlation distance. The same four As references used to fit the As speciation maps were used as the reference spectra in the As correlation-distance trees for all three cores. The Fe sample spectra were more diverse than the As spectra and no single set of references fit well with the Fe correlation-distance trees of all three cores. Iron references used in the correlation-distance trees were chosen by building a correlation distance tree with the entire Fe reference spectrum set, and then "pruning" branches made up entirely of references with no sample spectra by removing those reference spectra from the reference sample file for that tree. After removing these distant references from the reference set, the Fe correlation-distance trees were built again, and references more closely related to other references than to the samples were removed. This "pruning" brought the number of references used in the Fe trees down to ~10 references per Fe tree. Each reference set is somewhat different but all three include pyrite and goethite. SciPy (Jones et al. 2001, Oliphant 2007) was used for hierarchical clustering. Our script is available at
https://github.com/jklynch/mr-fitty/blob/master/notebooks/hc_sig_cut_archived_tills_As.i.pynb
and
https://github.com/jklynch/mrfitty/blob/master/notebooks/hc_sig_cut_archived_tills_Fe.ipynb.

2.2.9.3 Arsenic and Fe XANES Linear Combination Fitting

Linear combination fitting of a suite of As or Fe reference spectra was applied to each sample spectrum. Linear least-squares fitting was applied to all single references, pairs and combinations of three references for each sample spectrum, any fit with negative coefficients was rejected. Fits were selected based upon minimum values for the normalized sum of squares (NSS) for the residual. For parsimony, a second component or third component was only added if it reduced the NSS by more than 10%. Sample spectra best fits and scores were summarized according to individual references (i.e. arsenate sorbed to goethite pH7) and also according to broader species categories into which the individual references fall, e.g. "arsenate sorbed to goethite pH7" falls into the broader category "AsV". Tables of the As and Fe reference spectra including their broader species groups can be found in the Electronic Annex as EA Table1 and EA Table 2. We developed a program for linear combination fitting using SciPy (Jones et al. 2001, Oliphant 2007). Our program is available at: *https://github.com/jklynch/mr-fitty.*

2.2.9.4 Analysis of Co-located As and Fe XANES

The fractions of broader species categories for the co-located Fe and As XANES point spectra were used to generate a heat map and cosine-distance dendrograms to illustrate the relationship between As and Fe among the individual points and to identify populations of point types within the samples. Cosine-distance hierarchical clustering is often used for compositional data because it is sensitive to differences from a mean composition (D'haeseleer 2005). The horizontal dendrogram quantifies the similarity

among the fit composition of the sample spectra according to cosine distance, where in the horizontal u and v are the fractional contribution of each broad group at m spots. In the vertical dendrogram u and v are the fractional contribution of each spot to m broad groups. This quantifies the co-occurrence of the broad reference categories among the spots:

(Equation 5) $$Cosine\ distance\ = 1 - \frac{\sum_{i=1}^{m} u_i v_i}{\sqrt{\sum_{i=1}^{m} {u_i}^2}\sqrt{\sum_{i=1}^{m} {v_i}^2}}$$

For this analysis, the Fe XANES fits to primary Fe-bearing silicates were not included because these mineral surfaces are thought to be relatively inert with respect to As. For particles where primary Fe silicates were among the components, the primary Fe silicate component was removed from the total and the remaining components normalized to 100%. Heat maps and cosine-distance dendrograms were made using MatPlotLib (Hunter 2007).

2.3. RESULTS

2.3.1 Spatial Analysis of Well Water Chemistry

Water chemistry conditions in wells above and below the As 10μgL^{-1} maximum contaminant level in wells within 10km of the three cores are shown in Table 1.

Wells with elevated As near core OTT3 have slightly higher redox potential and lower pH (average 141eV, pH 7.2) than the nearby low As wells (114eV, pH7.7). Well water

Fe and S concentrations in the vicinity of core OTT3 are sub-equal (within 10%) in both elevated As and low-As wells. This is consistent with desorption as a mechanism liberating As to waters.

Wells near core TG3 with elevated As have somewhat lower redox potential and slightly lower pH (134eV, pH 7.2) than nearby low As wells (175eV, pH 7.3). Elevated As wells near core TG3 have higher Fe (3867μgL^{-1} Fe) in the elevated As wells than the low As wells (1416μgL^{-1} Fe), but the sulfate concentration varies less than 10% between the two sets of wells. This is consistent with reductive dissolution as a mechanism liberating As to waters.

High As wells near core UMBR2 have somewhat lower pH and much higher Eh (pH 7.3 and 224 mV) than the low As wells (pH 7.5, 134mV). The high As wells have much higher Fe and sulfate (Fe 3845μgL^{-1}, S 801mgL^{-1}) than low As wells (Fe 1351μgL^{-1}, S 480mgL^{-1}). This is consistent with oxidative dissolution as a mechanism liberating As to waters.

2.3.2 Bulk Chemical Analysis

The bulk chemical composition of the glacial sediments is displayed in Tables 2-4. Overall, the total As concentrations for the 46 samples are in the range of 2.6-12.3 mg As/kg sediment. Total Fe and S concentrations are in the weight % range with 0.9-3.6 wt. % Fe and 0.05- 2.9 wt. % S. The Fe/S ratio is reported as a first-order approximation of redox state, where we would interpret sediments with higher Fe/S to be more oxidized than a low Fe/S ratio.

Sediment analyses on 15 samples from core OTT3 (Table 2) show As concentrations ranging from 2.6 to 11.6 mg kg^{-1} with lower As concentrations in aquifer sands and gravels than in till. Iron concentrations ranged from 0.9 to 2.9 weight percent (wt. %) with lower Fe concentrations in aquifer sediments than in till. Sulfur concentrations ranged from 0.2 to 0.9 wt. % with lower concentrations of S in aquifer sediments than in till. The ratio of Fe/S tended to be higher in contact till and in the aquifer sands and gravels than in the mid-aquitard tills.

The 12 samples from core TG3 (Table 3) show As concentrations from 3.6 to 8.7 $mgkg^{-1}$. Iron concentrations range from 1.4 to 2.9 wt. % and sulfur (S) concentrations range from 0.05 to 2.9 wt. %. In the TG3 core in general, As, Fe and S concentrations are lower in aquifer sands and silts than in the till, and Fe/S ratios were higher in the near surface (TG3_28) sample and in the contact till and aquifer samples (TG3_56, 59 and 60), but in the aquifer sand at 31.4m (TG3_103) the Fe/S ratio was similar to the surrounding till.

Sediment analysis on 19 samples from core UMRB2 (Table 4, 19 samples) shows that the As concentrations of the samples range from 4.9 to 12.3 $mgkg^{-1}$. Iron concentrations range from 1.3 to 3.6 wt. % and S concentrations range from 0.3 to 1.8 wt. %. Fe/S ratios from core UMRB2 are lower overall than samples from the other two cores, and unlike the other two cores, S concentrations are not always lower in the aquifer sediments.

2.3.3 Solid-phase As and Fe Speciation

Work on these samples followed two tracks, one quantitative and the other descriptive. The quantitative track uses whole-rock digestions to measure total As, and speciation

mapping to measure the As species fraction for each sample. Speciation mapping collects spectroscopic data at hundreds of thousands of points in a sample, allowing us to calculate the relative abundance of As species groups. The descriptive track relies on detailed analysis of a relatively small number of point XANES to describe As and Fe speciation. The point XANES approach is necessary to "ground-truth" the speciation maps, as well as to identify the mineral species hosting As. This two-tiered approach to data collection, as applied to Fe geochemistry, is reviewed by Toner et al. 2014; 2016.

For the descriptive track, the first data analysis approach is correlation-distance hierarchical clustering (*Section 3.9.2*). This type of analysis groups As and Fe XANES spectra by pattern similarity and is data-base independent. Next, linear combination fitting (LCF) of As and Fe XANES spectra with reference spectra is conducted (*Section 3.9.3*); this is a data-base dependent approach (As and Fe reference spectra are described in Table EA1 and EA2). The final descriptive analysis relates co-located As and Fe species groups (derived from LCF of XANES) to each other using cosine-distance hierarchical clustering (*Section 3.9.4*).

In the following sections, we report on results from As speciation mapping, as well as As and Fe XANES analyses for three cores (OTT3, TG3, UMRB2). All Fe XANES reported are co-located with As XANES, but not all As XANES have a corresponding co-located Fe XANES spectrum.

2.3.3.1 Agreement Between Point XANES and Speciation Maps

Point XANES spectra generally confirmed the As species measured by the speciation maps. However, the maps tended to underestimate the As(III) mole fraction when compared with the point XANES; this may be due to differences in spot size and energy resolution between the maps and points. Speciation maps are collected with a 5 × 5 μm spot on the sample whereas the XANES spectra are collected at 15 × 4 μm to improve energy resolution and increase counts to the detector (horizontal × vertical; EA.Fig.2). The estimated As(III) fraction based on XANES spectra is up to 40% higher on small particles (< 10μm) than the As(III) per-pixel composition estimate from the maps. The discrepancy is much smaller or completely absent when XANES are collected on larger particles. The As(III) distribution tends to be diffuse throughout the sample, so small differences in beam position between the maps and the XANES tends to collect a larger fraction of As(III) from the diffuse background. We conclude that the XANES measurements on small particles include more overflow signal from the surrounding area than do the maps.

The speciation maps are less able to distinguish between As(-I) sulfides (Fe-As-type sulfides, where the As replaces S in a disulfide) and As(III) sulfides (orpiment-type sulfides in which As is the metal) than the point XANES spectra. This outcome is in agreement with the ~ 1 eV difference in the main spectral feature between the two As species groups, as well as the trade-off between speciation mapping and points XANES (i.e. number of observations increases while spectral resolution per point decreases). However, the summed As(-I) sulfides and As(III) sulfides components from LCF agrees very well between maps and point XANES when normalized without As(III). This

demonstrates that the speciation mapping is accurately detecting the total "As sulfide" species bin, but is not able to distinguish well between its components.

2.3.3.2 Ottertail County Core #3 (OTT3)

Results of As speciation maps and As and Fe XANES for core OTT3 are shown in Figure 4. The total As concentration in these samples is highest in the aquitard (OTT3_55), and decreases across the aquitard-aquifer contact (OTT3-74). The lowest As concentration is in the aquifer sediment (OTT3_73) (Table 5). The binned LCF results (specific reference spectra are assigned to a more general bin, e.g. goethite, α-FeOOH, is assigned to Fe(III) oxyhydroxide bin) for As and Fe are displayed in Tables 6 and 7, with full fit information available in Table EA3. OTT3 As speciation maps and multi-element xrf maps showing the location of XANES points are shown in EA Figures 3 and 4.

The speciation mapping allows us to calculate the relative proportions of As-sulfide (combined As(-I) sulfide and As(III) sulfide), As(III), and As(V) in the solid phase. From these data, we find that the As speciation in the aquifer (OTT3_73) is indistinguishable from the aquitard-aquifer contact (OTT3_74), and both are dominated by As(V). In contrast, the aquitard sample (OTT3_55) has more As sulfides. Overall, the aquitard has more total As and more As sulfide content. At the aquitard-aquifer contact, total As and As sulfide contents decrease and remain low in the aquifer.

The correlation-distance dendrogram for the As XANES spectra from OTT3 is shown in Figure 5a. The As spectra divide into four branches, with each branch containing one of

the four seeded reference spectra: arsenate As(V), arsenite As(III), orpiment As(III)-sulfide, and arsenopyrite As(-I)-sulfide. The spectra on these branches tend to resemble each other more closely than they do the reference spectra. Each branch contains spectra from most or all of the sampled strata. These results mirror the LCF output and indicate that most particles in the sample contain more than one of the As species types.

The correlation-distance dendrogram for the OTT3 Fe XANES spectra (Fig.5b) breaks into three main branches, as defined by seeded reference spectra. Unlike the As XANES spectra, the Fe spectra are largely segregated by stratum. The Fe(III) and mixed Fe(II,III) branches are composed primarily of spectra from the aquifer sample, and are defined by reference spectra that include Fe(III) (oxyhydr)oxides and secondary phyllosilicates, and Fe(II,III) oxides. The sulfide branch contains most of the aquitard-aquifer contact spectra and all of the aquitard spectra. These results corroborate the As speciation data by further demonstrating the chemically reducing conditions of the aquitard and oxidizing conditions in the aquitard-aquifer contact and aquifer.

Cosine-distance hierarchical clustering of the LCF output for As and Fe show three main populations of particles (Fig.6a). The "reduced" population is primarily composed of As(-I) sulfide and Fe sulfide materials from the aquitard and aquitard-aquifer contact. The "oxidized population" is composed of As(V) and Fe(III) oxyhydroxide and secondary phyllosilicate materials from the aquifer and aquitard-aquifer contact. The third group, designated "mixed redox population" is primarily composed of reduced As

(As(-I) and As(III) sulfide) and oxidized Fe. Particles with these mixed redox characteristics are primarily found in the aquifer sample.

2.3.3.3 Traverse Grant Core #3 (TG3)

Results of A speciation mapping and As and Fe XANES spectra for four strata from core TG3 are presented in Figure 7. From shallow to deep, the sampled strata are: an aquitard (TG3_45), an aquitard-aquifer contact (TG3_54), a silt layer (TG3-56), and an aquifer (TG3_59). The total As concentration is highest in the aquitard and aquitard-aquifer contact samples and lower in the silt and aquifer samples (Table 8). The binned LCF results for As and Fe XANES are displayed in Tables 9 and 10, with full fit information available in Table EA4.

The As speciation of the aquitard is dominated by As-sulfides (Fig.7b). The As(-I)-sulfide component decreases in the aquitard-aquifer contact and is replaced by As(V). The silt and aquifer strata have nearly identical As species composition and are dominated by As(V). In the TG3 core, the aquitard has higher As concentration and more reducing conditions than the aquifer. TG3 As speciation maps and multi-element xrf maps showing the location of XANES points are shown in EA Figures 5 and 6.

The correlation-distance dendrogram for As XANES spectra from TG3 show that, like spectra from OTT3, the sample spectra tend to be more similar to each other than to any of the reference materials (Fig.5c). The As XANES spectra divide into two branches. The arsenate As(V) branch, named for its seeded reference, has representatives from the

aquitard-aquifer contact, silt layer, and aquifer. All the remaining As XANES spectra, including all aquitard spectra, cluster within the As-sulfide branch with seeded reference spectra of arsenopyrite and orpiment. Spectra on the As sulfide branch come from all four strata. Arsenite As(III) is included in the dendrogram for consistency, but none of the TG3 As XANES spectra cluster closely with it.

The correlation-distance dendrogram for the co-located Fe XANES spectra of TG3 (Fig.5d) has four main branches. The Fe XANES spectra tend to segregate by stratum, but less so than OTT3. Overall, the aquitard and aquitard-aquifer contact are dominated by Fe sulfide content, as represented by mackinawite and pyrite seeded references. In contrast, the silt and aquifer strata are primarily Fe(II,III) and Fe(III), as represented by greenrust, magnetite, chromite, aegirine, Fe(III)-dextran, and goethite (see EA Table 2 for reference materials). These findings corroborate the As speciation: reducing conditions in the aquitard and aquitard-aquifer contact strata, and oxic conditions in the silt and aquifer strata.

Cosine-distance hierarchical clustering of the LCF output for As and Fe reveal three populations of particles (Fig.6b). The "oxidized" population is primarily composed of oxidized As and Fe, and has representatives from the silt and aquifer sediments. The "reduced" population is primarily composed of As and Fe sulfides, and has representatives from the aquitard and aquitard-aquifer contact. The "mixed redox population" (in which As sulfide is found with Fe(III)) forms two clusters, one with As(-

I)-sulfide and the other with As(III)-sulfide. This mixed redox population has representatives from the aquitard, silt, and aquifer.

2.3.3.4 Upper Minnesota River Basin Core #2 (UMRB2)

Results of As speciation mapping and and As and Fe XANES from core UMRB2 are presented in Figure 8. Strata sampled (from shallow to deep) are: an aquitard (UMRB2_159), an aquitard-aquifer contact or "above-aquifer contact" (UMRB2_164), an aquifer (UMRB2_165a2), and an aquitard-aquifer contact or "below-aquifer contact"(UMRB2_167). The total As concentration is highest in the below-aquifer contact, lesser in the aquitard and above-aquifer contact, and lowest in the aquifer (Table 11). UMRB2 As speciation maps and multi-element xrf maps showing the location of XANES points are shown in EA Figures 7 and 8.

The binned LCF results for As and Fe XANES are displayed in Tables 12 and 13, with full fit information available in Table EA5.

Speciation mapping (Fig.8b) of the aquitard (UMRB2_159) shows approximately equal fractions of all four As species. This is different from OTT3 and TG3, which both have chemically reduced aquitards. Both of the UMRB2 aquitard-aquifer contact samples (UMRB2_164 and UMRB2_167) have large fractions of As(-I)-sulfide, even more than the aquitard.

The correlation-distance hierarchical clustering dendrogram (Fig.5e) for As spectra has four main clusters. Like the As XANES spectra from OTT3 and TG3, the UMRB2 As

sample spectra resemble each other more than the reference spectra. The main feature of interest is the clustering of both contact strata (above and below the aquifer) with orpiment (As(III)-sulfide). The aquitard and aquifer strata contribute spectra to the arsenite As(III), arsenate As(V), and arsenopyrite branches. These data indicate more physical and chemical heterogeneity in the UMRB2 formation than in OTT3 or TG3.

The correlation-distance dendrogram (Fig.5f) for Fe spectra from UMRB2 shows that strata are more evenly distributed among the three branches than in the OTT3 and TG3 cores (i.e. grouping of Fe species by stratum is not present in UMRB2). The three branches are formed by Fe(II), mixed valence Fe(II,III), and Fe sulfide groups. Iron sulfides are distributed among all strata: aquitard, both aquitard-aquifer contacts, and the aquifer. The below-aquifer contact (UMRB2_167) is remarkably chemically reduced with Fe(II) and Fe sulfide branch affiliations. In the OTT3 and TG3 formations, the aquitard is chemically reduced, the contact is intermediate, and the aquifer is oxidized: UMRB2 does not follow this pattern.

Cosine-distance hierarchical clustering LCF output for co-located As and Fe XANES spectra (UMRB2; Fig.6c) show three main populations of particles. The “reduced” population is dominated by As(-I)sulfide, As(III) sulfide and Fe sulfide; all four of the sample strata are represented in this group. The “oxidized” population is dominated by As(V), As(III), and Fe(III) oxyhydroxides and secondary phyllosilicates; the aquifer and below-aquifer contact are represented in this group. The “mixed redox population” with As sulfide and Fe(III) is represented by the aquitard and both aquitard-aquifer contacts.

2.4. DISCUSSION

2.4.1 Solid-Phase Source of As to Groundwater

Earlier work on As in glacial aquifers (Erickson and Barnes 2005 a,b) led to an hypothesis that (bio)geochemical processes active at the interface between the aquitard and aquifer sediments were the probable cause of As release to groundwater. We then proposed that measurable changes in As and Fe chemistry should be observed in sediments at the stratigraphic contact between aquitard and aquifers. Our hypothesis was that a strong gradient in hydrologic conductivity and redox conditions present at the aquifer-aquitard contact would cause oxidative (e.g. As-bearing pyrite) or reductive (e.g. As-sorbed ferrihydrite) dissolution of minerals and release of As to groundwater. To test this hypothesis we compared As and Fe speciation in aquitard, aquitard-aquifer contact, and aquifer sediments from three rotosonic cores. Our main analytical approach was to develop methods to quantify As concentration and speciation in these sediments. The As speciation was then interpreted in the context of co-located Fe speciation and existing water chemistry databases for nearby wells to identify the process(es) liberating As to waters.

2.4.2 Geochemical Processes Liberating As to Waters

The minerals observed in the glacial sediments from this study are out of equilibrium with nearby well water. The water chemistry of wells near the locations of the three cores is plotted on an Eh-pH diagram (Fig.9). Currently available well-water chemistry indicates that the waters are suboxic and that the sulfide minerals identified by the point-

XANES analysis of the solid samples (As(III)-sulfide and As(-I) sulfide) are not in equilibrium with the waters of nearby wells.

The lack of chemical equilibrium between glacial sediment and well waters should be considered in light of the geologic processes that form glacial aquifers, as well as potential chemical artifacts in well-water samples. Glacial sediments are composed of transported materials entrained over hundreds (perhaps thousands) of kilometers: materials that formed under different geochemical conditions than those currently present in the till. These physically mixed materials are likely to have mineral components out of equilibrium within any particular stratigraphic layer. In addition to the large-scale mixing processes active in glaciers, disequilibrium may be caused by the integration of many microenvironments within and in proximity to wells. It is possible that well water samples have different redox, pH, element concentration, and chemical speciation than those that exist in pore waters. In particular, well-water samples could have different redox potential and pH values than *in situ* groundwaters (Gotkowitz et al. 2004). Despite this limitation, the water chemistry of wells surrounding these cores is an important tool in interpreting mineral populations in the aquifers and aquitard sediments. The Eh-pH diagram indicates that small changes in redox potential could change the stability of both iron and sulfide minerals in place with important implications for As chemistry. In particular, differences between the water chemistries of nearby wells with and without elevated As concentrations suggest possible mechanisms at work in As liberation near the three cores.

Arsenopyrite was detected in our samples. It is often observed out of equilibrium with its environment, and this disequilibrium persistence has been attributed to rinds of oxides forming on the outside of arsenopyrite grains in sediments and in lab-based oxidation experiments (Richardson and Vaughan 1989). Oxide rinds have been suggested as the cause of slowing dissolution of arsenopyrite (Craw et al. 2003). However, long-term experiments on mine wastes have shown that poorly crystalline Fe(III)(oxyhydr)oxide rinds are very effective at passivating the surface of arsenopyrite in air, but in aqueous solutions the rinds permit extensive leaching of As from the mineral grain into solution (Nesbitt and Muir 1998).

Oxidative dissolution of As sulfides has been identified as a source of As to groundwater in mine wastes (Yu et al. 2007; Nesbitt et al. 1995) and in bedrock aquifers that contain sulfide minerals (West et al. 2012; Schreiber et al. 2000). Redox potential and pH conditions are favorable for oxidation of sulfides in the wells near all three cores, and As sulfides were found in the aquifer and/or aquitard-aquifer contact sediments in each of the cores. Arsenic XANES data show that As in As-bearing sulfides makes up more than 30% of the As in the aquifer and aquitard-aquifer contact sediments from cores OTT3 and TG3, and approximately 50% of the As in core UMRB2.

2.4.3 Summary of Geochemical Conditions and Solid-phase Speciation

We have identified three mechanisms at work in liberating As to drinking-water wells near the three cores (Table 14). Desorption appears to be an important mechanism releasing As to waters near core OTT3 because the increased As concentration is not

accompanied by increases in sulfate or Fe. Well water Fe and S concentrations in the vicinity of core OTT3 are sub-equal (within 10%) in both elevated As and low-As wells. Wells near cores TG3 and UMBR2 have dissolved Fe concentrations approximately 2.7 and 2.8 times higher in the wells with elevated As than in the low As wells. Near core TG3, sulfate concentrations are sub-equal (within 10%) between the wells with elevated As and the low As wells. Wells near core TG3 with elevated As have lower redox potential and slightly lower pH (134eV, pH 7.2) than nearby low As wells (175eV, pH 7.3). This is consistent with reductive dissolution as a mechanism liberating As to well-waters near core TG3. In contrast to the wells near TG3, the elevated As wells near core UMRB2 have 1.6 times as much sulfate (801 mgL^{-1} SO_4^{-2}) as the low As wells (480 mgL^{-1} SO_4^{-2}).

While bulk well water chemistry conditions are favorable for sulfide dissolution at all the wells, high As wells near core UMRB2 have much higher Eh, Fe, and sulfate than the neighboring low As wells. Oxidative dissolution of As-bearing sulfides seems to be an important factor liberating As to well water near core UMRB2. The presence of particles in redox disequilibrium (As sulfide co-located with Fe oxides) in all three cores suggests that incongruent oxidative weathering is one of the processes at work liberating As to waters.

2.5 CONCLUSIONS

Our original hypothesis was that differences in As speciation between the aquifer, the aquitard and the aquifer-aquitard contact would indicate which processes are liberating As to waters in glacial aquifers. This hypothesis is predicated on the assumption that the

aquitard is the (relatively) unaltered parent material and the aquitard in contact in the aquifer has undergone weathering. We have evidence to validate this assumption in two of the cores examined, OTT3 and TG3, but not in the third core, UMRB2.

Correlation-distance hierarchical clustering of the As XANES spectra in cores OTT3 and TG3 shows samples grouping across the different sampled strata. These results point to a common parent material with different degrees of weathering. In core OTT3, we observe a small reduction in overall As concentration between the two tills but a large speciation transformation in which much of the original As sulfide has oxidized to As(V). Modern water chemistry of wells near core OTT3 are consistent with desorption as the primary process currently liberating As to waters. In core TG3 we observe a small (<10%) increase in overall As concentration between the two tills, and a large speciation transformation in which much of the original As sulfide has oxidized to As(V). Water chemistry of wells near core TG3 suggest reductive dissolution and desorption as the primary processes currently liberating As to waters. The oxidation seen in the aquitard sediments in contact with the aquifer relative to the out-of contact aquitard sediments may have occurred during deposition when the sediments were first deposited by the glacier and could also have occurred in situ over the last 14,000 years, from exposure to oxic groundwater. It is likely that some oxidation of all sediment types occurred in storage after the cores were collected.

Solids from the UMRB2 core, and water chemistry of nearby wells, are very different from those of cores OTT3 and TG3. Unlike solids from cores OTT3 and TG3, correlation distance hierarchical clustering of both As and Fe point XANES spectra from core UMRB2 groups the spectra according to stratum, which suggests dissimilar parent materials. Solid-phase As concentrations in samples from core UMRB2 are significantly higher in the below-aquifer contact till than in the mid-aquifer till or the above-aquifer contact till. The simplest explanation for these results is that the mid-aquifer till is not the parent material of the contact till. If that is the case, the sampled strata from UMRB2 cannot be used to test the hypothesis that differences in As speciation between the mid-aquitard till and the contact till indicate redox processes liberating As to waters. Overall, the UMRB2 contact till have much higher concentrations of As sulfide than the mid-aquitard till, and As sulfide is a large fraction of the aquifer As. Water chemistry of wells near UMRB2 is consistent with oxidative dissolution processes liberating As to waters.

In this contribution, we have developed an analytical method to address the geochemical complexity underlying the release of As from sediments to groundwater. Drinking-water wells with elevated As concentrations are a hazard to public health. For wells in Des Moines lobe provenance glacial aquifers the problem is complicated by the strong geographic heterogeneity of elevated-As wells, the relatively low As concentration in aquifer sediments, and the lack of a correlation between solid-phase and aqueous-phase As concentrations. Through the application of this method to archived rotasonic cores, we have identified three major As release mechanisms: desorption (OTT3), reductive dissolution (TG3), and oxidative dissolution (UMRB2). The diversity of As release

mechanisms is consistent with the geographic heterogeneity observed in the distribution of elevated-As wells. Our results confirm that in two of the three locations studied, the glacial till forming the aquitard is the source of As to the aquifer sediments. Further, we have confirmed that the interface between the aquitard and aquifer is a geochemically active zone for As release to water.

Table 2.1. Water chemistry of wells within 10km of sampled cores (MDH 2001 and MPCA 1999). Wells with any type of water treatment in place are not included. Wells are grouped by core and separated into two sub-groups: The "As exceeds MCL" subgroups have As concentrations in excess of the USEPA Maximum contaminant level of 10µgL^{-1} , the "As below MCL" subgroups have As concentrations below 10µgL^{-1}.

Average parameter results	OTT3		TG3		UMRB2	
	As exceeds MCL	As below MCL	As exceeds MCL	As below MCL	As exceeds MCL	As below MCL
	n = 8	n = 6	n = 5	n = 5	n = 4	n = 3
As µgL^{-1}	25.3	3.6	34.0	3.1	45.3	0.5
Eh mV	141	114	134	175	224	133.9
pH	7.2	7.7	7.2	7.3	7.3	7.5
Fe µgL^{-1}	1792	1950	3867	1416	3845	1351
Sulfate mgL^{-1}	312	289	1062	1153	801	480

Table 2.2 Ottertail County Core-3 (OTT3) whole-rock As, Fe and S concentrations.

Sample Name	Sample Description	Depth (m)	[a]As mg/kg	[b]Fe %	[b]S %	Fe/S
OTT3-55	Upper Goose Formation till (aquitard)	16.8	8.7	1.8	0.94	2
OTT3-56	Upper Goose Formation till (aquitard)	17.1	7.3	2.28	0.66	3
OTT3-65	Upper Goose Formation contact till (aquitard)	19.8	7.2	2.45	0.4	6
OTT3-66	outwash sand and gravel (aquifer)	20.1	4.7	1.81	0.36	5
OTT3-73	outwash sand and gravel (aquifer)	22.3	3.9	1.83	0.43	4
OTT3-74	Upper Goose Formation contact till (aquitard)	22.6	7.8	2.79	0.44	6
OTT3-75	outwash sand and gravel (aquifer)	22.9	3.1	1.31	0.21	6
OTT3-120	James River till (aquitard)	36.6	5.7	1.91	0.46	4
OTT3-133	James River till (aquitard)	40.5	5.6	1.87	0.39	5
OTT3-134	outwash sand and gravel (aquifer)	40.8	3.1	1.05	0.18	6
OTT3-146	outwash sand and gravel (aquifer)	44.5	2.6	0.89	0.15	6
OTT3-147	James River till (aquitard)	44.8	5.8	1.85	0.44	4
OTT3-161	James River till (aquitard)	49.1	11.6	2.03	0.59	3
OTT3-165	Ottertail Formation (aquitard)	50.3	6.5	2.34	0.54	4
OTT3-184	James River till (aquitard)	56.1	7.9	1.98	0.59	3

a - Arsenic measured via continuous-flow hydride-generation atomic absorption spectrometry after total acid extraction.

b - Iron and S measured via a combined inductively coupled plasma atomic emission spectrometry or mass spectrometry method after a 4-acid near total extraction (Taggart 2002).

Table 2.3. Traverse Grant County Core-3 (TG3) whole-rock As, Fe and S concentrations.

Sample Name	Sample Description	Depth (m)	[a]As mg/kg	[b]Fe %	[b]S %	Fe/S
TG3-28	Heiberg Formation till (aquitard)	8.5	8	2.42	0.12	20
TG3-41	Heiberg Formation till (aquitard)	1.0	8.1	2.26	0.61	4
TG3_45	Heiberg Formation till (aquitard)	1.0	8.3	2.3	0.65	4
TG3-54	Heiberg formation contact till (aquitard)	16.5	8.7	2.57	0.75	3
TG3-56	silt in Heiberg Formation	17.1	5.6	1.44	0.09	16
TG3-59	sand lens (aquifer)	18.0	3.6	1.65	0.06	28
TG3-60	Villard Formation contact till (aquitard)	18.3	3.9	1.49	0.05	30
TG3-83	Villard Formation till (aquitard)	25.3	6.8	1.57	0.43	4
TG3 95	Villard Formation till (aquitard)	29.0	4.8	1.78	0.48	4
TG3-103	sand lens (aquifer)	31.4	4.6	1.43	0.39	4
TG3-138	Gervaise formation till (aquitard)	42.1	7.3	2.06	0.5	4
TG3-149	Gervaise formation till (aquitard)	45.4	8.4	2.87	0.53	5

a - Arsenic measured via continuous-flow hydride-generation atomic absorption spectrometry after total acid extraction.

b - Iron and S measured via a combined inductively coupled plasma atomic emission spectrometry or mass spectrometry method after a 4-acid near total extraction (Taggart 2002).

Table 2.4. Upper Minnesota River Basin Core-2 (UMRB2) whole-rock As, Fe and S concentrations.

Sample Name	Sample Description	Depth (m)	[a]As mg/kg	[b]Fe %	[b]S %	Fe/S
UMRB2-132	unnamed till (aquitard)	40.2	6.6	1.81	0.53	3
UMRB2-134	unnamed till (aquitard)	40.8	7.1	1.77	0.56	3
UMRB2-135	unnamed till (aquitard)	41.1	7.4	1.91	0.65	3
UMRB2-136	sand (aquifer)	41.5	5.6	1.64	0.5	3
UMRB2-137	unnamed till (aquitard)	41.8	7.2	1.7	0.46	4
UMRB2-147	unnamed till (aquitard)	44.8	7.7	1.74	0.55	3
UMRB2-152	sand (aquifer)	46.3	9.7	1.71	0.55	3
UMRB2-153	unnamed till (aquitard)	46.6	6.4	1.76	0.59	3
UMRB2-157	unnamed till (aquitard)	47.9	7.2	1.74	0.48	4
UMRB2-159	unnamed till (aquitard)	48.5	6.9	1.74	0.51	3
UMRB2-161	unnamed till (aquitard)	49.1	6.5	1.71	0.5	3
UMRB2-164	unnamed till (aquitard)	50.0	7.2	1.7	0.53	3
UMRB2-165	sand (aquifer)	50.3	5.1	1.58	0.33	5
UMRB2-167	unnamed till (aquitard)	50.9	12.3	3.61	1.81	2
UMRB2-175	sand and gravel (aquifer)	53.3	6.6	1.7	0.55	3
UMRB2-176	unnamed till (aquitard)	53.6	7.8	1.88	0.52	4
UMRB2-183	unnamed till (aquitard)	55.8	7.1	1.91	0.57	3
UMRB2-184	sand and gravel (aquifer)	56.1	6.5	1.78	0.59	3
UMRB2-185	sand and gravel (aquifer)	56.4	4.9	1.33	0.36	4

a - Arsenic measured via continuous-flow hydride-generation atomic absorption spectrometry after total acid extraction.

b - Iron and S measured via a combined inductively coupled plasma atomic emission spectrometry or mass spectrometry method after a 4-acid near total extraction (Taggart 2002).

Table 2.5. Distribution of As species in core OTT3.

	OTT3-55 (aquitard)	OTT3-73 (aquifer)	OTT3-74 (aquitard-aquifer contact)
[a]**total As mg/kg**	8.7	3.9	7.8
As(V) mg/kg	2	2	3
As(III) mg/kg	2	1	2
As sulfide mg/kg	5	2	3

a – Arsenic concentration as measured via continuous-flow hydride-generation atomic absorption spectrometry after total acid extraction (Table 2).
b – Arsenic species abundance calculated by multiplying relative abundance (Fig.6b) by total As.

Table 2.6. Arsenic XANES linear combination fit results, reported as mol %, for OTT3. Sample spectra best fits and scores shown here are summed into broad species groups. EA Table 1 lists all As reference spectra, including broader species groupings. Comprehensive individual fits at each point measured in OTT3 are listed in EA Table 3.

Spot Name	As(-1)sulfide	As(III) sulfide	As III	As V
OTT3_55_spot0.e	51	40	0	9
OTT3_55_spot1.e	70			30
OTT3_55_spot2.e		7		93
OTT3_55_spot3.e	90			10
OTT3_55_spot4.e	33	15		50
OTT3_55_AsQXANES_spot_0_a2.e	79	0	0	21
OTT3_55_AsQXANES_spot_1_a2.e	79	0	0	21
OTT3_55_AsQXANES_spot_3_a2.e	93	0		7
OTT3_55_AsQXANES_spot_4_a2.e			87	12
Ott3_73_AsQXANES_spot_0.e			13	86
Ott3_73_AsXANES_spot_1.e	42	58		
Ott3_73_AsXANES_spot_2.e	84		16	
Ott3_73_AsXANES_spot_3.e	21	64	14	
Ott3_73_AsXANES_spot_4.e			17	82
Ott3_73_AsXANES_spot_5.e	18			79
Ott3_73_AsXANES_spot_6.e	48		41	10
Ott3_73_AsXANES_spot_7.e	36		50	13
Ott3_74_AsXANES_spot_0.e			15	85
Ott3_74_AsXANES_spot_2.e	31	54		15
Ott3_74_AsXANES_spot_1.e	59	26		15
OTT3_74_AsQXANES_spot_0a2.e	87			13
OTT3_74_AsQXANES_spot_1_a2.e	41	43		16
OTT3_74_AsQXANES_spot_2_a2.e	90			10
OTT3_74_AsQXANES_spot_3_a2.e	96			4
OTT3_74_AsQXANES_spot_4_a2.e	71	29		

Table 2.7. Iron XANES linear combination fit results, reported as mol %, for OTT3. Sample spectra best fits and scores shown here are summed into broad species groups. EA Table 2 lists all Fe reference spectra including broader species groupings. Comprehensive individual fits at each point measured from Core OTT3 are listed in EA Table 3.

Spot Name	Fe Sulfide	Native Fe	Fe phyllo-silicates	Fe(III) (oxyhydr) -oxides	Fe(II,III) (oxyhydr) -oxides + Fe(II)oxides	Fe primary silicates
OTT3_55_FeQXANES_spot_0_a2.e	93	7				
OTT3_55_FeQXANES_spot_1_a2.e	14		55	31		
OTT3_55_FeQXANES_spot_3_a2.e	50		19			31
OTT3_55_FeQXANES_spot_4_a2.e	66				34	
Ott3_73_FeXANES_spot0.e			44	28		28
Ott3_73_FeXANES_spot1.e			69			30
Ott3_73_FeXANES_spot2.e			37	36		27
Ott3_73_FeQXANES_spot3.e			47	34		19
Ott3_73_multi_FeQXANES_spot4.e			75		25	
Ott3_73_FeQXANES_spot5.e			60			40
Ott3_73_FeXANES_spot6.e			64			36
OTT3_74_FeQXANES_spot_0_a2.e	100					
OTT3_74_FeQXANES_spot1_a2.e	84	16				
OTT3_74_FeQXANES_spot2_a2.e	55				45	
OTT3_74_FeQXANES_spot3_a2.e	88				12	
OTT3_74_FeQXANES_spot_4_a2.e			62	38		

Table 2.8. Distribution of As species in core TG3.

	TG3_45 (aquitard)	TG3_54 (aquitard-aquifer contact)	TG3_56 (silt horizon)	TG3_59 (aquifer)
total As mg/kg	8.3	8.7	5.6	3.6
As(V) mg/kg	1	3	3	2
As(III) mg/kg	2	3	1	1
As(-1)sulfide mg/kg	4	2	1	1
As(III)sulfide mg/kg	0	1	1	0

a – Arsenic concentration as measured via continuous-flow hydride-generation atomic absorption spectrometry after total acid extraction (Table 3).
b – Arsenic species abundance calculated by multiplying relative abundance (Fig.9b) by total As.

Table 2.9. Arsenic XANES linear combination fit results, reported as mol %, for TG3. Sample spectra best fits and scores shown here are summed into broad species groups. EA Table 1 lists all As reference spectra, including broader species groupings. Comprehensive individual fits at each point measured from TG3 are listed in EA Table 4.

Spot Name	As(-1)sulfide	As(III)sulfide	As III	As V
TG3_45_As_XANES_spot_1.e	80		19	
TG3_45_As_XANES_spot_2.e	60	27		13
TG3_45_As_XANES_spot_3.e	99			
TG3_45_As_XANES_spot_4.e		64		35
TG3_45_As_XANES_spot_6.e	34	26	39	
TG3_45_As_XANES_spot_7.e		73	27	
TG3_45_As_XANES_Spot_8.e	80		20	
TG3_45_As_XANES_spot_10.e	34	43		22
TG3_54_As_XANES_spot_0.e	64	21		15
TG3_54_As_XANES_spot_1.e	11	17		72
TG3_54_As_XANES_spot_2.e	33	46		20
TG3_56_AsQXANES_spot_0.e	50	14	35	
TG3_56_AsQXANES_spot_1.e	56		29	14
TG3_56_AsQXANES_spot_2.e			26	73
TG3_56_AsQXANES_spot_3.e	33	41		26
TG3_59_AsQXANES_spot_0.e	5		29	66
TG3_59_AsQXANES_spot_1.e	88		11	
TG3_59_AsQXANES_spot_2.e	53	24		23
TG3_59_AsQXANES_spot_3.e	72		19	7

Table 2.10 Iron XANES linear combination fit results, reported as mol%, for TG3. Sample spectra best fits and scores shown here are summed into broad species groups. EA Table 2 lists all Fe reference spectra including broader species groupings. Comprehensive individual fits at each point measured from Core OTT3 are listed in EA Table 4.

Spot Name	Fe Sulfide	Fe phyllo-silicates	Fe(III) (oxyhydr)-oxides	Fe(II,III) (oxyhydr)-oxides + Fe(II)oxides	Fe primary silicates
TG3_45_FeQXAS_spot_1.e	35	65			
TG3_45_FeQXAS_spot_4.e	88	12			
TG3_45_FeQXAS_spot_6.e	100				
TG3_54_FeQXANES_spot_0.e	75	15		10	
TG3_54_FEQXANES_spot_1.e	71			29	
TG3_54_FeQXANES_spot_2.e	71			29	
TG3_56_FeQXANES_spot_0.e	21		45		34
TG3_56_FeQXANES_spot_1.e		26		43	30
TG3_56_FeQXANES_spot_2.e	10		71		19
TG3_56_FeQXANES_spot_3.e	44		56		
TG3_59_FeQXANES_spot_0.e	31	14	54		
TG3_59_FeQXANES_spot_1.e			55	45	
TG3_59_FeQXANES_spot_2.e	28	20	52		
TG3_59_FeQXANES_spot_3.e	36	19	45		

Table 2.11. Distribution of As species in core UMRB2.

	UMRB2-159 (aquitard)	UMRB2-164 (aquitard-aquifer contact)	UMRB2-165 (aquifer)	UMRB2-167 (aquitard-aquifer contact)
total As mg/kg	6.9	7.2	5.1	12.3
As(V) mg/kg	2	2	2	4
As(III) mg/kg	2	1	1	2
As(-1)sulfide mg/kg	1	4	2	4
As(III)sulfide mg/kg	2	1	1	1

a – Arsenic concentration as measured via continuous-flow hydride-generation atomic absorption spectrometry after total acid extraction (Table 4).
b – Arsenic species abundance calculated by multiplying relative abundance (Fig.10b) by total As.

Table 2.12 Arsenic XANES linear combination fits results, reported as mol%, for UMRB2. Sample spectra best fits and scores shown here are summed into broad species groups. EA Table 1 lists all As reference spectra, including broader species groupings. Comprehensive individual fits at each point measured from TG3 are listed in EA Table 5.

Spot Name	As(-1) sulfide	As(III) sulfide	As III	As V
UMRB2_159_AsXANES_spot_0.e	93			7
UMRB2_159_AsXANES_spot_1.e	39	51		10
UMRB2_159_AsXANES_spot_2.e			28	71
UMRB2_159_AsXANES_spot_3.e	61	27	12	
UMRB2_159_AsXANES_spot_4.e	91			9
UMRB2_159_AsQXANES_spot_0_a2.e	42	37	21	
UMRB2_159_AsQXANES_spot_1_a2.e	92			7
UMRB2_159_AsQXANES_spot_2_a2.e	84			16
UMRB2_159_AsQXANES_spot_3_a2.e	41		21	36
UMRB2_159_AsQXANES_spot_4_a2.e	56	30		14
UMRB2_164_As_QXANES_spot_0.e	26	59		15
UMRB2_164_As_QXANES_spot_1.e	92		8	
UMRB2_164_As_QXANES_spot_2.e	88	12		
UMRB2_164_As_QXANES_spot_3.e	37	48		15
UMRB2_164_As_QXANES_spot_4.e	43	42		15
UMRB2_165_As_QXANES_spot_1.e	52	8		40
UMRB2_165_As_QXANES_Spot_3.e			42	57
UMRB2_165_As_QXANES_spot_4.e	86			13
UMRB2_165_AsQXANES_spot_0_a2.e	47	21		32
UMRB2_165_AsQXANES_spot_1_a2.e	81			19
UMRB2_165_AsQXANES_spot_2_a2.e		73	16	11
UMRB2_167_As_QXANES_spot_0.e		52	35	13
UMRB2_167_As_QXANES_spot_1.e	42	43		15
UMRB2_167_As_QXANES_spot_2.e	45	44		12
UMRB2_167_As_QXANES_spot_3.e	26	57	16	
UMRB2_167_As_QXANES_spot_4.e			22	78

Table 2.13. Iron XANES linear combination fit results, reported as mol %, for UMRB2. Sample spectra best fits and scores shown here are summed into broad species groups. EA Table 2 lists all Fe reference spectra including broader species groupings. Comprehensive individual fits at each point measured from Core OTT3 are listed in EA Table 5.

Spot Name	Fe Sulfide	Fe phyllo-silicates	Fe(III) (oxyhydr)-oxides	Fe(II,III) (oxyhydr)-oxides + Fe(II)oxides	Fe primary silicates
UMRB2_159_FeQXANES_spot_0_a2.e	100				
UMRB2_159_FeQXANES_spot_1_a2.e			70		30
UMRB2_159_FEQXANES_spot_2_a2.e	100				
UMRB2_159_FeQXANES_spot_3_a2.e	6		44		50
UMRB2_159_FeQXANES_spot_4_a2.e	100				
UMRB2_164_Fe_XANES_spot_0.e	45				55
UMRB2_164_Fe_XANES_spot_1.e	11			48	41
UMRB2_164_Fe_XANES_spot_2.e	69	31			
UMRB2_164_Fe_XANES_spot_3.e	100				
UMRB2_164_Fe_XANES_spot_4.e	86		14		
UMRB2_165_FeXANES_spot_1.e	92				8
UMRB2_165_FeXANES_spot_3.e		11	70		19
UMRB2_165_FeXANES_spot_4.e	100				
UMRB2_167_Fe_XANES_Spot_1.e		46		37	18
UMRB2_167_Fe_XANES_Spot_2.e	83			16	
UMRB2_167_Fe_XANES_Spot_3.e			50	36	13
UMRB2_167_Fe_XANES_Spot_4.e		64		9	27

Table 2.14. Comparison of low and high As wells within 10km of each studied core (MDH 2001 and MPCA 1999). The U.S. Environmental Protection Agency maximum contaminant level (MCL) for As is 10 µg As L^{-1}.

	Gradient of average chemical conditions in wells (wells below MCL → above MCL)		
	OTT3	**TG3**	**UMRB2**
As ($\mu g L^{-1}$)	3.6 → 25.3	3.1 → 34.0	0.5 → 45.3
Redox gradient (mV)	Slightly positive 114 → 141	Negative 175 → 134	Very positive 134 → 224
pH gradient	Very negative 7.7 → 7.2	Slightly negative 7.3 → 7.2	Slightly negative 7.5 → 7.3
Fe gradient ($\mu g L^{-1}$)	Slightly negative (<10%) 1950→1792	Very positive 2.7 times higher 1416 → 3867	Very positive 2.8 times higher 1351 → 3845
Sulfate gradient ($mg L^{-1}$)	Slightly positive (<10%) 289 → 312	Slightly negative (<10%) 1153 → 1062	Very positive 1.7 times higher 480 → 801
As Release Mechanism	Desorption	Reductive dissolution and desorption	Oxidative dissolution

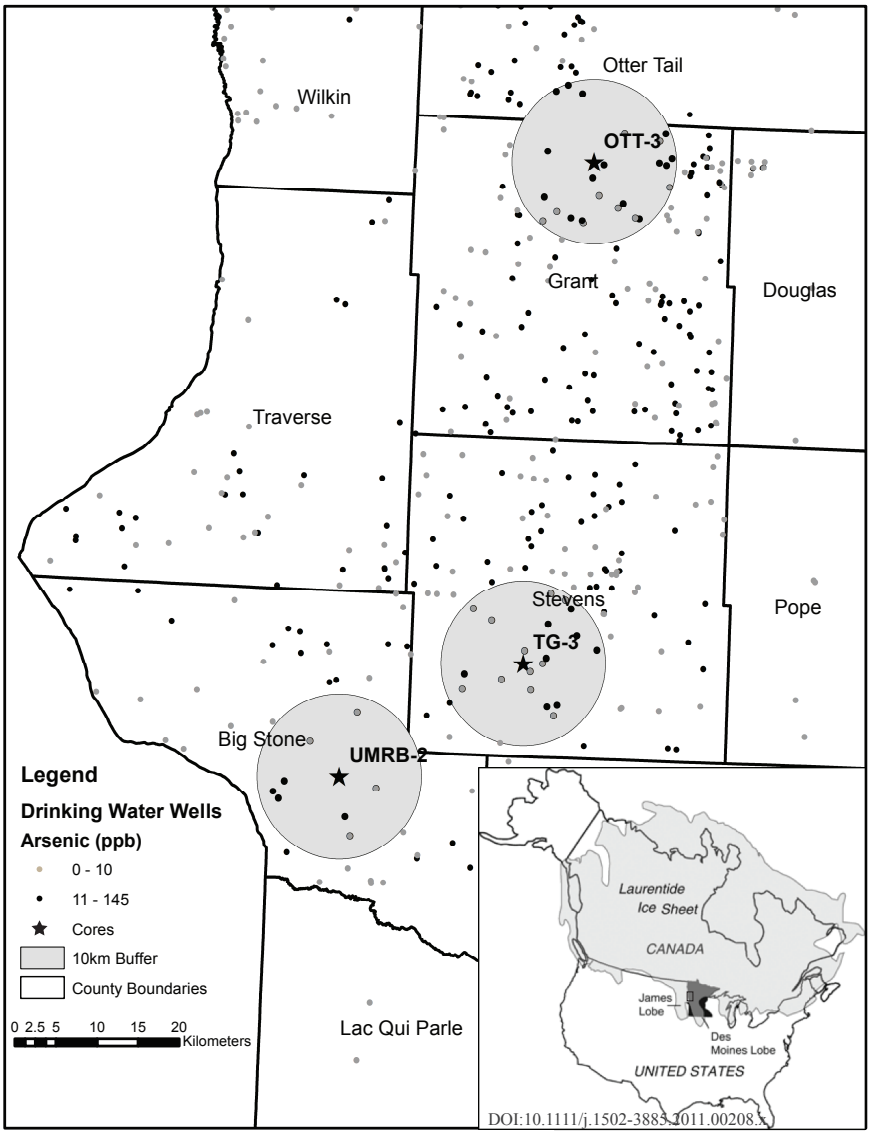

Figure 2.1 Map of Des Moines lobe glacial advance, west-central Minnesota, USA, showing As-affected wells, and 10km buffer around cores.

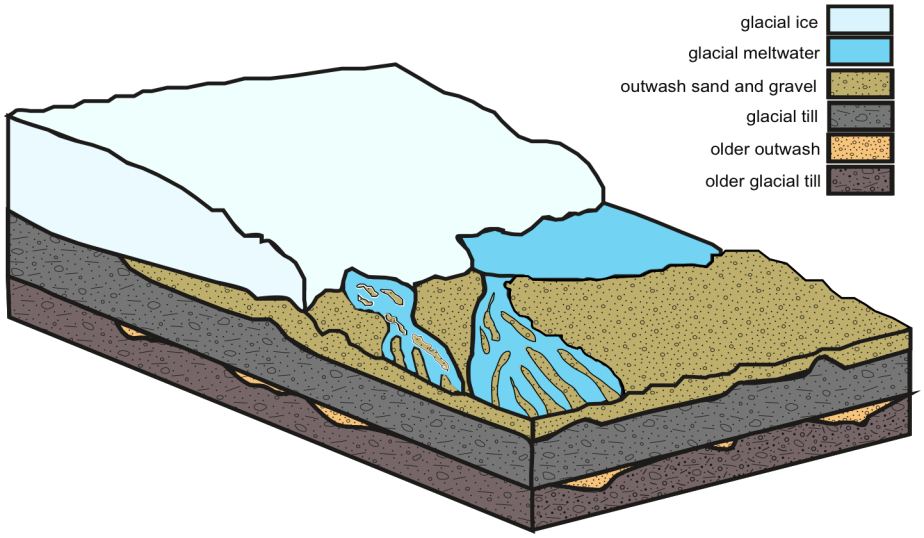

Figure 2.2 Block drawing of glacier, periglacial lake, periglacial braided stream, and till and outwash layers. Modified from Ojakangas and Matsch 1982. Tills make up the aquitards and outwash sediments are the aquifers. Aquifer deposits are dendritic and discontinuous making it common for wells drilled within short horizontal distances to have very different properties.

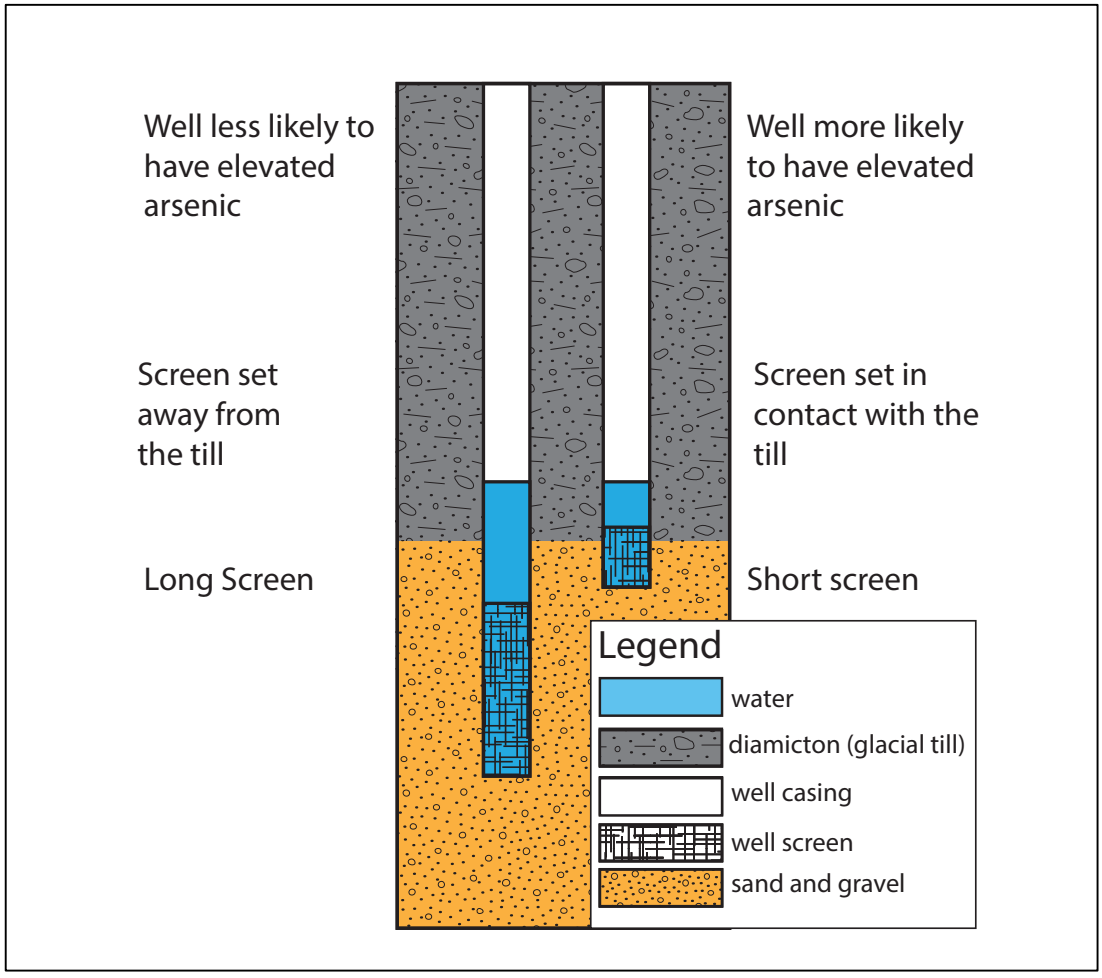

Figure 2.3 Cartoon of well construction in a glacial aquifer, modified from Erickson and Barnes 2005b. Wells constructed like the one on the right are more likely to have elevated As than the well on the left. The well on the right has a short screen, set close to (in this case set partially within) the glacial-till aquitard. The well on the left has a long screen set deep down into the aquifer, far from the contact with the glacial-till aquitard.

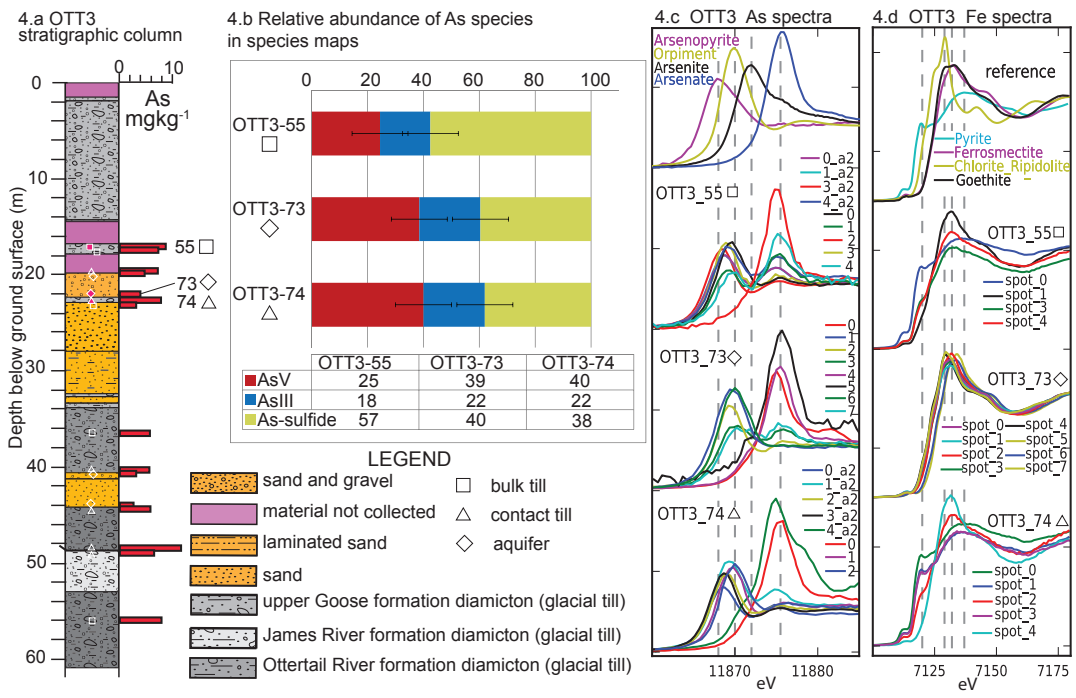

Figure 2.4 Stratigraphic column, quantitative As speciation, and As and Fe XANES spectra for Ottertail County Core-3 (OTT3). (a) Stratigraphic representation of sediments in core OTT3 simplified from Harris et al. 1999. Whole-rock As concentrations (measured via hydride) shown in red. Symbols mark depths where sample collection occurred. Square symbols mark unaltered tills (aquitard samples), triangles for contact tills (aquitard-aquifer contact samples), diamonds for aquifer sediments. (b) Bar graph showing relative proportions of AsV(red), AsIII(blue), and As-sulfide (green). Error bars mark estimated error of 10% (Bargar et al. 2000). (c) Arsenic reference and point XANES spectra. Reference spectra and marked energies are the references and energies used to fit the speciation maps. (d) Iron reference and point XANES spectra. Reference spectra and marked energies were chosen to represent a typical range of Fe species absorption features.

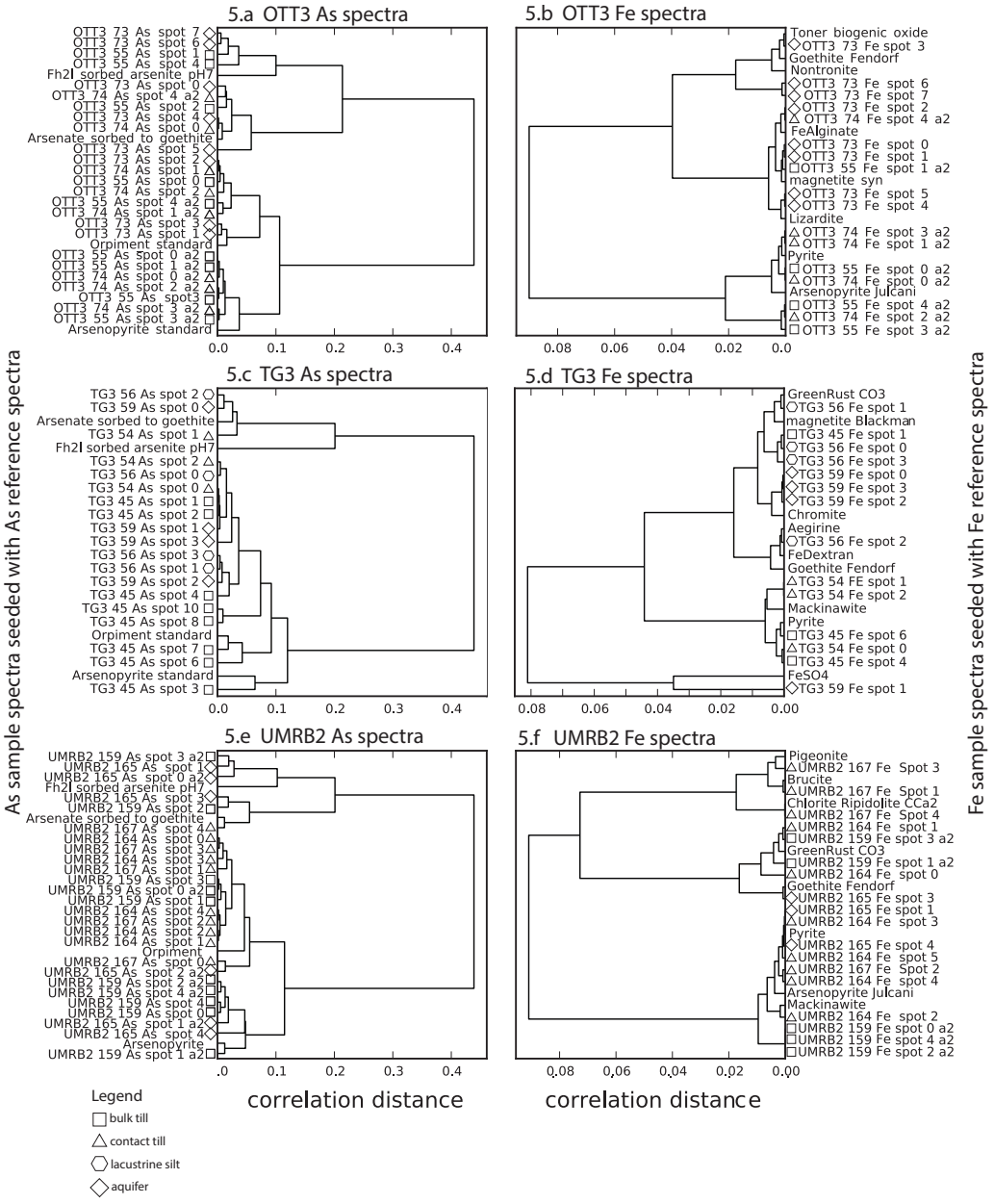

Figure 5

Figure 2.5 Correlation-distance hierarchical clustering dendrograms showing As and Fe samples spectra seeded with As reference spectra. Square symbols indicate unaltered tills

(aquitard samples), triangles indicate contact tills (aquitard-aquifer contact samples), hexagons indicate lacustrine sediments, and diamonds indicate aquifer sediments. (a) OTT3 As sample spectra seeded with As reference spectra. (b) OTT3 Fe sample spectra seeded with Fe reference spectra. (c) TG3 As sample spectra seeded with As reference spectra. (d) TG3 Fe sample spectra seeded with Fe reference spectra. (e) UMRB2 As sample spectra seeded with As reference spectra. (f) UMRB2 Fe sample spectra seeded with Fe reference spectra.

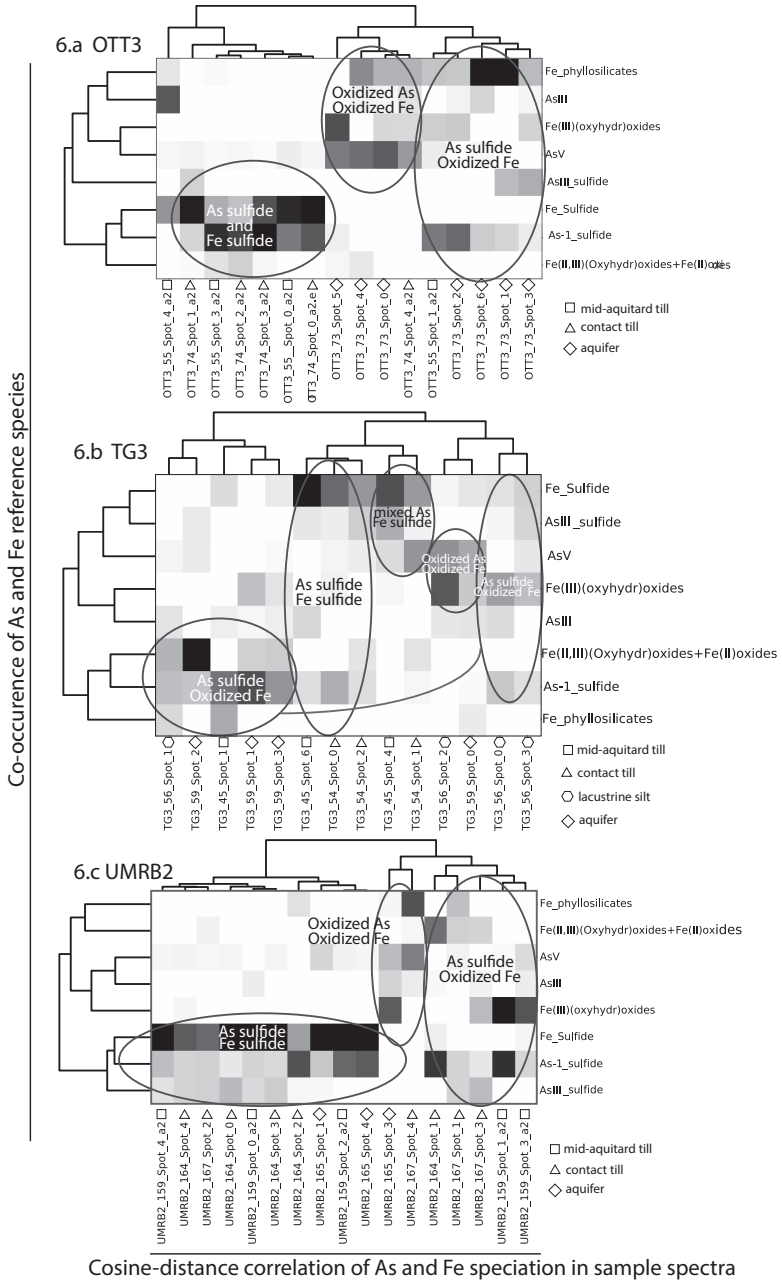

Figure 6

Figure 2.6 Results of hierarchical dendograms clustering via cosine-distance and heatmaps of fitted reference components measured at points of co-located As and Fe

XANES: (a) OTT3, (b) TG3, and (c) UMRB2. The horizontal dendrogram at the top shows the relationship of the sample spectra to each other based on the LCF results for each sample spectrum. The vertical dendrogram to the left shows the frequency of co-occurrence of the types (generalized bins) of Fe and As species fitted with LCF. The heatmap illustrates clusters of co-occurrence, showing three populations of co-located As and Fe species types. Relative abundance of the four As species groups and the four Fe species groups in each heatmap is indicated by shading, where darkness indicates greater abundance of a species group. Ellipses indicate sub-populations of points within the set. Square symbols indicate unaltered tills (aquitard), triangles indicate contact tills (aquitard-aquifer contact), hexagons indicate lacustrine sediments, and diamonds indicate aquifer sediments.

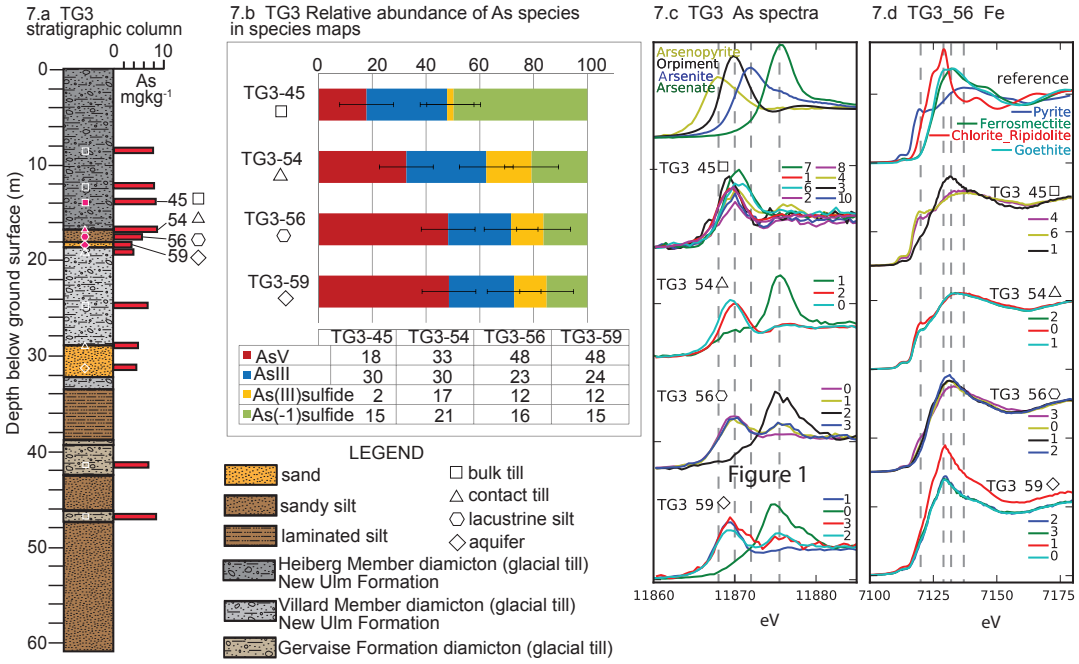

Figure 2.7 Stratigraphic column, quantitative As speciation, and As and Fe XANES spectra for Traverse Grant County Core-3 (TG3). (a) Stratigraphic representation of sediments in core TG3 (Harris and Berg 2006). Whole-rock As concentrations (measured via hydride) shown in red. Symbols mark sample collection depths. Square symbols mark unaltered tills, triangles for contact tills, diamonds for aquifer sediments. Lacustrine silt marked with a hexagon. (b) Bar graph showing relative proportions of AsV(red), AsIII(blue), As(III)sulfide (yellow) and As(-1) sulfide (green). Error bars mark estimated error 10% (Bargar et al 2000). (c) Arsenic reference and point XANES spectra. Reference spectra and marked energies are the references and energies used to fit the speciation maps. (d) Iron reference and point XANES spectra. Reference spectra and marked energies were chosen to represent a typical range of Fe species absorption features.

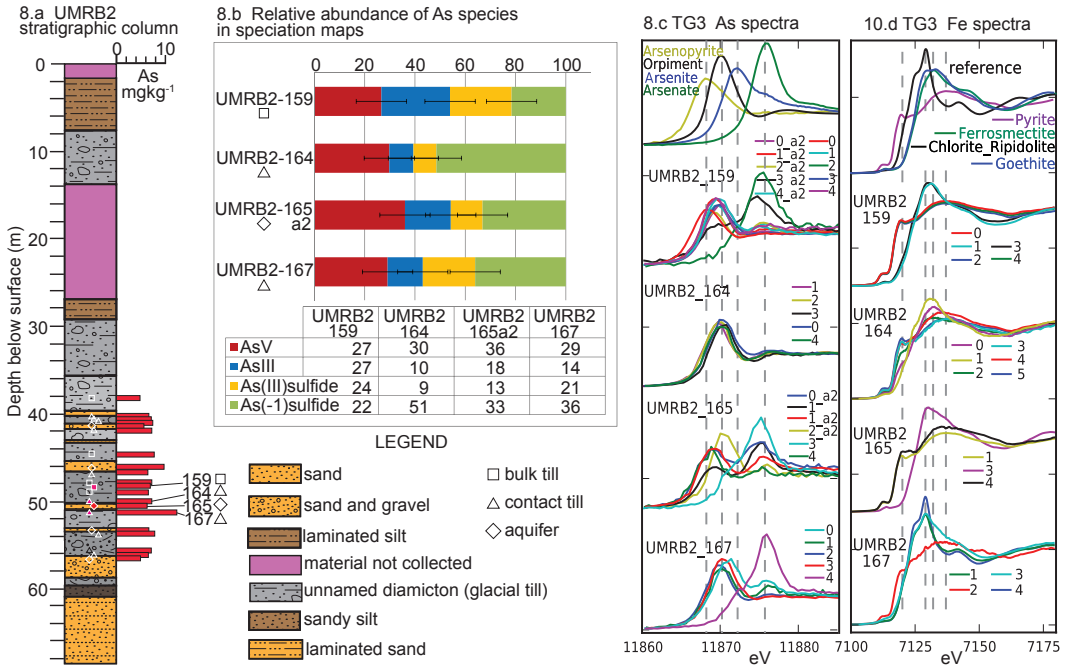

Figure 2.8 Stratigraphic column, quantitative As speciation, and As and Fe XANES spectra for Upper Minnesota River Basin Core-2 (UMRB2). (a) Stratigraphic representation of sediments in core UMRB2 (Patterson et al. 1999). Whole-rock As concentrations (measured via hydride) shown in red. Symbols mark sample collection depths. Square symbols mark unaltered tills, triangles for contact tills, diamonds for aquifer sediments. (b) Bar graph showing relative proportions of AsV(red), AsIII(blue), As(III)sulfide (yellow) and As(-1) sulfide (green). Error bars mark estimated error 10% (Bargar et al 2000). (c) Arsenic reference and point XANES spectra. Reference spectra and marked energies are the references and energies used to fit the speciation maps. (d) Iron reference and point XANES spectra.

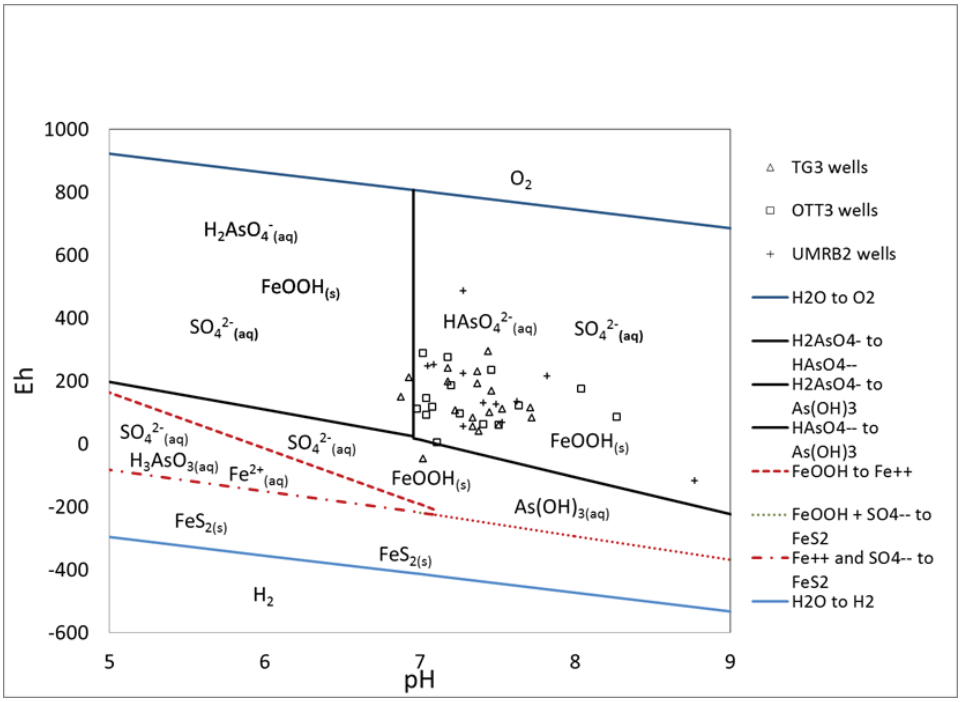

Figure 2.9 Eh/pH diagram showing predominance of As, Fe, and S species at 10ºC. Dashed lines indicate the points of equal activity between Fe species, solid lines indicated the points of equal activity between the arsenic species. Sulfur speciation follows the Fe species lines. Eh and pH measured in well water from wells within 10km of each core are plotted with a square for wells near OTT3, a triangle for wells near TG3 and a plus-sign for wells near UMRB2. Wells with water treatment (water softeners and/or iron removers) were not included.

CHAPTER 3: SOLID-PHASE ARSENIC SPECIATION IN ANAEROBICALLY-PRESERVED GLACIAL AQUIFER SEDIMENTS

Sarah L. Nicholas[1,2], Angela Gowan[3], Melinda L. Erickson[4], Laurel G. Woodruff[4], Matthew A. Marcus[5], Brandy M. Toner[1]*

1 Department of Soil, Water, and Climate, University of Minnesota-Twin Cities, Saint Paul, MN, USA

2 Department of Earth and Ocean Sciences, National University of Ireland, Galway, Ireland

4 United States Geological Survey, Minnesota Water Science Center, Mounds View, MN, USA

3 Minnesota Geological Survey, Saint Paul, MN, USA

5 Advanced Light Source, Lawrence Berkeley National Laboratory, Berkeley, CA, USA

*Corresponding Author

Abstract

Previous work on the source of well-water As in west-central Minnesota identified glacial tills as the solid-phase source of As to well water and the aquitard/aquifer interface as the likely source of As from solids to water. Because the solid-phase reservoirs of As are often redox-sensitive species, we froze glacial sediments from a new core under argon in order to preserve their redox state. Anaerobically preserved glacial aquifer sediments from an area with a large number of As-contaminated domestic wells were examined by bulk chemistry and X-ray Absorption Spectroscopy (XAS). Solid-phase As and Fe speciation was examined on two stratigraphically separate triplets of 1)aquifer, 2)aquitard, and 3)contact sediments (6 strata). Solid phase As and Fe speciation was compared with water chemistry of nearby wells. Bulk water chemistry favors $HAsO_4^{-2}$ (aq) and FeOOH (s). Wells with As concentrations greater than the US EPA maximum contaminant level of 10 μgL^{-1} had higher median dissolved Fe and sulfate concentrations than wells with As concentrations less than 10 μgL^{-1}. Co-located As and Fe microprobe-XANES on discrete points within the strata show that most of co-located As and Fe particles are either As(V) with Fe(III) or As with Fe in sulfides. Both populations were found in all examined strata. A subset with co-located As-bearing sulfide and Fe(III)(oxyhydr)oxide was also found. This indicates that there are both a reduced and an oxidized reservoir of As sequestered in the solid phase of these sediments. Arsenic speciation mapping on the two sets of strata show that As in the aquitard material is dominantly As-bearing sulfide, while As in the contact material is dominantly As(V).

Arsenic in the deeper aquifer stratum was dominantly oxidized As while As in the shallower aquifer stratum was predominantly As-bearing sulfide. An exposure experiment in which two different depths of aquitard strata were prepared both anaerobically and in the open air found large differences in As speciation between the two treatments in one of the strata, but very little difference between the two treatments of the other stratum.

Introduction:

In the upper Midwest of the United States geogenic arsenic (As) contamination of groundwater has been associated with sulfide minerals in Wisconsin (Schreiber et al 2000, Gotkowitz 2004; West et al. 2012) and Michigan (Kolker et al 2003). In Minnesota and South Dakota it is linked to glacial sediments (Welch et al 2000; Grosz et al. 2004; Erickson and Barnes 2005a, b). West-central Minnesota is a geographic nexus of private drinking-water wells with As concentrations exceeding the US EPA maximum contaminant level of 10 $\mu g\ L^{-1}$. Most private wells in western Minnesota are installed in small glacial aquifers within the footprint of the Des Moines Lobe of the late Wisconsinan glaciation (Marine isotope stage 2) but no single formation source has been identified as the solid-phase source of As to well water.

Glacial aquifers typically form in glacial-outwash sediments composed of sands and gravels (aquifer sediments) deposited by fast-moving glacial meltwater but may also form in sandy lake sediment. The aquitard sediments confining these aquifers are glacial tills composed of poorly sorted sediments in a matrix of finely-ground clay-sized material. Glacial aquifers tend to be laterally discontinuous which likely contributes to the geographic heterogeneity observed in groundwater properties, including As concentrations (Toner et al. 2011).

In general, As in aquifer sediments is usually associated with iron (Fe) and sulfur (S) minerals, primarily Fe (oxyhydr)oxides and Fe sulfides. Arsenic-bearing Fe sulfide

minerals such as arsenopyrite, FeAsS, or As-rich pyrite $FeS_{2-x}As_x$ are favored under chemically reducing conditions (Schreiber and Rimstidt 2013). Under chemically oxidizing conditions As is associated with Fe(oxyhydr)oxides such as goethite and ferrihydrite, through sorption and co-precipitation reactions. These mineral reservoirs are oxidation-reduction (redox) end-members for the sequestration of As in the solid phase. Each end member presents the potential for As release when (bio)geochemical conditions, especially redox, in aquifers change.

The complex distribution of elevated-As wells in Minnesota glacial aquifers is a longstanding public health problem. The strong geographic heterogeneity of elevated-As wells, the relatively low As concentration in aquifer sediments, and the lack of a correlation between solid-phase and aqueous-phase As concentrations have contributed to the intractability of the problem. In addition to these factors, it is now known that changes in redox conditions near the aquitard-aquifer contact zone contribute to several different As release modes within the Des Moines Lobe glacial advance (Nicholas et al. in review).

Previous work on the source of well water As in west-central Minnesota identified glacial tills as the solid-phase source of As to well water (Welch, 2000) and the aquitard/aquifer interface as the likely source of As from solids to water (Erickson and Barnes 2005 a,b). Previous solid-phase speciation work on As speciation in solids at the aquitard/aquifer interface using archived (stored in open-air) rotary-sonic cores found evidence of

reductive desorportion and dissolution and oxidative dissolution as geochemical mechanisms releasing As to waters (Nicholas et al. in review).

In this contribution we examine As and Fe speciation in anaerobically preserved glacial aquifer sediments from a 10 cm diameter rotary-sonic core collected in Clay County, west-central Minnesota. We use bulk sediment chemistry, X-ray absorption spectroscopy (XAS), and nearby well-water chemistry to identify mechanisms releasing As to well waters in samples protected from ambient air from the time of collection in the field through sample preparation and analysis for As and Fe XAS. Co-located As and Fe XANES were collected to describe the species present and As speciation mapping was used to quantify the As species distribution.

Materials and Methods

Geologic Setting and Groundwater Chemistry. Clay County (Figure 1 Map) has a complex Quaternary history with strata preserved from the advances of the Wadena, Des Moines, and Red River lobes of the late Wisconsinan glaciation (Marine isotope stage 2) (Wright 1972; Patterson 1998; Hooyer and Iverson 2002; Jennings 2006; Lusardi et al. 2011). It sits in a bedrock low and parts of it have been occupied before and after the different glacial advances by different stages of Glacial Lake Agassiz (Hobbes and Gowan 2014; Gowan 2014).

Samples were collected from core CYR-1, Clay County, Minnesota, USA, 46.740N, (96.238W). Clay County has many private drinking-water wells that exceed the US Environmental Protection Agency maximum contaminant level (MCL) of 10 µg As L^{-1}, however As concentrations in the aquifer materials are not particularly high (< 9 mg kg^{-1}). The distribution of As-affected wells in the area is heterogeneous with respect to location and well depth (Erickson and Barnes 2005a) and no single formation has been identified as the source of As to well waters.

Well-water pH, Eh, and Fe and sulfate concentrations used in this study came from previous statewide and regional groundwater chemistry studies conducted in 1998 and 1999 (MPCA 1999; MDH 2001). The reported water chemistry comes from single sampling events (each well was sampled once) so temporal variability and seasonal effects cannot be evaluated from these data.

Initial aqueous species activities for the predominance diagram were generated with Geochemist's Workbench REACT sub-program (Bethke 2008). Redox and dissociation constants used to delineate the predominance fields were generated using published constants (James and Bartlett 1999; Wagman et al. 1982; Eary 1992) and enthalpies (Bryndzia and Kleppa 1988). These were adjusted to 10ºC using the van't Hoff equation (van't Hoff 1874) to reflect the average well-water temperature.

Sample Collection, Preservation, and Handling. Glacial sediments were collected in cooperation with the Minnesota Geological Survey County Atlas Project for Clay County

in November and December 2010 (Gowan 2014). Sub-samples for solid-phase As analysis were collected in the field from 10 cm diameter rotary-sonic drill cores immediately after they were brought to the surface (Figure 3.2).

Samples were chosen in sets of three to represent specific stratigraphic features: (1) aquifer sediments, (2) glacial till in contact with the aquifer sediments ('contact till'), and (3) glacial till out of contact with aquifer sediments ('mid-aquitard till').

The strata sampled for the shallower triplet are CYR_1_38 (aquifer) CYR_1_40.5 (contact till) and CYR_1_46 (mid-aquitard till'). These aquitard strata are Upper member till of the Red Lake Falls Formation and the aquifer stratum is a sand and gravel deposit in the Upper member of Red Lake Falls Formation. The Red Lake Falls Formation was deposited by the Red River Lobe of the of the late Wisconsinan glaciation (Marine isotope stage 2) (Gowan 2014). It has a mixed Riding Mountain and Winnipeg provenance (now central Manitoba, Canada). The Riding Mountain provenance has shale and carbonate bedrock and the Winnepeg provenance has carbonate bedrock (Johnson et al. 2016).

The sampled strata for the deeper triplet are CYR_1_61 (mid-aquitard till), CYR_1_78bc (contact till) and CYR_1_80ac (aquifer). These aquitard strata are St. Hillaire member till of the Goose River formation and the aquifer stratum is a sand and gravel deposit within the St. Hillaire member (Gowan 2014). The St. Hillaire member was deposited

by the Red River lobe of the late Wisconsinan glaciation (Marine isotope stage 2) (Gowan 2014) and has a mixed Riding Mountain and Winnipeg provenance (Johnson et al. 2016), like the Upper member of the Red Lake Falls Formation sampled for the shallower triplet. The two sampled members are texturally and lithologically similar but the St. Hillaire member has more shale (Hobbes and Gowan 2014).

For sub-sampling, the core was scraped with a plastic putty knife to reveal sediments less affected by drilling fluids. The sampled area was photographed in the core. An aliquot was removed with a plastic putty knife and wrapped tightly in Saran® wrap. On a clean work-surface, the sample was sub-divided for microbiology and geochemistry. Using a sterile spoon, sediment was placed in a sterile 15 mL Falcon tube under ambient conditions and stored frozen until returned to the lab for final -80 ºC storage.
A second geochemistry aliquot was collected with the same spoon, placed in a 50 mL Falcon® tube and flushed with 1 L of argon (Ar) for 1 minute at 1 psi (equivalent to ~ 20 tube volumes). The flushed tubes were then sealed and placed in a portable Ar glove bag operated under positive pressure conditions. The tubes were allowed to equilibrate with the Ar atmosphere for 20 minutes prior to packaging. Within the glove bag, each tube was sealed in a minigrip® bag, and then sealed inside an 8 mil Mylar® bag with an Anaeropak® oxygen scavenger. These "anaerobic" samples were kept above freezing for an hour after sealing in mylar to encourage scavenging of residual O_2 (g) by the Anaeropak, and then frozen. Photographs of the portable glove bag and sample sealing apparatus can be seen in the Supplementary Information (SI Fig.SX).

The remaining sediment sample was re-wrapped in Saran wrap, in ambient air, sealed in a ziplock bag and then frozen, these bulk frozen samples were used for the bulk sediment chemistry and for the air-dried "ambient" described below.

The "anaerobic" geochemistry samples were handled in an H_2N_2 anaerobic chamber (Coy) at all times. Sediments were thawed, dried at room temperature, ground with a corundum mortar and pestle, and passed through a 150 μm sieve. For micro-probe XAS analysis, processed sediments were mounted on adhesive that was physically stabilized by a Rinzle® coverslip. The adhesive/coverslip was fixed to an aluminum sample holder for the Advanced Light Source beamline 10.3.2. Sample exposure to ambient atmosphere was limited by sealing the front and back of the prepared sample with low-S mylar (Zeng et al. 2013). The entire mounted sample, ready for the sample stage, was stored in a sealed mylar bag with an Anaeropack until analysis at the beamline.

To examine the effect of different storage methods on As speciation, aliquots of the "anaerobic" geochemistry samples were also 1) dried in ambient air and 2) anaerobically preserved with subsequent thawing (two months) and re-freezing. To prepare the "ambient" air samples, sediments from the bulk frozen samples were prepared benchtop under ambient conditions using the exact process described above for the "anaerobic" samples. To prepare the "thawed anaerobic" samples, splits of the anerobic samples were prepared using the "anaerobic" process with the exception of two months storage at ambient temperature (instead of -20 C). The purpose of the "thaw anaerobic" handling was to emulate a freezer failure that occurred in June-August 2010 which affected some

samples that had been collected during the January-March 2010 field season. All the samples described in this paper underwent the complete "anaerobic" handling procedure and were collected in November 2010.

Bulk Sediment Chemistry. Approximately 100 g of bulk frozen sediment was thawed, dried, disaggregated with a ceramic mortar and pestle, sieved to remove pebbles > 2 mm, and stored in plastic tubes in dark ambient conditions. For dissolution chemistry, subsamples of the < 2 mm fraction were sent to a United States Geological Survey (USGS) contract laboratory for analysis using published methods (Taggart 2002). The < 2 mm fractions were digested in a four-acid decomposition (nitric, hydrochloric, perchloric, and hydrofluoric acids). Forty-two major and trace elements were measured by a combined inductively coupled plasma atomic emission spectrometry/mass spectrometry (ICP-AES/MS) method. Arsenic and selenium (Se) were measured separately by continuous-flow, hydride-generation, atomic absorption-spectrometry, and mercury (Hg) was analyzed by cold-vapor, atomic-absorption spectrometry. Three of the samples (CYR_1 37bc, 38ac and 38c) were analyzed at the University of Minnesota Earth Sciences ICP-MS lab. These samples had the four-acid digestion and were then analyzed on a via ICP-MS. Sulfur was not measured in these samples.

X-ray Absorption Spectroscopy. Microprobe X-ray fluorescence (μXRF) maps, As and Fe 1s microprobe X-ray absorption near edge structure (point-XANES) spectroscopy, and As "speciation maps" were measured at the X-ray micro-probe beamline 10.3.2,

ALS, Lawrence Berkeley National Laboratory, USA (Marcus et al. 2004). For As measurements the monochromator was calibrated by setting the main resonance of the As XANES spectrum of sodium arsenate to 11,875 eV. For Fe measurements, the monochromator was calibrated using Fe foil with the inflection point of the XANES spectrum set to 7110.75 eV. Fluorescence mode measurements were made with a Canberra 7-element germanium solid-state detector, or with Vortex or Amp-Tek silicon drift diode detectors. Measurements were conducted at room temperature in ambient atmosphere. All As and Fe point-XANES data were collected in "quick" mode with a full sweep of the monochromator in 30 seconds. The number of sweeps per point varied depending on the quality of the spectra, for most points 30-45 sweeps were collected while more diffuse spots required more than 60 sweeps to resolve the spectra sufficiently for fitting.

The speciation of As in the samples was described in two steps (Nicholas et al. in review):

1) The spatial distributions of total As, Fe, and other elements were mapped using XRF with a resolution of 5 μm^2 pixels (beam size 6 μm × 6 μm). Then As point-XANES data were collected in the area of the XRF map. These As spectra were fit with a set of 25 As reference spectra using linear least-squares combination fitting (LCF) (see SI). The best-fitting As species were used to design the "speciation mapping" protocol (step two).
2) An As speciation mapping protocol was developed for glacial sediments (Toner et al. 2014). The method has the same components as chemical-speciation-multi-energy

mapping methods developed for S (Zeng et al. 2013; Pickering et al. 2009) and Fe (Lam et al. 2012; Mayhew et al. 2011; Toner et al. 2012; Marcus et al. 2010). Multiple XRF maps were collected from sample areas with energies spanning the As 1s absorption edge. The number of XRF maps and the incident energy for each were chosen based on the observed As species present (point-XANES observations) and the degree to which the absorbance at specific energies could distinguish among the species present. This selection process was aided by a custom beamline program *chem map error estimator* (see SI).

The following six incident energies were used for As speciation mapping: 11830eV (pre-edge), 11868 eV (arsenopyrite), 11869 eV (orpiment), 11871.5 eV (arsenite), 11875 eV (arsenate), and 11979 eV (post-edge). The species listed for each energy are those for which mapping at that energy provides the greatest sensitivity, but all species contribute to the signals at all energies. The speciation map data sets were composed of six XRF maps that yield a six-point absorption profile at each pixel in the aligned composite map, with an error estimate for the calculated species in a speciation map of less than 10 mol% for each species type.

The speciation maps were fit pixel-by-pixel using custom beamline software (Marcus 2010) using linear combination fitting (LCF) with reference spectra and a spectrum collected on an empty sample preparation as a material blank. We used four reference spectra to fit to the map:

1) *arsenate sorbed to goethite* as representative of As(V),

2) *arsenite sorbed to ferrihydrite* as representative of As(III),

3) *orpiment* as representative of As-sulfides in which As(III) is the metal bound to reduced S,

4) *arsenopyrite* as representative of As(-I) sulfide, in which As substitutes for sulfur in the disulfide and is bound to both Fe and reduced S.

The quality of the speciation-map fits was evaluated with the whole-map, mean-squared error. The agreement between the speciation-map fits and point-XANES data was evaluated by comparing the species fraction from the maps with the species fraction from the point-XANES using the same 4-species reference set as the map, and allowing 4-member fits. The mole fraction of each As species was calculated by summing the mole fraction from all pixels in the speciation map and normalizing by the number of pixels (Nicholas et al., submitted).

Additional point As point-XANES spectra were collected within the area of the speciation map to ensure that the pixel-by-pixel fits and point XANES collected on the same spot were in agreement. Co-located Fe point-XANES spectra were collected on the same locations as the As point XANES to describe As-bearing or -associated minerals in greater detail.

As described in detail by Nicholas et al. (in review), As and Fe point-XANES spectra were compared with each other and suites of As and Fe reference spectra using a

correlation-distance hierarchical clustering approach. This statistical analysis allows one to compare spectra in a way that is not sensitive to scaling and differences in mean values (D'haesseleer 2005). Sample spectra and selected reference spectra were organized into dendrograms according to correlation distance. The same four As references used to fit the As speciation maps were used as the reference spectra in the As correlation-distance trees.

Data derived from LCF of co-located Fe and As point-XANES spectra (fractional species bins) were used to generate heat map and cosine-distance dendrograms to: (1) illustrate relationships between As and Fe for individual points within samples, and (2) identify populations of point types within the samples. Cosine-distance hierarchical clustering is often used for compositional data because it is sensitive to differences from a mean composition (D'haeseleer 2005).

For this analysis, the Fe point-XANES spectra best fit by primary Fe-bearing silicates were not included because they are thought to be relatively inert mineral surfaces with respect to As. For particles where primary Fe silicates were among the components, the primary Fe-silicate component was removed from the total and the remaining components normalized to 100%.

Results

Bulk Geochemistry. Dissolution major and trace element chemistry was done on 17 samples of glacial sediments from Core CYR-1 and include glacial till (aquitard), glacial stream sediment (aquifer), and glacial lacustrine sediments (**Figure 2: Core stratigraphy with sample locations**). Results for As, Fe and S concentrations are shown in **Table 1** and complete results for all elements are presented in SI Table 1. Arsenic concentrations ranged from 2.6 mg kg^{-1} to 8.1 mg kg^{-1} with a median value of 6.1 mg kg^{-1}. Iron and S concentrations are reported as elemental weight percent (rather than an oxide basis). Iron concentrations ranged from 0.9% to 2.4% and S concentrations ranged from 0.04% to 0.46% with median value of 0.3%. Iron and S ratios show no clear pattern with regard to sediment type.

Well-Water Chemistry. Of the 113 private drinking water wells near core CYR-1 (**Figure 3.1: Buffer map**) 84 have As concentrations in excess of the US EPA MCL of 10 µg L^{-1}. (Minnesota Pollution Control Agency 1999; Minnesota Department of Health 2001; Minnesota Department of Health 2002; Minnesota Geological Survey and Minnesota Department of Health 2004). End-point domestic water treatment is quite common in this area and of the 113 wells, 63 had some kind of water softener, Fe remover, or other water treatment in places (treated wells excluded from analysis). Of the 50 remaining untreated wells within 20 km of core CYR-1, As concentrations ranged from 0.06 to 67 µg L^{-1} with a median concentration of 8.9 µg L^{-1}. Dissolved Fe concentrations ranged from 7 to 11,345 µg L^{-1} with a median Fe concentration of 1168.7

µg L^{-1}. Sulfate was reported for only 40 of the 50 untreated wells, of those 40 the range of sulfate concentrations was from 5 to 827 mg L^{-1} with a medium sulfate concentration of 68 mg L^{-1}. **Figure 3.3** is an Eh/pH predominance diagram showing the 50 untreated wells. Wells with As concentrations above and below 10 µg L^{-1} tend to group together in the predominance diagram. Most of the untreated wells (44 of the 50) are in the stability field for $HAsO_4^{-2}$ (arsenate), four are in the stability field for $H_2AsO_4^-$ (arsenate), and two are in the stability field for $As(OH)_3$(arsenite). **Table 2** shows the median water chemistry conditions for wells above and below the 10 µg L^{-1} US EPA MCL for arsenic. The 10 km buffer contains only one untreated well with As below 10 µg L^{-1} so it is difficult to identify trends within the 10km buffer. Within the 15 and 20 km buffers we see that there is very little difference in pH and Eh between wells with As concentrations above and below 10 µg L^{-1}. In both the 15 and 20 km buffer, wells with As greater than 10 µg L^{-1} also have much higher median dissolved Fe and dissolved sulfate than the wells with As below 10 µg L^{-1}wells. The wells with As in excess of 10 µg L^{-1} also have a somewhat shallower median depth of 85m.

Arsenic and Fe Point-XANES. Arsenic point-XANES collected on the anaerobically preserved samples (**Figures 3.4 and 3.5** As stacked spectra) show a that most points appear to be either chemically reduced As or oxidized As with only one point showing a mixed valence spectrum (contact till CYR 1 78 spot 5). Iron point-XANES collected at the same locations show Fe(III) in all levels and Fe-sulfides in the aquifer and the aquitard **(Figures 3.6 and 3.7).** The five Fe point-XANES spectra in the contact till are

nearly identical. Correlation-distance hierarchical clustering of the As and Fe spectra show that As point-XANES tend to be diverse among the strata, with points from each stratum represented in each cluster (**Figure 8** As tree). Iron spectra tend to cluster by stratum (**Figure 9** Fe tree) with extremely close clustering of the Fe spectra from the CYR-1-78 (contact till).

Complete linear combination fitting (LCF) results for the As and Fe point-XANES can be found in SI Tables 2 and 3. These show both the specific reference to the spectra fit and the "binned" results in which specific reference spectra were assigned to a more general group, e.g. pyrite is assigned to the more general Fe(-I)-sulfide bin. The binned results and cosine-distance hierarchical clustering were used to generate a heat map (**Figure 10** Heat Map) showing both As and Fe LCF results for the same points. This figure shows that there are two main populations of As and Fe co-located particles: one that is almost exclusively As(V) with Fe(III), and one that is almost all As- and Fe-sulfide. Fit results from two points, CYR-1-80-spot 3 in the aquifer and CYR-1-78-spot 5 in the contact till are dominantly As-sulfide and Fe(III)oxyhydr(oxides).

Arsenic Speciation Mapping. Relative abundance of As species in the chemical maps are shown in **Figure 11** (bar chart) and **Table 3**. Two sets of three strata are shown. In the upper triplet we see similar total As concentrations in the mid-aquitard and contact tills, with slightly higher As in the contact till. The aquifer sediments have a much lower As concentration. The aquifer and the mid-aquitard till are mostly As-sulfides while the

contact till is dominated by oxidized As. In the lower triplet we see higher As concentrations overall, similar As concentrations in the mid-aquitard and contact tills with slightly higher overall As in the contact till and a lower As concentration in the aquifer sediments. The mid-aquitard till is dominantly As-sulfide, the contact till is entirely oxidized As and the aquifer is dominantly oxidized As.

Results of As speciation mapping on the thaw/exposure experiment are shown in **Figure 12** and **Table 4**. CYR1-61 and CYR1-46 are both mid-aquitard till samples from the St. Hillaire member of the Goose River formation. Three treatments of CYR1-61 were mapped. Compared with the anaerobic treatment which was predominantly As sulfides the thawed anaerobic and open air samples from CYR1-61 were more oxidized and had similar fractions of combined As sulfides and combined AsV and AsIII. The open air sample from CYR1-61 was dominated by end members As(-I) sulfide and As(V) while the thawed anaerobic sample had larger fractions of As(III) and As(III)sulfide. Results for CYR1-46 were different from those of CYR1-61. Two treatments of CYR1-46 were mapped and the Anaerobic and open-air treatments of CYR1-46 were indistinguishable within the error.

Discussion

Mechanisms of As Release from Sediments to Groundwater. Linear combination fitting of As and Fe point-XANES indicates the presence of As- and Fe–sulfides, as well as oxidized As and Fe in all of the sampled strata. Results of As speciation mapping

show that As(V) and As-sulfides are the dominant As species present.. These species are out of equilibrium with the well water near core CYR1 (Figure Eh pH diagram). Well-water conditions favor Fe oxyhydr(oxides) and As(V) aqueous species. This suggests oxidative dissolution of Fe and As-bearing sulfides as a mechanism liberating As to waters (Equation 1).

Equation 1:

$$4FeAsS_{(s)} + 11O_{2(g)} + 6H_2O_{(l)} \rightarrow 4Fe^{2+}_{(aq)} + 4H_3AsO_{3(aq)} + 4SO^{2-}_{4(aq)}$$

In circumneutral pH environments, $Fe^{2+}_{(aq)}$ oxidizes to Fe(III) and precipitates as an Fe(oxyhydr)oxide (Schrieber and Rimstidt 2013)

Equation 2:

$$Fe^{2+}_{(aq)} + 2H_2O_{(l)} \rightarrow FeOOH_{(s)} + 3H^{+}_{(aq)} + e^{-}$$

The freshly formed (oxyhydr)oxide presents favorable binding sites for the dissolved As (Yu et al. 2007).

Two of the wells within the 20 km buffer zone favor As(III) aqueous species and many of the wells are near the equilibrium between As(V) and As(III) aqueous species. Changes in redox would tend to favor the reduction of As(V) to As(III) and this would be expected to cause some desorption of As into waters (Saalfield and Bostick 2009). It is important to note that the well-water-chemistry data present a snapshot of water chemistry at a single moment, and chemical conditions of the pore water, where most of the rock-water

interactions are taking place, are likely to be different from the bulk well-water chemistry (Gotkowitz et al. 2004).

Comparison of water chemistry conditions between wells with As concentrations above and below the 10 μg l^{-1} MCL shows higher concentrations of Fe and S in well waters with elevated As (**Table 2**) and this also consistent with oxidative dissolution of sulfides as a mechanism liberating As to waters.

Median redox conditions are slightly higher in wells with As above the MCL within the 15 km buffer, but median redox conditions are lower when we include wells out in the 20 km buffer. A drop in redox conditions where wells are near the equilibrium of As(V) and As(III) would favor the reduction and desorption of As(V) to As(III) (Cullen and Reimer 1989; Erbs et al. 2010).

Equation 3:

$$HAsO_4^{2-} \cdots FeOOH\ (s) + 3H^+(aq) + \ e^- \rightarrow Fe^{2+}(aq) + 2H_2O\ (l) + \ HAsO_4^{2-}$$

Correlation-distance clustering of As point-XANES shows the sample spectra clustering more closely with each other than with any of the reference spectra, with samples from different strata clustered together (**Figure 8**). This suggests samples undergoing similar weathering processes at different rates and for different lengths of time. Correlation-

distance clustering of the Fe point-XANES co-located with As tended to be by stratum (**Figure 9**), which suggests an overprint of the Fe parent material.

The heatmap of LCF output for the co-located As and Fe point-XANES (**Figure 10**) also points to a weathering process with the As- and Fe-sulfides as one end member and the oxidized As and Fe as another end-member. The presence of the mixed group (As-sulfide with Fe oxy(hydr)oxides) is interesting because it was also found during analysis of co-located As and Fe point-XANES from archived cores that had been stored in the open air (Nicholas et al. in review). The appearance of the mixed group in anaerobically preserved cores suggests that this may be a stage of *in-situ* weathering rather than an artifact of sample storage.

Arsenic Sulfide Accumulation – Evidence for Past Sulfate Reducing Conditions. A finding that was very surprising was that most of the As in the upper aquifer (CYR1-38c) fit in the speciation map as As(III)sulfide. A column-reactor study by Onstott et al. (2011) in which the authors stimulated sulfate-reducing bacteria in sediments and porewaters collected from an As-contaminated aquifer by injecting additions of sulfate, lactate, phosphate, and Fe found that this treatment resulted in the formation of As-rich microcrystaline sulfides. Concentrations in the reactor experiment were much higher than those found in the area of core CYR1, but it presents an interesting avenue for further research.

Preservation of Redox Sensitive Sediments. Speciation mapping results for the three treatments of CYR1-61 (anaerobic, thaw anaerobic, and open-air) (**Figure 12**) show a slight relative increase in oxidized As between the anaerobic and the thaw-anaerobic treatments and a larger increase in oxidized As between the anaerobic and the open-air treatment. The greatest change was in the relative proportion of As(III)-type sulfide which may indicate that this species is more labile over a short period of time. Differences between the two treatments (anaerobic and open-air) of CYR1-46 were very slight and both treatments were dominated by As(-I)-sulfide and As(V). These data are not conclusive but suggest that As(III) and As(III)sulfide may be more labile in ambient-air than As(-1) sulfide.

Acknowledgments

Funding for this work came from grants to Toner from the Center for Urban and Regional Affairs, the UMN Office of the Vice President for Research, and a USGS Water Research Grant (jointly funded by the USGS's Water Resources Research Initiative Program and the Minnesota Agricultural Experiment Station's Center for Agricultural Impacts on Water Quality). We thank Prof. Bernhardt Saini-Eidukat, and undergraduate researcher Lane Folkers at North Dakota State University for assistance in the field and lab space. We thank synchrotron scientists Sirine Fakra and Josep Roque-Rosell (Advanced Light Source, ALS, BL10.3.2). The ALS is supported by the Director, Office of Science, Office of Basic Energy Sciences, of the U.S. DOE under Contract No. DE-AC02-05CH11231.

Table 15 CYR-1 wet chemistry results

Samples labeled USGS were analyzed in a USGS contract lab and samples labeled UMN were run in the University of Minnesota Earth Sciences ICP-MS lab.

Sample name	Sample Description	Depth (m)	As mg/kg	Fe %	S %	Fe/S	lab
CYR1_25	Silt loam till with sand and gravel (aquitard) Upper Member, Red River Falls Formation	7.6	6.5	1.9	0.3	6.7	USGS
CYR1_31_i	Silt loam till (aquitard) Upper Member, Red River Falls Formation	9.4	8.3	2.1	0.04	51.3	USGS
CYR1_37ac_i	Silt loam till (aquitard) Upper Member, Red River Falls Formation	11.3	8.8	2.4	0.2	9.9	USGS
CYR1 _37bc	fine silty sand (aquifer) outwash in Red River Falls Formation	11.3	2.87	0.9	na		UMN
CYR1 _38ac	fine silty sand (aquifer) outwash in Red River Falls Formation	11.5	2.58	1.1	na		UMN
CYR1_38c	sand and gravel (aquifer) outwash in Red River Falls Formation	11.6	6.47	1.8	na		UMN
CYR1_40.5	Silt loam till (aquitard) Upper Member, Red River Falls Formation	12.3	5.4	1.5	0.4	3.5	USGS
CYR1_41ac	fine sandy silt with lignite (aquifer) slow water sediment, Red River Falls Formation	12.5	8.5	1.9	0.1	18.7	USGS
CYR1_41_bc_i	pebbly silt loam till with possible sulfides (aquitard) Upper Member, Red River Falls Formation	12.5	7.8	2.0	0.1	16.5	USGS
CYR1_46	Silt loam till (aquitard) Upper Member, Red River Falls Formation	14.0	4.6	1.7	0.4	4.6	USGS

Sample name	Sample Description	Depth (m)	As mg/kg	Fe %	S %	Fe/S	lab
CYR_1_56ac	silty fine sand (aquifer) outwash in Goose River formation	17.1	3	0.9	0.2	5.7	USGS
CYR1_61	Loam till (aquitard) St. Hillaire member, Goose River formation	18.6	6.1	1.9	0.4	4.3	USGS
CYR_1_64ac	Loam till (aquitard) St. Hillaire member till, Goose River formation	19.5	4.9	1.6	0.4	4.2	USGS
CYR1_64bc	Loam till (aquitard) St. Hillaire member till, Goose River formation	19.5	6	1.4	0.3	4.3	USGS
CYR_78bc	Loam till (aquitard) St. Hillaire member till, Goose River formation	23.8	8.9	2.3	0.1	33.1	USGS
CYR1_80ac	fine silty sand (aquifer) outwash in Goose River formation	24.4	3.9	1.8	0.3	7.1	USGS
CYR1_208_i	clay with silt (lacustrine sediment) Otter Tail River formation	63.4	7.4	2.3	0.5	5.0	USGS

Table 16 Well water chemistry near core CYR-1

Gradient of median well-water chemistry conditions in wells near core CYR-1						
Distance	**10km**		**15km**		**20 km**	
	As below 10 µg L^{-1}	As above 10 µg L^{-1}	As below 10 µg L^{-1}	As above 10 µg L^{-1}	As below 10 µg L^{-1}	As above 10 µg L^{-1}
n	1	4	8	9	27	23
As µgL^{-1}	7.2	15.5	1	18.5	1.8	31.4
depth (m)	107	24	27	26	37	26
Eh (mV)	132	196	124	135	124	98
pH	7.5	7.2	6.8	6.8	7.3	7.3
Fe µg L^{-1}	393	962	445	1976	522	1405
SO_4 mg L^{-1}	47	44	52	68	63	75

Table 2 caption: Median water chemistry conditions for wells above and below the 10 µg L^{-1} US EPA MCL for arsenic.

Table 17 in upper and lower anaerobic triplets

Stratum	Total As	As (V)	As(III)	As(III) sulfide	As(-I) sulfide
CYR1-38c Aquifer outwash in Red River Falls Formation	100%	[a] 38%	[a] 0%	[a] 52%	[a] 10%
	[b] 1.8 mg/kg	[c] 0.7 mg/kg	[c] 0.0 mg/kg	[c] 0.9 mg/kg	[c] 0.2 mg/kg
CYR1_40.5 contact till Red River Falls Formation	100%	[a] 76%	[a] 10%	[a] 4%	[a] 10%
	[b] 5.4 mg/kg	[c] 4.1 mg/kg	[c] 0.5 mg/kg	[c] 0.2 mg/kg	[c] 0.5 mg/kg
CYR1_46 mid-aquitard till Red River Falls Formation	100%	[a] 19%	[a] 15%	[a] 18%	[a] 48%
	[b] 4.6 mg/kg	[c] 0.9 mg/kg	[c] 0.7 mg/kg	[c] 0.8 mg/kg	[c] 2.2 mg/kg
CYR1_61 mid-aquitard till St. Hillaire member, Goose River formation	100%	[a] 11%	[a] 11%	[a] 44%	[a] 34%
	[b] 6.1 mg/kg	[c] 0.7 mg/kg	[c] 0.7 mg/kg	[c] 2.7 mg/kg	[c] 2.1 mg/kg
CYR_78bc contact till St. Hillaire member, Goose River formation	100%	[a] 73%	[a] 27%	[a] 0%	[a] 0%
	[b] 8.9 mg/kg	[c] 6.5 mg/kg	[c] 2.4 mg/kg	[c] 0.0 mg/kg	[c] 0.0 mg/kg
CYR1_80ac Aquifer outwash in Goose River formation	100%	[a] 32%	[a] 47%	[a] 21%	[a] 0%
	[b] 3.9 mg/kg	[c] 1.2 mg/kg	[c] 1.8 mg/kg	[c] 0.8 mg/kg	[c] 0.0 mg/kg

a – Arsenic species fraction as measured by speciation mapping (Figure X)
b – Arsenic concentration as measured via continuous-flow hydride-generation atomic absorption spectrometry after total acid extraction (Table 2).
c – Arsenic species abundance calculated by multiplying relative abundance by total As.

Table 18

Thaw experiment samples	As(V)	As(III)	As(III) sulfide	As (-I) sulfide
CYR-1 61 anaerobic	11%	11%	44%	34%
CYR-1 61 thawed anaerobic	18%	22%	18%	32%
CYR1-61 open air	35%	15%	6%	44%
CYR1-46 anaerobic	15%	19%	18%	48%
CYR1-46 open air	21%	20%	16%	43%

Supplementary file "*Nicholas dissertation supplementary files 1 to 5.xlsx"* was submitted to the UMN digital conservancy with this thesis. It is an excel workbook with five tables. Tables 1 and 2 are the complete provenance and citation information for all As and Fe reference spectra used. Tables 3, 4, and 5 are the reference spectra fits, fractions, and scores for the sampled spectra from cores OTT3, TG3, and UMRB2.

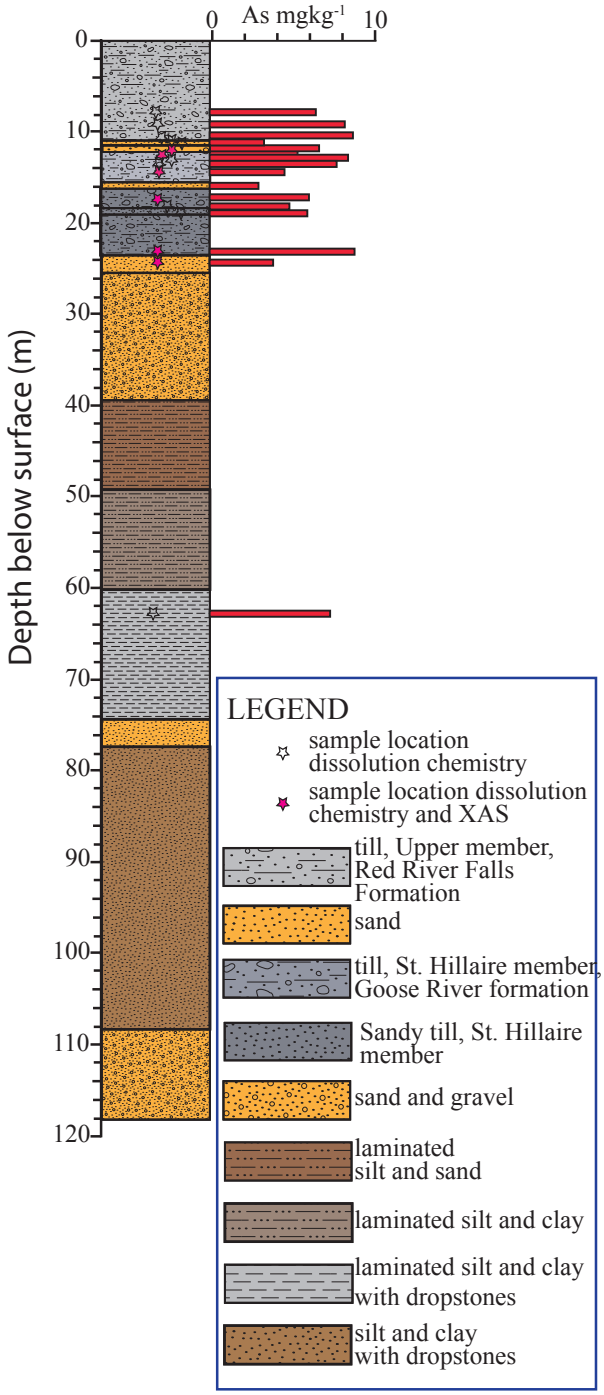

Figure 10 Simplified descriptove stratigraphy of core CYR-1. Simplified from Gowan 2014. Sample depths are shown by stars. Red bars show As concentration as measured by dissolution chemistry. Filled red stars show samples for XAS.

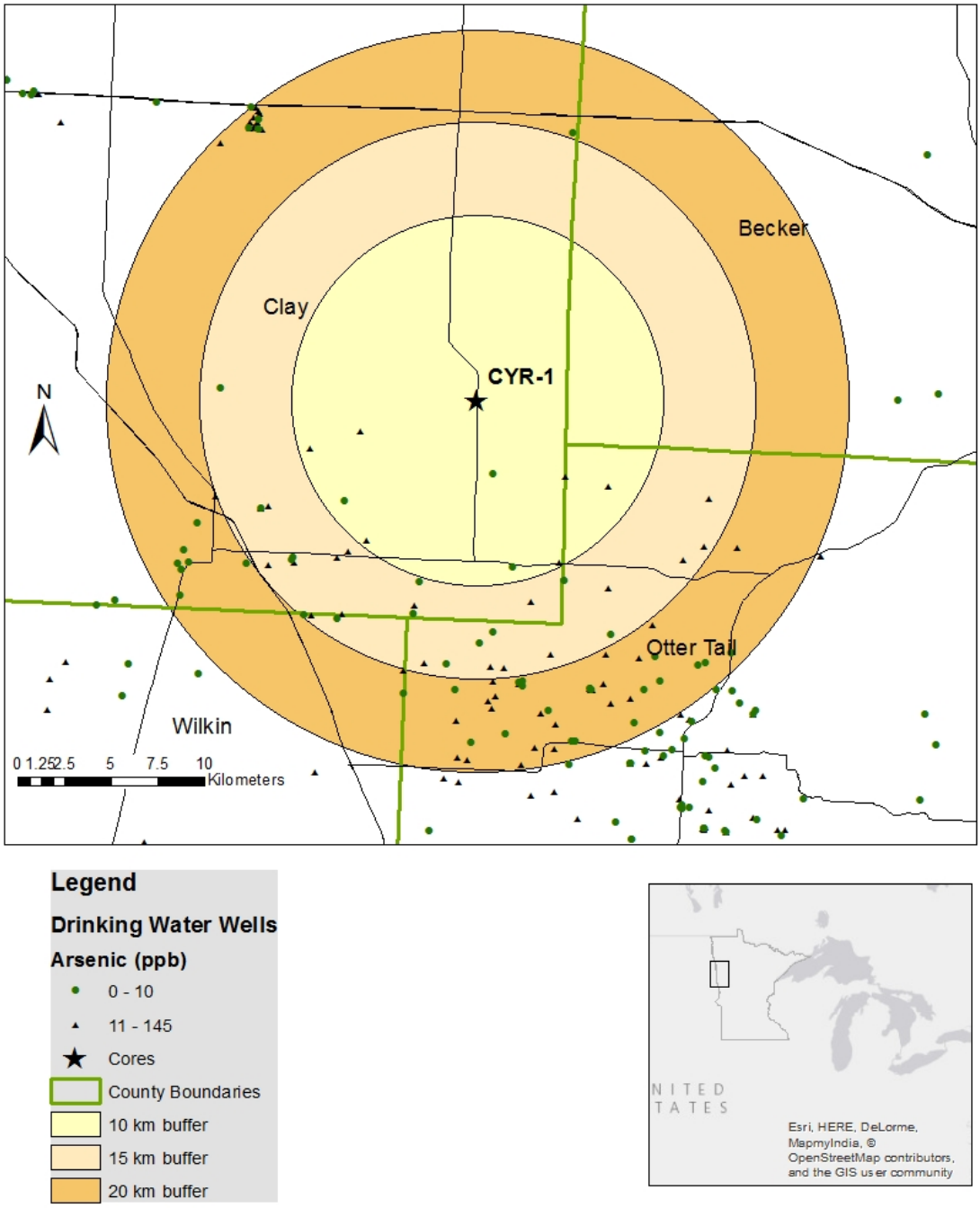

Figure 11 Location of core CYR-1 and nearby drinking-water wells, with 10, 15 and 20km buffers shown.

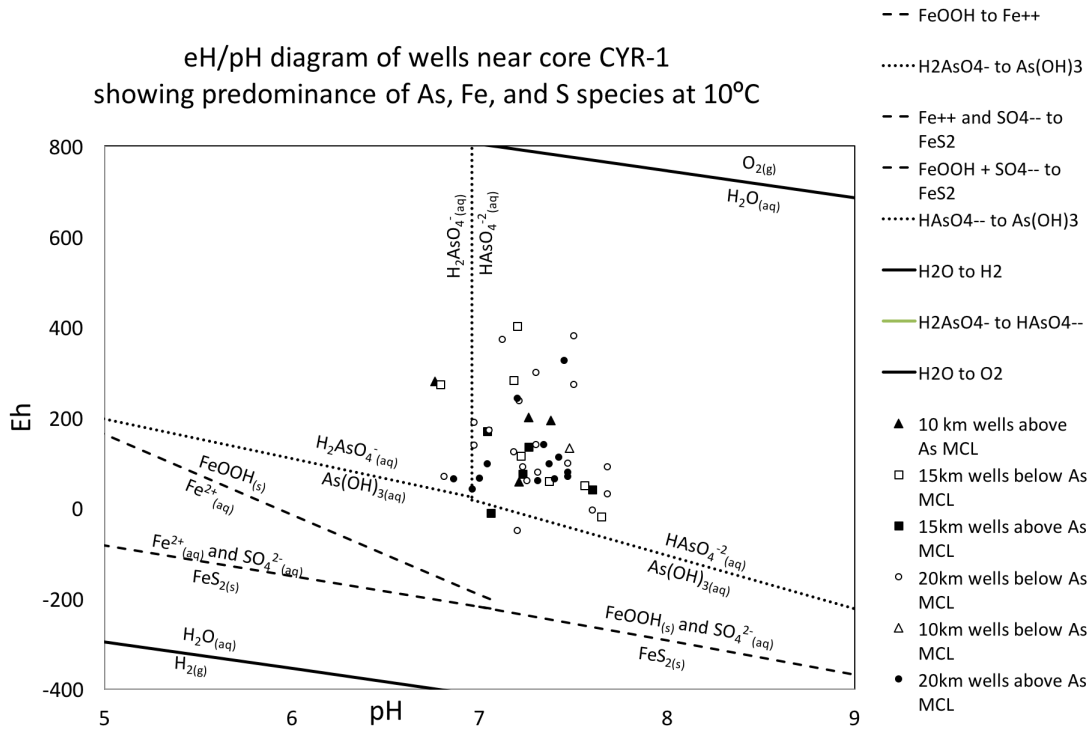

Figure 12 Eh/pH diagram showing predominance of As, Fe, and S species at 10ºC 10, 15, and 20km buffers. High and low As wells within 10, 15 and 20 km of CYR-1 cluster together on the Eh/pH diagram. Using this as a predictive model we see that the favored Fe species is FeOOH and the favored S species is sulfate. The favored As species would be arsenate, with two wells more favorable for arsenite.

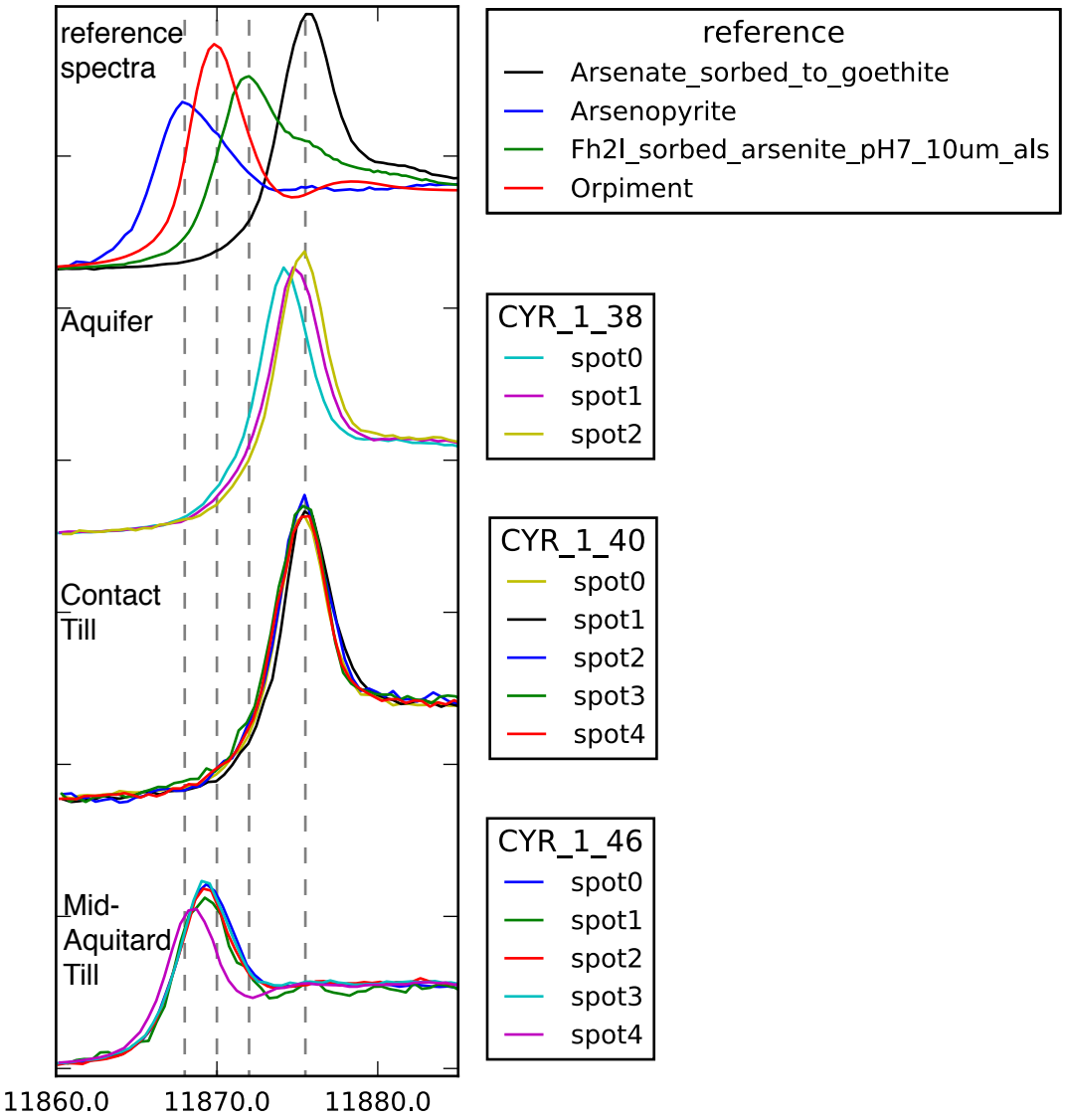

Figure 13 Till and stream sediments from the Upper member of the Red River Falls Formation

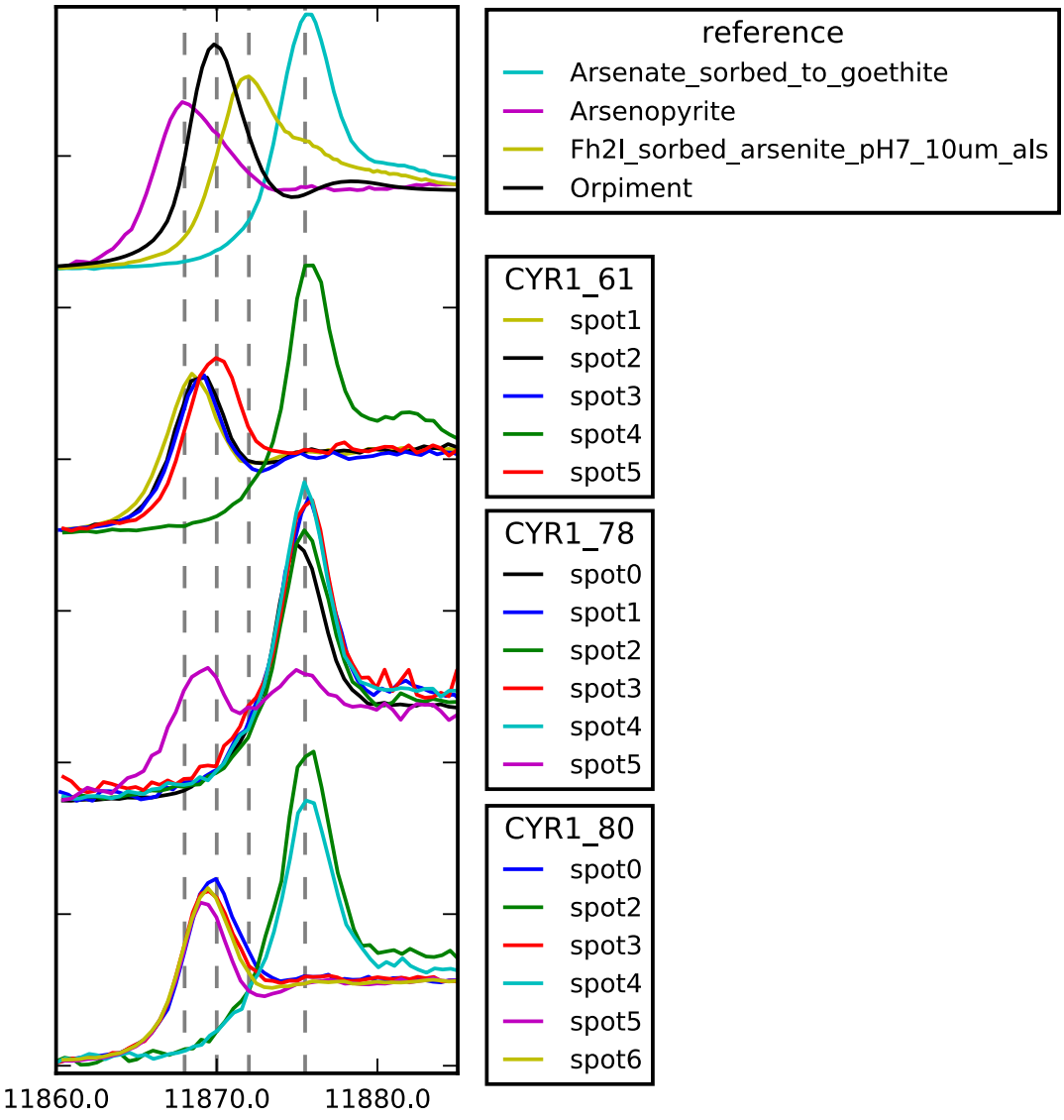

Figure 14 till and stream sediments from the St. Hillaire member oft the Goose River formation.

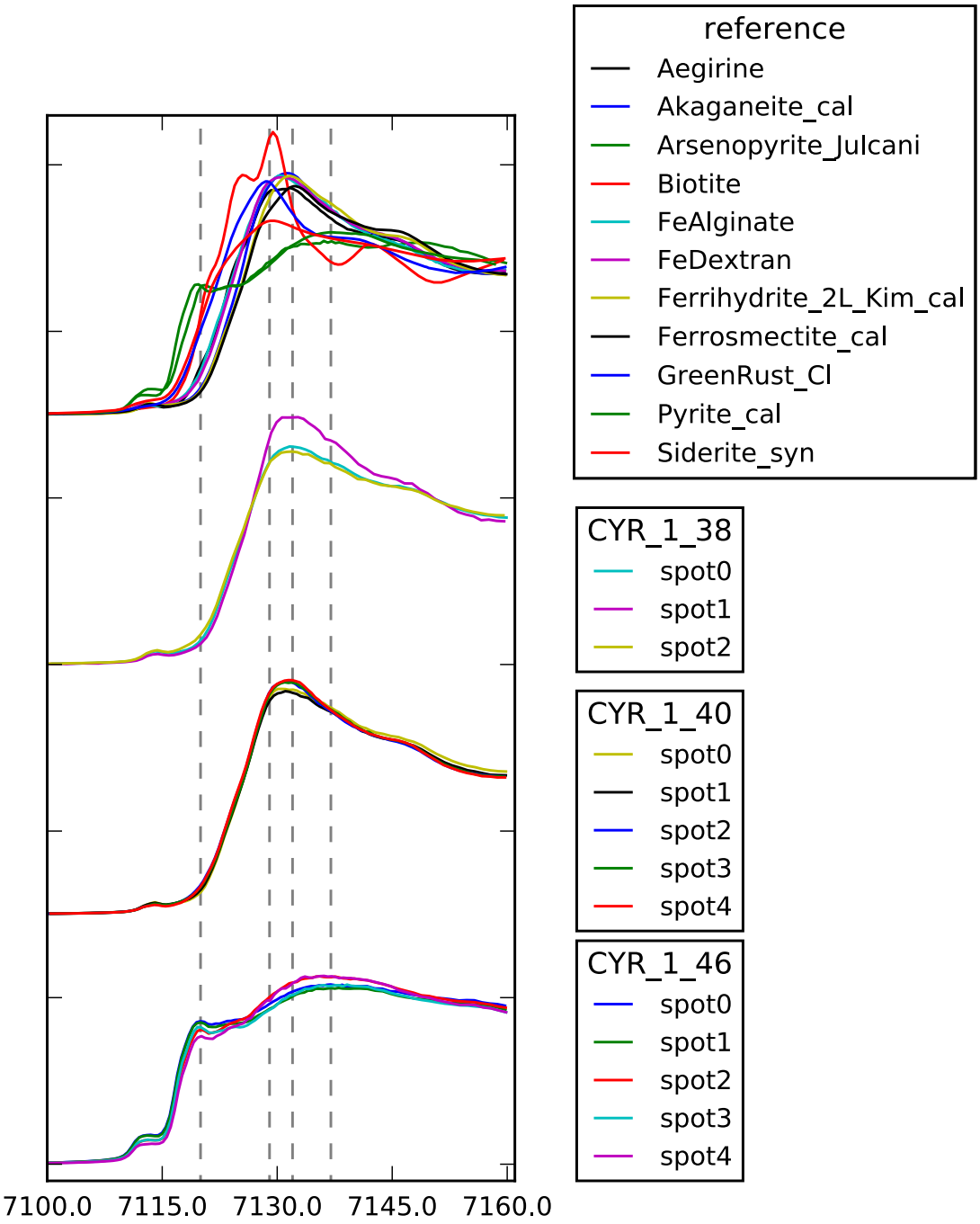

Figure 15 till and stream sediments from the Upper member of the Red River Falls Formation

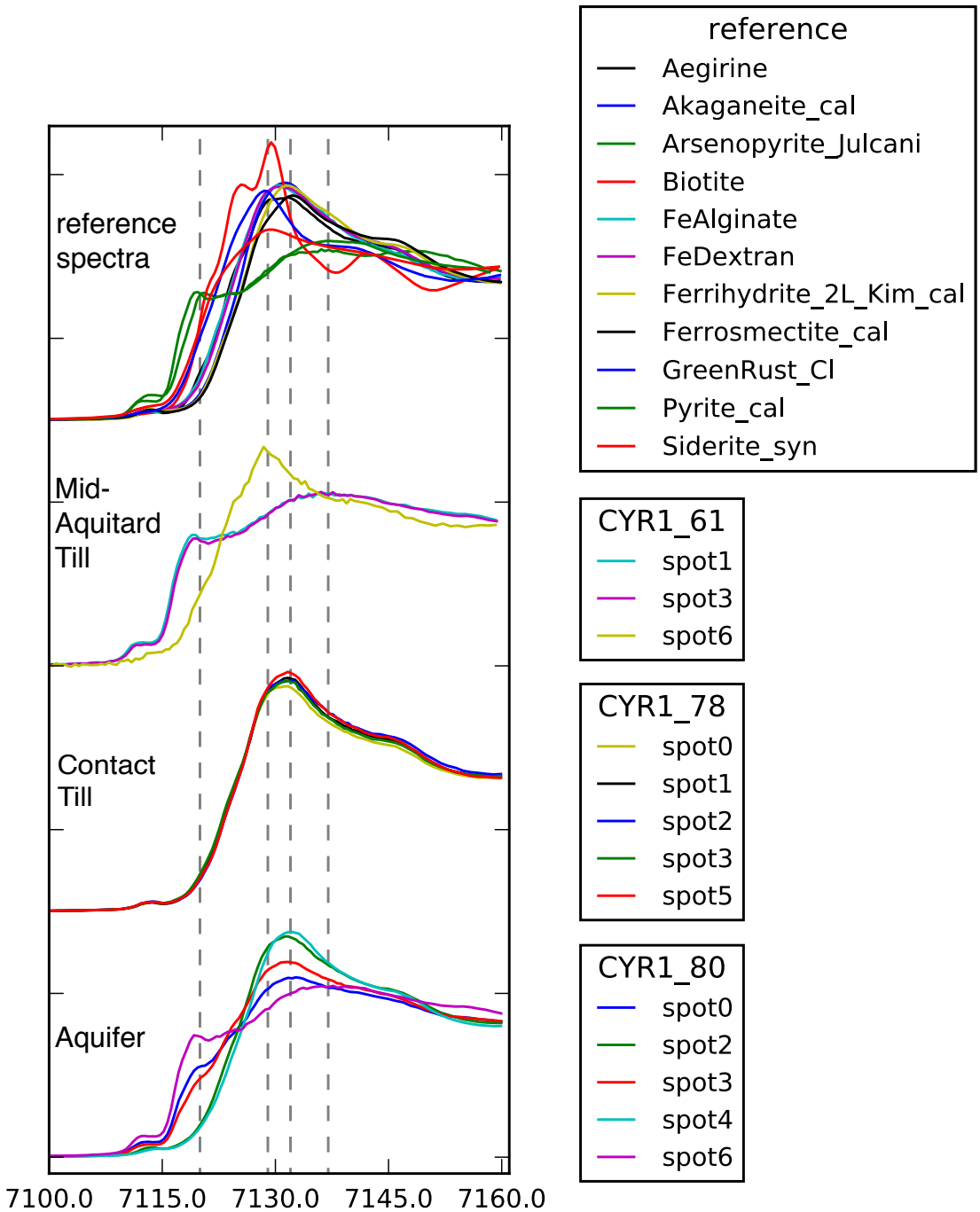

Figure 16 Till and stream sediments from the St. Hillaire member of the Goose River formation.

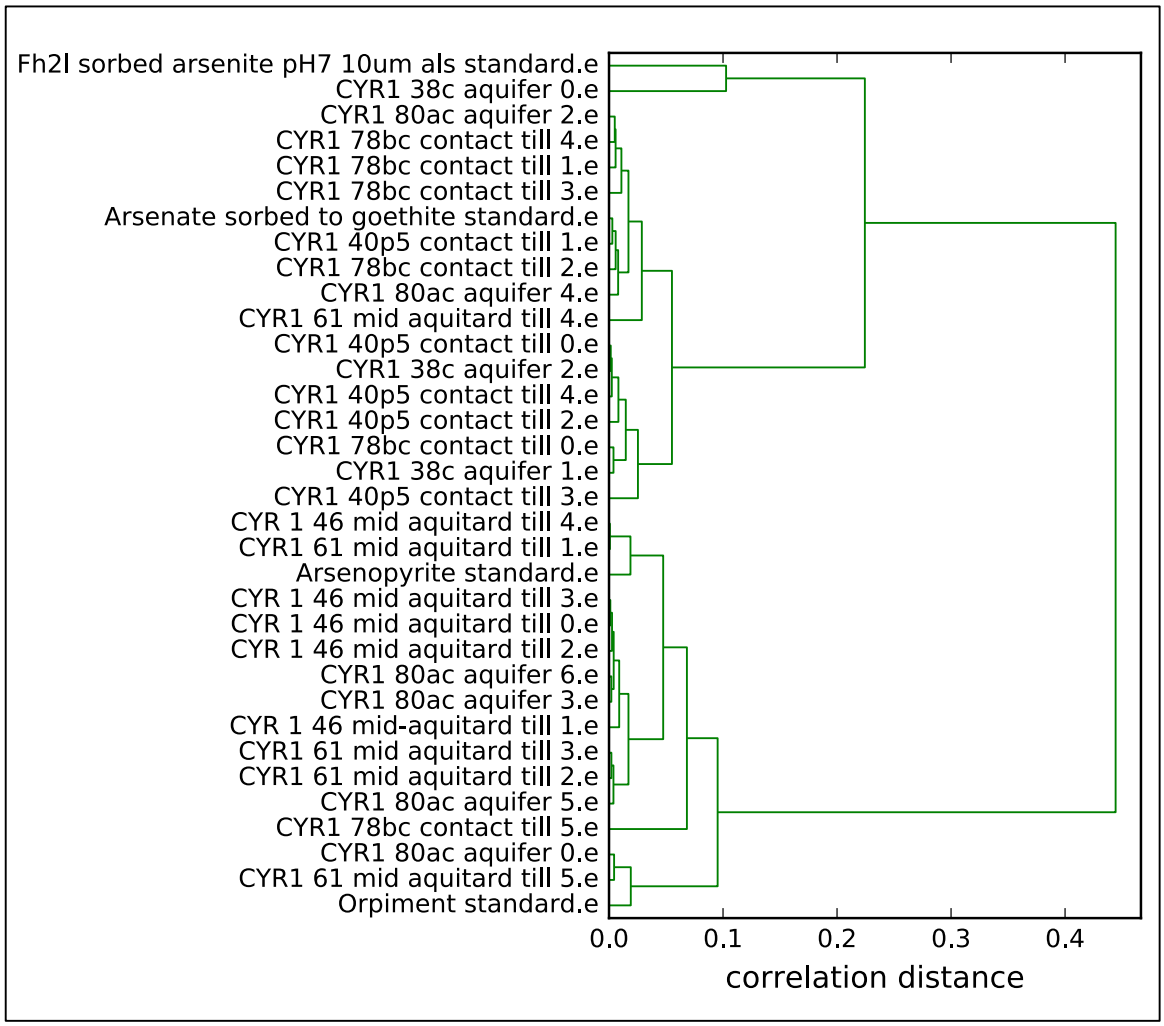
Fh2l sorbed arsenite pH7 10um als standard.e
CYR1 38c aquifer 0.e
CYR1 80ac aquifer 2.e
CYR1 78bc contact till 4.e
CYR1 78bc contact till 1.e
CYR1 78bc contact till 3.e
Arsenate sorbed to goethite standard.e
CYR1 40p5 contact till 1.e
CYR1 78bc contact till 2.e
CYR1 80ac aquifer 4.e
CYR1 61 mid aquitard till 4.e
CYR1 40p5 contact till 0.e
CYR1 38c aquifer 2.e
CYR1 40p5 contact till 4.e
CYR1 40p5 contact till 2.e
CYR1 78bc contact till 0.e
CYR1 38c aquifer 1.e
CYR1 40p5 contact till 3.e
CYR 1 46 mid aquitard till 4.e
CYR1 61 mid aquitard till 1.e
Arsenopyrite standard.e
CYR 1 46 mid aquitard till 3.e
CYR 1 46 mid aquitard till 0.e
CYR 1 46 mid aquitard till 2.e
CYR1 80ac aquifer 6.e
CYR1 80ac aquifer 3.e
CYR 1 46 mid-aquitard till 1.e
CYR1 61 mid aquitard till 3.e
CYR1 61 mid aquitard till 2.e
CYR1 80ac aquifer 5.e
CYR1 78bc contact till 5.e
CYR1 80ac aquifer 0.e
CYR1 61 mid aquitard till 5.e
Orpiment standard.e
0.0
0.1
0.2
0.3
0.4
correlation distance

Figure 17

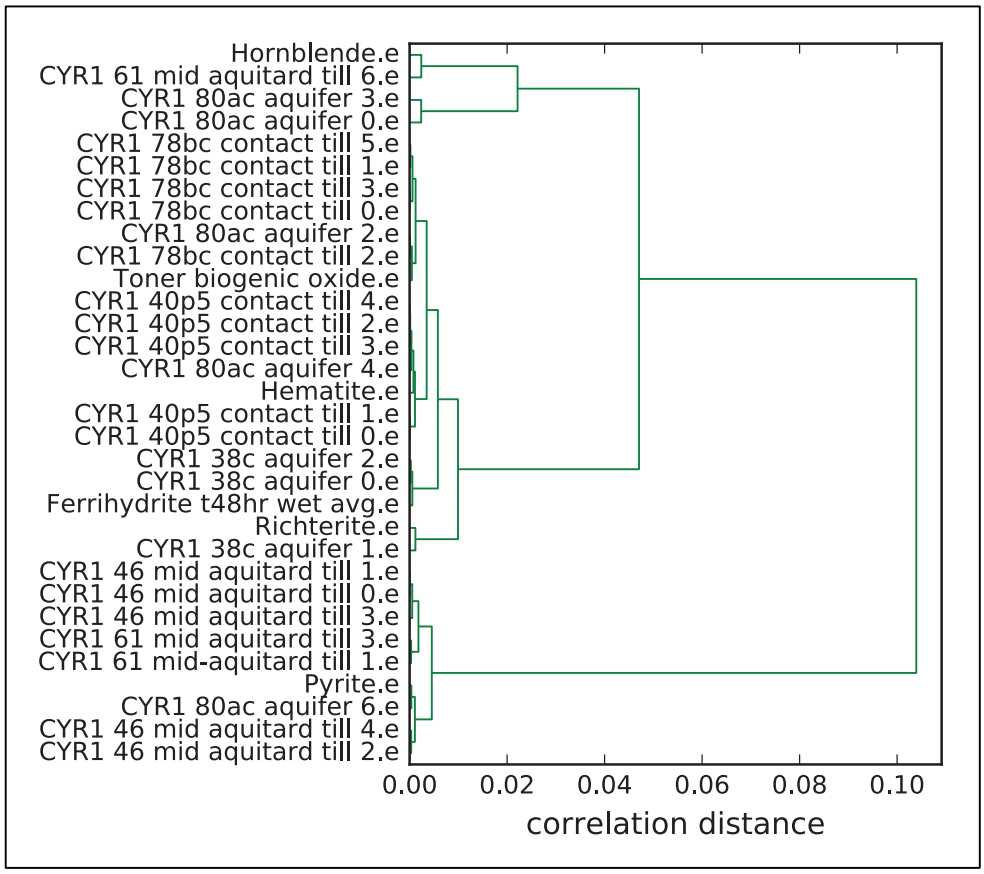
Hornblende.e
CYR1 61 mid aquitard till 6.e
CYR1 80ac aquifer 3.e
CYR1 80ac aquifer 0.e
CYR1 78bc contact till 5.e
CYR1 78bc contact till 1.e
CYR1 78bc contact till 3.e
CYR1 78bc contact till 0.e
CYR1 80ac aquifer 2.e
CYR1 78bc contact till 2.e
Toner biogenic oxide.e
CYR1 40p5 contact till 4.e
CYR1 40p5 contact till 2.e
CYR1 40p5 contact till 3.e
CYR1 80ac aquifer 4.e
Hematite.e
CYR1 40p5 contact till 1.e
CYR1 40p5 contact till 0.e
CYR1 38c aquifer 2.e
CYR1 38c aquifer 0.e
Ferrihydrite t48hr wet avg.e
Richterite.e
CYR1 38c aquifer 1.e
CYR1 46 mid aquitard till 1.e
CYR1 46 mid aquitard till 0.e
CYR1 46 mid aquitard till 3.e
CYR1 61 mid aquitard till 3.e
CYR1 61 mid-aquitard till 1.e
Pyrite.e
CYR1 80ac aquifer 6.e
CYR1 46 mid aquitard till 4.e
CYR1 46 mid aquitard till 2.e
0.00
0.02
0.04
0.06
0.08
0.10
correlation distance

Figure 18

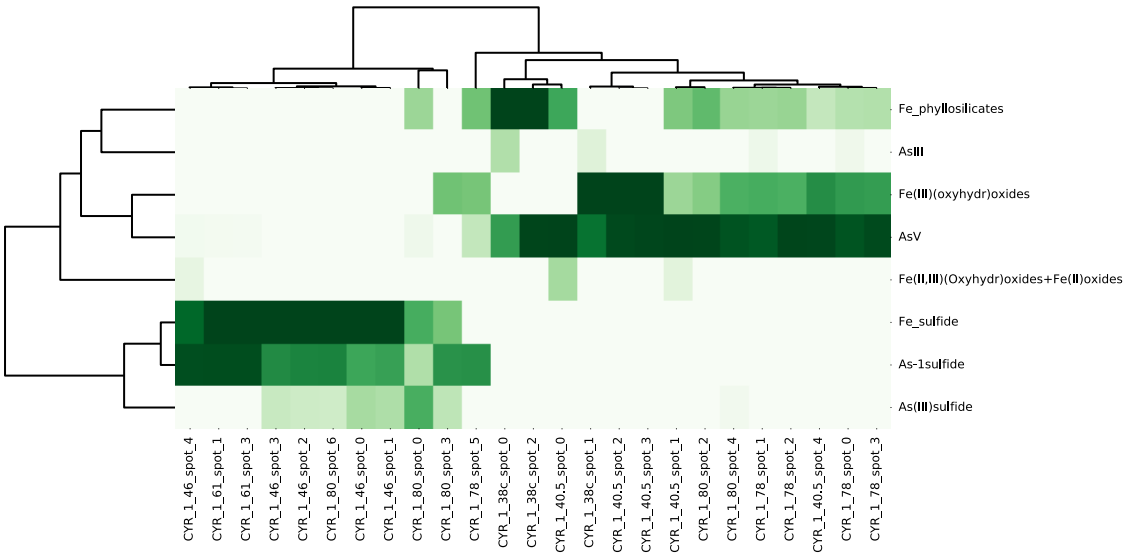
Fe_phyllosilicates
AsIII
Fe(III)(oxyhydr)oxides
AsV
Fe(II,III)(Oxyhydr)oxides+Fe(II)oxides
Fe_sulfide
As-1sulfide
As(III)sulfide
CYR_1_46_spot_4
CYR_1_61_spot_1
CYR_1_61_spot_3
CYR_1_46_spot_3
CYR_1_46_spot_2
CYR_1_80_spot_6
CYR_1_46_spot_0
CYR_1_46_spot_1
CYR_1_80_spot_0
CYR_1_80_spot_3
CYR_1_78_spot_5
CYR_1_38c_spot_0
CYR_1_38c_spot_2
CYR_1_40.5_spot_0
CYR_1_38c_spot_1
CYR_1_40.5_spot_2
CYR_1_40.5_spot_3
CYR_1_40.5_spot_1
CYR_1_80_spot_2
CYR_1_80_spot_4
CYR_1_78_spot_1
CYR_1_78_spot_2
CYR_1_40.5_spot_4
CYR_1_78_spot_0
CYR_1_78_spot_3

Figure 19

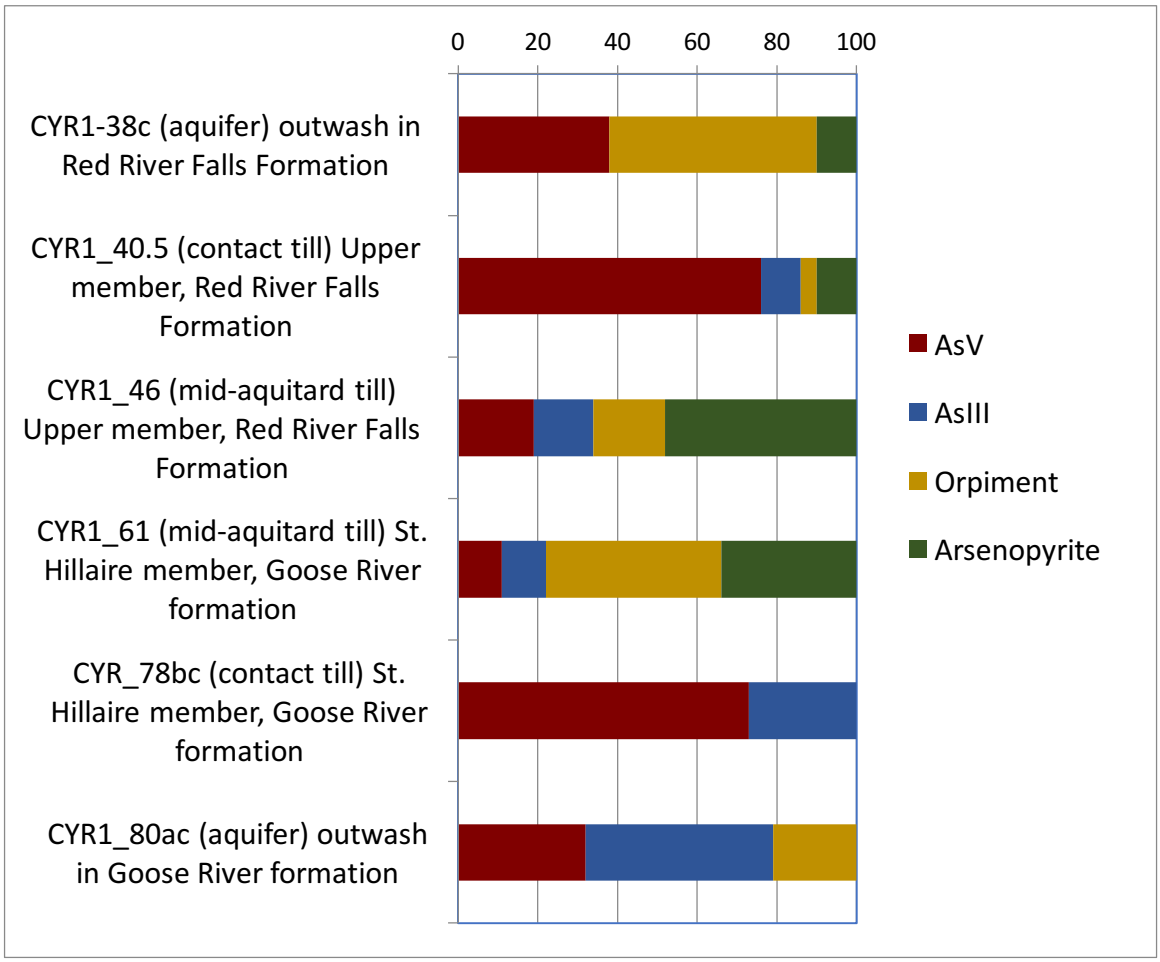

Figure 20 Relative abundance of As species measured via As speciation mapping, upper and lower anaerobic triplets.

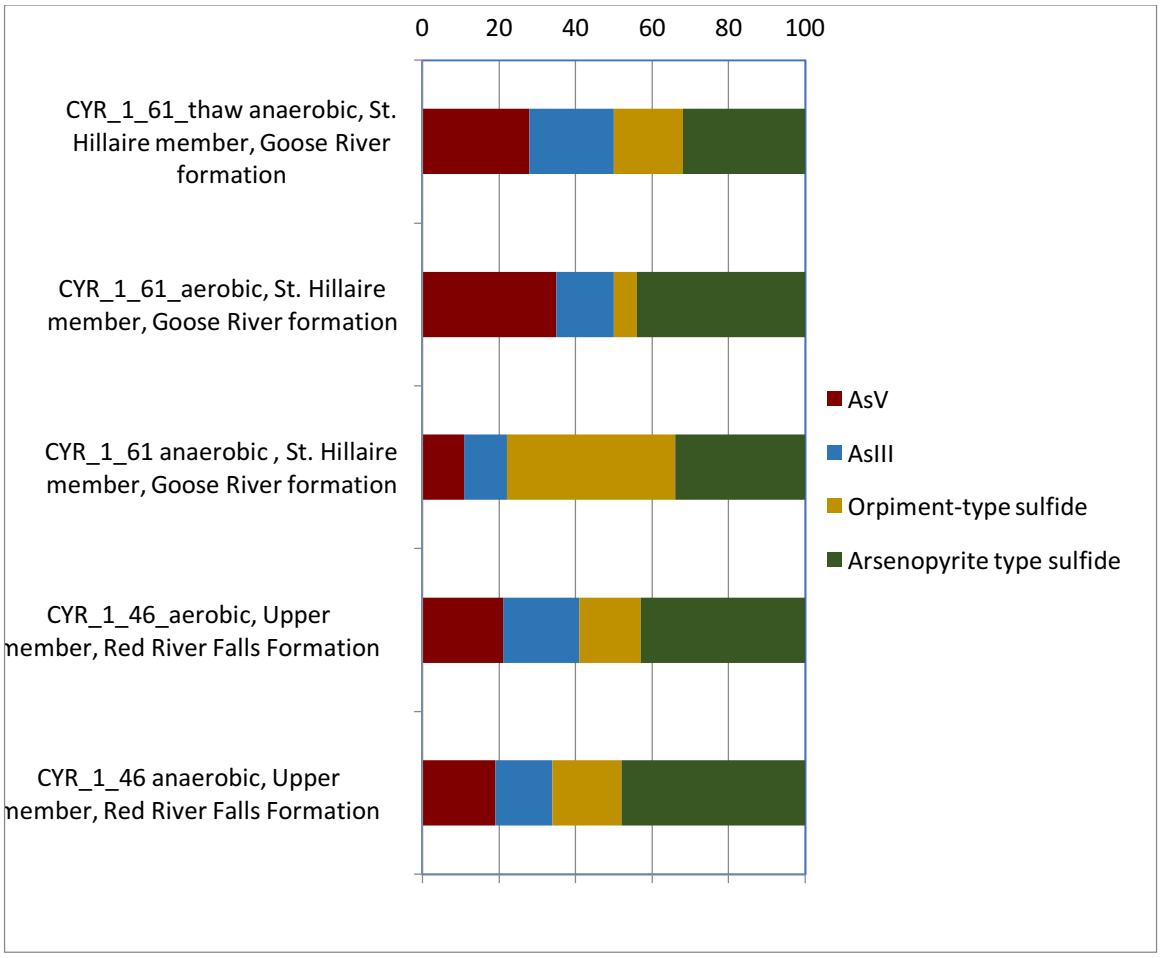

Figure 21 Relative abundance of As species measured via As speciation mapping, thaw experiment.

Chapter 4: NOVEL APPLICATIONS OF STATISTICAL METHODS AND NEW SOFTWARE

Section 1, Introduction:

In this chapter I describe the statistical methods that were used to analyze the XANES data (Chapters 2 and 3) and describe the motivation for writing new XANES data analysis software *mrfitty.py*. **Section 2** describes traditional methods of linear combination fitting (LCF) and principle component analysis (PCA). **Section 3** describes and illustrates the use of some statistical tools commonly used in genomics and data mining that, to my knowledge, have not been applied to XAS data before. *Correlation distance hierarchical clustering* was used to compare normalized sample spectra to each other. C*osine distance hierarchical clustering* was used to identify patterns of co-occurrence between linear combination fits (LCF) of As and Fe reference spectra to co-located As and Fe XANES sample spectra. These two methods were illustrative and helpful. **Section Four** describes novel statistical methods that were applied without success. I applied cosine distance hierarchical clustering to the dissolution chemistry seeking a chemical fingerprint of different till groups but found no relationship between the trace or major element composition of the till matrix and the named till groups. I applied the LASSO variant of linear least squares fitting to the LCF data hoping to limit the number of references used in LCF but found that this method tended to give larger sets of references than were indicated by the traditional method.

The first paper submitted from this project (Chapter 2) introduces and presents a link to the *mrfitty* Python program for linear combination fitting, correlation-distance

hierarchical clustering, and cosine-distance hierarchical clustering of XAS data. The original motivation for writing original software was to deal with re-fitting when new reference for arsenic became available. Before *mrfitty.py* I fit each sample spectrum one at a time to a set of reference spectra using the data analysis software written in LabView by Matthew Marcus, the beamline scientist at 10.3.2. This is still how I do it at the beamline when the data first comes in, because I want to do a rough fit on each sample spectrum right away. This is a very iterative process and it is necessary to re-fit the data using different sets of reference spectra. As my work moved forward I was in contact with other scientists who were studying As. I was sent new reference materials from which I collected spectra (e.g.As and Fe spectra on lollingite, and arsenopyrite from the Smithsonian minerals collection) or new reference spectra (e.g As-pyrite and scorodite As spectra from Andrea Foster, arsenopyrite Fe spectra from Rob Root before they were published in 2015). This was exciting but it also meant that I had to re-fit every sample spectrum one at a time to the set of references with the new reference spectrum. Watching me re-fit my spectra one at a time prompted Joshua Lynch, a scientific programmer of my acquaintance, to propose that we write a program that would allow me to fit all the spectra to all the references at one time. This program, *mrfitty.py* has been through several iterations but the roughest version was ready to try out in about a week and it was a revolution for me; it made curiosity cheap. If I wanted to see how adding and removing reference spectra from consideration changed the fits to all the spectrum instead of taking a week it took about 5 minutes to write a new configuration file and

then 70 seconds to fit all the As spectra and 5 minutes to fit all the Fe spectra (the iron database is much larger than the arsenic database).

The software and instructions for the use of *mrfitty.py* are available at Github. The software development work was done in collaboration with Joshua Lynch (at that time UMN Bioinformatics and Computational Biology) who is a co-author on the first paper. The correct citation for *mrfitty.py* is the paper that was submitted to GCA in June (Chapter 2). The software is copyrighted 2014 by Lynch and Nicholas under an MIT license. The MIT license allows anyone to use or modify the software for his or her use. Originally the hierarchical clustering (*mstree*) and the table-generating software (*msreport*, *mspie*) were separate programs but now they are included in *mrfitty*. *https://github.com/jklynch/mr-fitty.*

Section 2: Orthodox statistical methods applied to XANES data analysis in the usual way:

XAS spectroscopy usually relies on two main statistical methods. *Linear combination fitting* (LCF) of a reference database is used to assign proportions of different chemical species. *Principle component analysis* (PCA) is to a number of spectra and find the number of components in them such that the number of components is less than the number of spectra.

Linear combination fitting All the spectroscopy data in this study except for correlation-distance hierarchical clustering are direct results of linear combination fitting (LCF) of a reference database. Linear combination fitting is commonly described as a

Laplacian or classical statistical method. The origins of LCF are with the use of determinants to solve simultaneous linear equations by Liebniz in 1693 (Berlin-Brandenburg Academy of Sciences and the Academy of Sciences in Gottingen 190x). As applied here LCF is a reference-database-dependent analysis (Figure 1). **Figure 1.**

The model for linear combination fitting is:

Equation 1

$$f = \beta_0 + \beta_1 \mathrm{r}_1 + \beta_2 \mathrm{r}_2 + \cdots + \beta_q \mathrm{r}_q + \epsilon$$

Where Y is the measured spectrum, β_0 is a constant, β_1 to β_q are the coefficients of r_1 to r_q, the constituent parts, and ε is an error term representing noise. (James et al. 2014).

In practice, this model is applied through a linear least squares fitting (LLS) approach that estimates the coefficients $\hat{\beta}_0, \hat{\beta}_1, \hat{\beta}_2, \cdots, \hat{\beta}_q$ of reference components (predictors) and estimating the fit (solution).

Equation 2:

$$\hat{f}_i = \hat{\beta}_0 + \hat{\beta}_1 \mathrm{r}_1 + \hat{\beta}_2 \mathrm{r}_2 + \cdots + \hat{\beta}_q \mathrm{r}_q$$

In this context, "linear" means that a series of reference spectra are fit to an experimental spectrum by multiplying reference spectra (r_i) by a coefficient $\hat{\beta}_i$ and adding a constant to arrive at a fit.

The residual sum of squares (RSS) is then used to compare the fit outcome to the experimental spectrum and as a tool for ranking different fit outcomes. For the RSS, f_i is the measured fluorescence (experimental spectrum) at a given incident X-ray energy *i* and $\hat{f}_i$ is the estimated fluorescence (sum of fit component spectra) at given energy *i*.

Equation 3:

$$RSS = \sum_{i=1}^{n} (f_i - \hat{f})^2$$

Which can be expanded using Equation 2:

$$RSS = \sum_{i=1}^{n} (f_i - \hat{\beta}_0 - \hat{B}_1 r_{i1} - \hat{B}_2 r_{i2} - \cdots - \hat{B}_q r_{iq})^2$$

Equation 4.

where $\hat{\beta}_q$ is the estimated coefficient of the reference r_q at incident energy i. (James et al. 2014 pp 71-75).

In order to compare reference spectra of different lengths or with different numbers of sampling points (e.g. different energy resolution) it is necessary to compare the normalized sum of squares (NSS) of fits. NSS is the RSS divided by the number of points (incident X-ray energies) fitted.

By this method, using ALL the reference spectra will always produce the lowest NSS (James et al. 2014). In the standard LCF fitting approach, we generate a list of NSS ranked one, two, and three component fits using a variety of custom freeware packages (e.g. SixPack, Webb et al. 2005; ALS 10.3.2, Marcus et al. 2004). The number of allowable components is typically limited to a maximum of three or four components based on the sensitivity of the XANES method (detection limit) and the error associated with LCF (often difficult to assign for complex systems because the fitting is database dependent). However, the estimated error for LCF-derived components is often reported as 5 - 10 mol % on a per atom basis. In studies reporting calibration curves with simple binary and ternary mixtures, the error is lower but remains high relative to other analytical methods and is highly element and absorption-edge specific (e.g. 1 – 3 mol %

on a per atom basis for ternary mixtures of Mn(II), Mn(III), and Mn(IV); Bargar et al. 2000). For natural materials with a large number of chemical species and physical heterogeneity, a microprobe XANES approach can be used to effectively simplify the experimental spectra to counteract the 3-to-4 fit component limitation (for review; Toner, Nicholas, and Coleman Wasik 2014).

The components (i.e. reference spectra) included in LCF analysis are chosen to best represent the physical, biological, and chemical conditions present for the sample *in situ*. Vetting of the reference spectra database is often conducted prior to LCF through a database independent step that uses principle component analysis (PCA) and target transformation analysis (TTA) (Malinowski 1977; 1978; Manceau et al. 2002; Webb 2005; Toner et al. 2006; 2012).

Linear combination fits are also constrained to be physically realistic. For example, the reference components are not allowed to take on negative contributions (e.g. – 0.5 mol % pyrite is not allowed even when it improves the NSS). An LCF approach that is unconstrained by knowledge of the system being studied (geology, chemistry, mineralogy) will get the best NSS by using a large, and physically unrealistic, number of reference compounds, many with very small coefficients and near-equal contributions of similar references. The increment of improvement to the NSS will decrease as the number of references increases.

The detection limits and error estimates discussed above protect analysts against this potential problem, but ultimately the operator also has to have an understanding of chemistry and mineralogy of the system she is studying. As an anecdotal example, once

right after switching from measurements on As to Fe, I had two iron spectra that fit as mostly kamacite. This was extremely surprising because kamacite is elemental Fe and is pretty much only found in meteorites. As it turns out I had left the Fe foil (elemental Fe) that is used to calibrate the instrument in the holder behind the sample stage and enough x-rays were getting through the sample to fluoresce the foil. This is also a cautionary tale about always doing at least a rough fit right away as the data come in.

Both the 10.3.2 software and *mrfitty* solve for all the 1, 2, and 3 reference non-negative solutions and then report them in order of smallest NSS. In practice this method works quite well in that it provides good fits (low NSS) and sparse solutions that tend not to have closely-related constituent parts. If the operator wanted to, she could easily set either set of software to solve for more than three references but in practice this is unlikely to give a realistic solution.

Principal component analysis was invented independently by Karl Pearson (Pearson 1901) and Harold Hotelling (1933). It is an orthogonal transformation of data in which the principal component of the data is the one responsible for most of the variance in the dataset. Often a cloud of data points is described when using PCA. In this case we can imagine that the spectra are points in an n-dimensional cloud, and the first principal component is the longest of the vectors (Manceau et al. 2002). The components determined by PCA are not reference spectra, they are vectors through an n-dimensional cloud of datapoints. The second principal component is the longest vector orthogonal to the first one. In the case of XANES data, PCA is used to query a set of sample spectra to see if they can be described (expressed) as a smaller number of basis spectra. These basis

spectra are abstract components; they are not reference spectra. The first principle component typically looks like a smoothed average of the queried XANES sample spectra, and the subsequent components (orthogonal to the first) don't even look like XANES spectra.

Target transformations can be used to identify references spectra that are good candidates for constituent parts of the abstract spectrum. They are used by removing all the features of the reference spectra that are not present in the abstract spectrum and then judging the extent to which the reference spectra are modified by the subtraction (Manceau et al. 2002). The difference between the reference spectrum before and after these features have been removed can be evaluated objectively following the SPOIL method of Malinowsky (1978). This method quantifies changes in the fit error when abstract spectra are replaced by a references spectrum. The reference spectra can then be chosen based on their SPOIL numbers where lower numbers (smaller fit error) are better. Malinowski's indicator function (1977) is often used as a guide to the number of reference spectra to be used in fitting.

Principle component analysis is useful for data compression, description, and visualization (Marcus and Lam 2014). It has been used successfully to limit the number of reference spectra allowed in LCF fits (Ressler et al 2000). Its use for this purpose requires that the system from which the samples spectra comes is well understood.

Section 3: Novel applications of statistical methods:

Correlation-distance hierarchical clustering is statistical tool that is often used for pattern recognition and data mining. For the archived tills (Chapter 2) and the anaerobically preserved samples (Chapter 3) correlation distance $D_{x,y}$ was calculated between all pairs of spectra where x_{μ}^{i} is normalized fluorescence of the sample spectrum at incident energy *i*, $\bar{x}_{\mu}$ is the mean of the normalized fluorescence for the first spectrum, y_{μ}^{i} is the normalized fluorescence of the second spectrum at incident energy *i*, and $\bar{y}_{\mu}$ is the mean of the normalized fluorescence of the second spectrum:

(Equation 5)

$$D_{x,y} = 1 - \frac{\sum_{i=1}^{n} \left(x_{\mu}^{i} - \bar{x}_{\mu}\right)\left(y_{\mu}^{i} - \bar{y}_{\mu}\right)}{\sqrt{\sum_{i=1}^{n}\left(x_{\mu}^{i} - \bar{x}_{\mu}\right)^{2}}\sqrt{\sum_{i=1}^{n}\left(y_{\mu}^{i} - \bar{y}_{\mu}\right)^{2}}}$$

Correlation-distance fitting is relatively insensitive to scaling (D'haeseleer 2005) because of the centering in the numerator. All the spectra are compared two at a time and the mean is subtracted from each data point in each spectrum, so spectra with peaks in phase with each other correlate well and have a smaller correlation distance than peaks that are out of phase (Figure 2). This makes correlation-distance fitting useful for comparing the raw spectra among themselves (database independent) but not very good for evaluating composition (Friedman and Alm 2012).

Using correlation distance we were able to quantify the similarities among the spectra themselves without reference to their fits with reference spectra. It is a database-independent method of comparing spectra and of all the methods used involves the least

interpretation. Linear-combination fitting requires that a database be chosen and cosine-distance clustering uses the results from linear-combination fitting.

In most cases, the sample spectra resembled other sample spectra more closely than they resembled any of the reference spectra. This is consistent with particles that are weathering. It would have been very surprising if the spectra had closely resembled those of lab-synthesized standards or reference materials from the Smithsonian.

The As XANES spectra did not cluster by stratum, rather they clustered together in a way that was consistent with the proportions of different As species present in the particles as indicated by the linear least-squares fitting. The sampling for point XANES was non-random and skewed towards denser particles (Chapter 2 Section 3.7). The As XANES correlation distance hierarchical clustering data were interpreted as showing stages of convergent weathering from a reduced As sulfide end-member to an As(V) end-member that was present to some degree in all the sampled strata.

Fe XANES sample spectra clustered by strata in all three of the archived core data sets (Chapter 2 Figures 5.a-f) and in the anaerobic core data set (Chapter 3 Figures 7 and 8) although it was much weaker in the Fe XANES from core UMRB2 (archived till) than in the other three cores. Fe XANES spectra were collected only where Fe was co-located with As, because the samples contain approximately10^4 times more Fe than As. The stratum-specific clustering seen in Fe XANES is interpreted as reflecting the Fe parent material with which the As interacts.

The initial impetus for using correlation distance was to look at “chemistry agnostic” differences between the spectra, because I wanted to know how consistently I was

calibrating and normalizing my data. At the time I was curious about the difference between samples that I had measured on different days. I thought this would be a good way to be sure that all the data collected on a particular day didn't group together because of an artifact of my processing. I didn't find any obvious indication of an artifact effect, but most of the spectra from a stratum of a core are measured during the same beamtime. I typically got through one core (3 or 4 strata per core) or fewer during a single beamtime, using the same initial calibration.

That the As data showed no clustering by stratum tends to support the idea that artifacts were less important than chemical differences in the samples but I don't think they could be said to *prove* that. The correlation distance data turned out to be useful and illustrative, but not for the reason I had initially intended.

Cosine-distance hierarchical clustering is frequently used to analyze similarity in compositional data because it can accommodate a large number of components without introducing scaling artifacts (Friedrich and Alm 2012). It is a popular method used to illustrate patterns of gene expression within a group of organisms (Eisen et al 1998) and is also a common method used in data mining to evaluate document similarity and for name disambiguation in search engines.

Equation 6:

$$Cosine\ distance\ =\ 1\ -\ \frac{\sum_{i=1}^{m} u_i\ v_i}{\sqrt{\sum_{i=1}^{m} {u_i}^2}\sqrt{\sum_{i=1}^{m} {v_i}^2}}$$

where u_i and v_i are the fractional contribution of each broad group at *m* spots.

This can be used to make a heat map by placing two dendrograms normal to each other, clustering the data in two dimensions. A heat map is a graphical approach that displays the hierarchy of a matrix using colors. (Wilkinson and Friendly 2008).

The fractions of broader species categories for the co-located Fe and As XANES point spectra were used to generate a heat map and cosine-distance dendrograms to illustrate the relationship between As and Fe among the individual points and to identify populations of point types within the samples from both the archived cores (Chapter 2 Figures 6.a-c) and the anaerobically preserved core (Chapter 3 Figure 9).

Heat maps made in this way can be seen in Chapter 2 Figures 6.a-c and in Chapter 3 Figure 9. The horizontal dendrogram quantifies the similarity among the fit composition of the sample spectra according to cosine distance, where in the horizontal u and v are the fractional contribution of each broad group at m spots. In the vertical dendrogram u and v are the fractional contribution of each spot to m broad groups. This quantifies the co-occurrence of the broad reference categories among the spots.

Tables showing all the reference spectra used, correct citation for each reference and the broader category to which the reference was assigned can be found in Appendix 2.

Cosine-distance hierarchical clustering was applied to the database-dependent LCF results for both As and Fe speciation. It is the *most interpreted* analysis in the study and it relies on several assumptions but the most significant are:

1) It uses LCF fitting data which limits the fits to references within the database.

2) It normalizes the fits to those references to 100%.

3) It only addresses Fe that is co-located with As, and removes from consideration Fe primary silicates (minerals that form from melts were excluded).

Important differences between the correlation-distance clustering and cosine-distance clustering.

Correlation-distance clustering was used on the spectra themselves, and treats them as squiggly lines. It can compare two squiggly lines at different scales by centering the data (Figure 3). The $\left(x_{\mu}^{i} - \bar{x}_{\mu}\right)$ terms are subtracting the average from each point. It would be inappropriate to use a centering method like correlation-distance fitting on the composition from the linear combination fitting, because those data *have already been centered* by being set to 100% in the LCF. By this method any two-component mixture is constrained on a line (**Figure 4**); any three-component mixture is constrained on a plane; a four component mixture is constrained on a volume, and five or more components are constrained on different hyperplanes.

Section 4: Examining Linear Least squares fitting subset selection methods: In this study I used linear combination fitting (Section 2) for balancing goodness of fit with sparse solutions. The single-reference solution with the lowest NSS was identified, and the two-sample solution with the lowest NSS was identified and compared with the lowest single-spectrum NSS. If the NSS of the two-sample spectrum was a 10% or more improvement (reduction) in NSS then that solution supplanted the single-reference solution. If the three-reference solution with the lowest NSS was a better than 10%

improvement over the two-solution fit then the three-reference solution superseded the two-reference solution. Using this method I did not allow solutions with more than three references. Both the 10.3.2 software and *mrfitty.py* solve for all the 1, 2, and 3 reference non-negative solutions and then report them in order of smallest NSS.

I was curious about other ways to limit the set size and tried a LLS variant called the LASSO (Tibshirani 1996) which seeks sparse solutions by punishing solutions that contain a large number of references. Essentially a penalty is imposed for every additional component, so as the set grows larger the bar is raised higher. The user can run *mrfitty* either following the 10% NSS improvement method or using the LASSO. The surprise in running with the LASSO is that while it gave mathematically sparse solutions, they often had 6-9 components. Nine iron references out of a reference set of 68 iron reference spectra are a sparse set to a statistician. These solutions did not agree well with the error of the measurements or with the physical realities of the glacial sediments.

I am curious about other methods of subset selection. From a mathematical perspective, one that I think might be very good is called cross validation. It works by randomly removing a fraction of datapoints, fitting a solution to the remaining data (via LSS or another method). The goodness of fit would then be evaluated by the RSS of the held-out datapoints (James et al 2014).

From the mineralogy point-of-view, another method that would be interesting to pursue would be one that would penalize solutions that contain very similar references. In practice, this doesn't happen very often with the current method, especially when the

quality of the measured sample spectrum is high. By high quality I mean lots of counts so that the noise tends to average itself out of the spectrum. By this metric, the Fe spectra in this study are high quality and the As spectra are of low quality; a lot of noise persists in the As sample spectra. "First-cousin fits", where two of the references in a solution are very similar, occurred fairly frequently in the arsenic fits and very infrequently in the Fe fits. One way to limit fits with similar references would be to punish the addition of a similar second reference. Similarity could be assigned based on chemistry, for example by grouping together Fe oxyhydroxides. It could also be assigned arbitrarily by not permitting the addition of a component that was within a certain correlation distance of a component already included in the fit.

Section 5: Applying Cosine-distance hierarchical clustering to dissolution chemistry data

We had a large dataset of dissolution chemistry from the USGS analysis of the different till samples. So far I had only made use of the arsenic, iron and sulfur data from the archived cores and from CYR-1. We also had dissolution chemistry from 10 cores collected in southern Minnesota during the winter of 2010 as part of the Minnesota Geological Survey Southern County Atlas project. These cores were collected for County Atlases of Nicollet, Sibley, and Blue-Earth Counties. Our intention was to also do spectroscopy on samples from these cores, but they thawed in a freezer failure the summer after they were collected. Aliquots for wet chemistry had already been sent away for analysis and when the data came back they were effectively orphaned, because

we didn't have well-preserved core samples to which we could attach them. In examining these data Laurel Woodruff (USGS) had found a weak correlation between Fe and S using a logarithmic transform.

I was curious about whether different named till groups could be identified using cosine-distance clustering on the dissolution chemistry. The method is intended for compositional data like these. So far this has not been successful. First I tried all the samples of named tills (I did not include unnamed till samples, lacustrine samples or stream sediment) and all the measured chemical concentrations, then I tried all the named tills and all the major elements, then all the named tills and all the trace elements. No patterns emerged that seemed related to the different till groups. Then I limited the till samples to the "unaltered" tills to remove samples that had signs of weathering. No patterns emerged that seemed related to the different till groups, or to the general flow path of the Des Moines lobe where the tills were deposited.

The way tills are identified is through the lithic composition of the coarse-sand size fraction, and we had dissolution chemistry on the matrix, having removed the pebble and sand size fraction. So it may be that the relationship between the lithic composition and the fine-grained matrix sediments of the tills is not very strong. The composition of the till matrix can be diluted with different amounts of sand (quartz dilution) but because the method relates the relative proportions of different components that should not have mattered. I have not resolved this to my satisfaction.

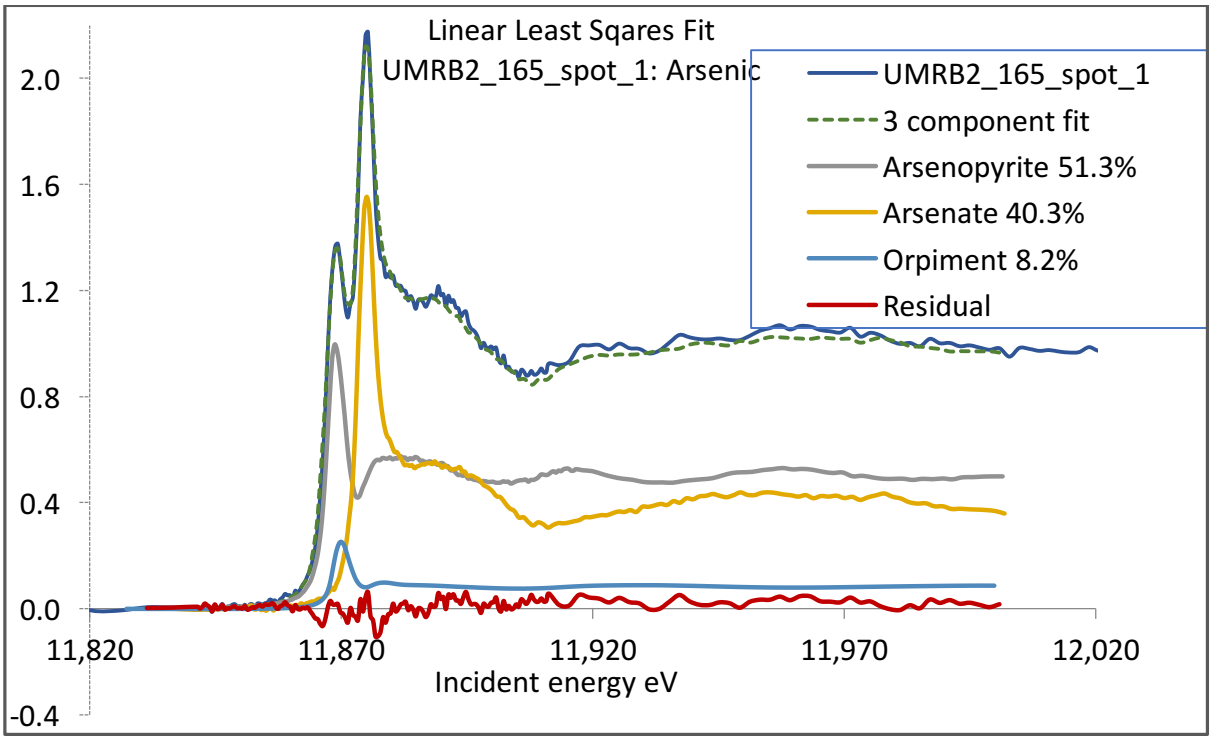

Figure 22 Example of linear combination fit (LCF) of an experimental As XANES spectrum, with three reference spectra.

The blue line is the normalized experimental spectrum, the three references have been combined to produce the 3-component best fit (dashed green line). The red line is the residual, which is the part of the sample spectrum left unaccounted for by the 3 component fit.

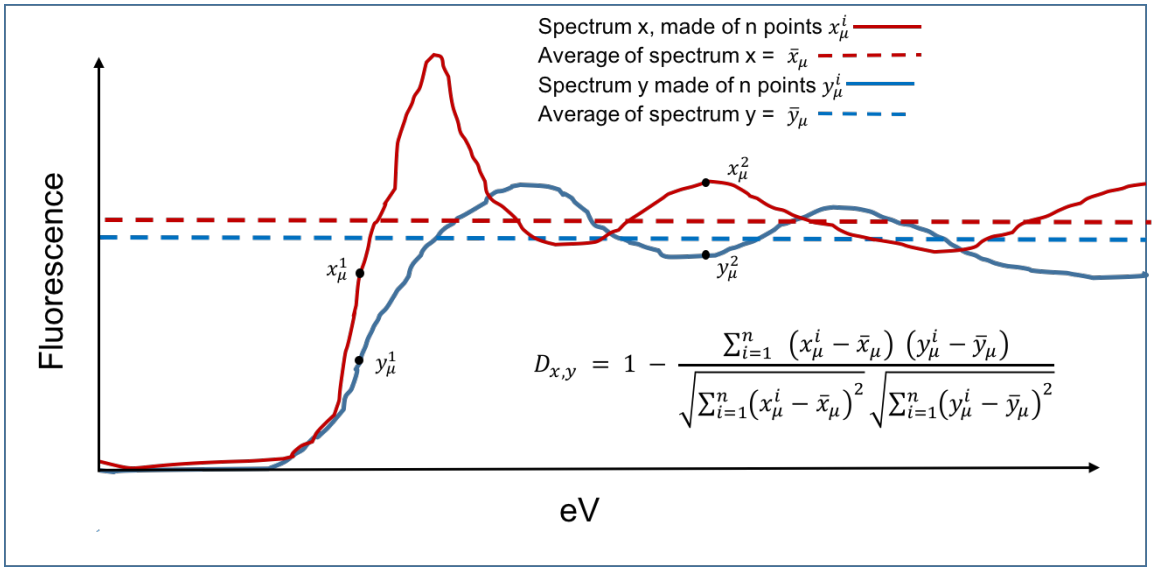

Figure 23 Example showing how correlation distance approaches zero when spectra are in phase and approaches one when spectra are out of phase.

At point 1 we see that both spectrum x and spectrum y are below their average, each term in the numerator is negative, so correlation is positive and correlation distance is small (closer to zero). At point 2 we see that spectrum x is above its average while spectrum y is below its average, so correlation is negative, and correlation distance is large (closer to one).

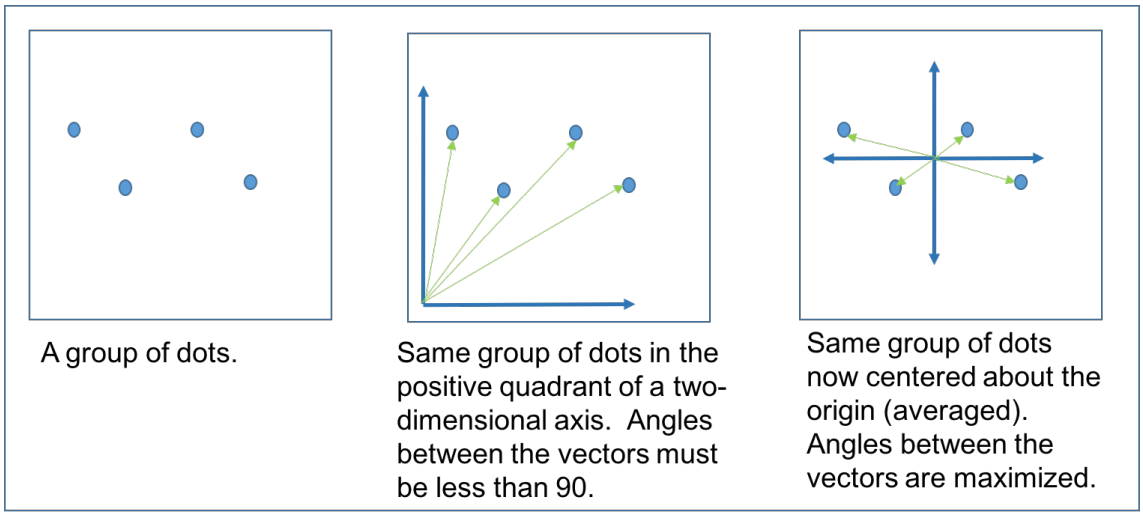

Figure 24 Cartoon illustrating effect of centering data for illustrating correlation

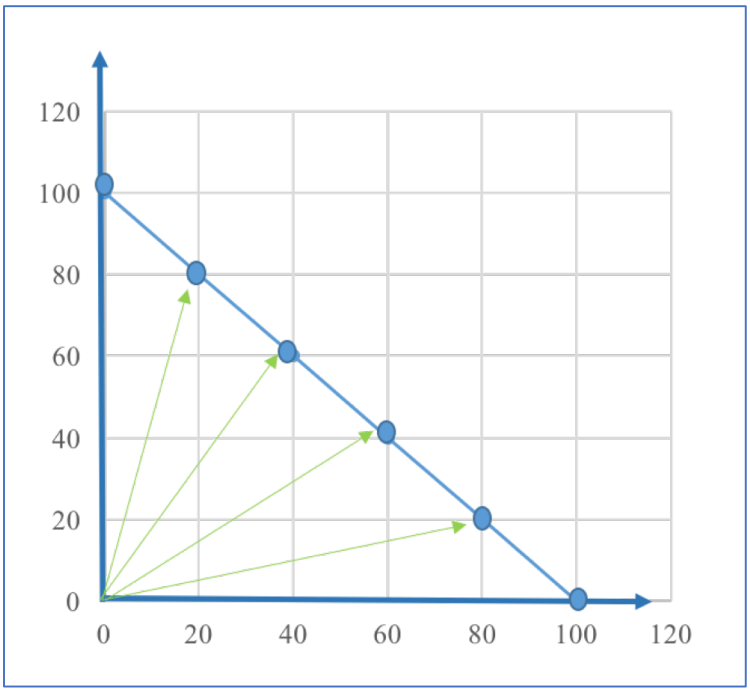

Figure 25 Cartoon showing the effect of normalizing compositional data to 100%.

CHAPTER 5: CONCLUSIONS AND FUTURE DIRECTIONS

This dissertation is predicated on the paradigm articulated by McMahon (2001) that hydrogeochemical gradients found at interfaces between different sediment types create active biogeochemical reaction zones.

Model and its assumptions: I used a thought experiment as a tool to predict what the effect of different processes acting on the solids would have on the water, and then compared the water chemistry of wells that were above and below the 10 μgL^{-1} US EPA MCL for arsenic. This was a very simple model that said that:

1) Oxidative dissolution of As-bearing sulfides would lead to elevated As, Fe and sulfate.

2) Reductive desorption of As sorbed to oxides would lead to elevated As without elevated Fe or sulfate.

3) Reductive dissolution of As co-precipitated with oxides would lead to elevated As and Fe without elevated sulfate.

Within that model I could go through the wells near the cores that were above and below the MCL and then ask "Do the solids present in these sediments support the process suggested by the model"?

The strong point of the model is that it allows for the formation of testable hypotheses. The weakest points of any model lie in its assumptions and this model is predicated on

the assumption that the water chemistry from single-time sampling of well water accurately reflects water chemistry in the minute pore-spaces of the sediment water-interface. We know this assumption to be false.

Chapter Two is a study of solid-phase As speciation on archived tills from cores collected in Grant, Pope, Stevens and Ottertail counties in western Minnesota. Chapter Three is a study of solid-phase As speciation on glacial sediments from Clay County, Minnesota, preserved anaerobically at the time the core was collected. All the cores are within the footprint of the Des Moines Lobe but there are geologic, land-use, and well-distribution differences between locations of the archived cores and the fresh core. The area of the archived cores is mostly farmland, and the domestic wells tend to lie along the grid of sections as demarcated by the 1831 US Land Survey, as do the roads. The area near CYR-1 has fewer farms and more wetland and marginal land. Near CYR-1 the roads follow the topography and there are dispersed houses with private wells, as well as clusters of houses with private wells in unincorporated settlements (Chapter 3 Figure 1). This distribution did not lend itself well to the 10km buffer method because there were few wells within 10km of core CYR-1, but it has the potential to allow closer examination of dense clusters of wells with As concentrations above and below $10 \mu g L^{-1}$. These clusters are not close to any existing or currently planned stratigraphic core.

This dissertation project is rooted in earlier work by Welch, that identified the glacial strata as the source of arsenic to groundwater and in the work of Erickson and Barnes that identified the tills as the solid-phase As reservoir and the aquifer-aquitard interface.

What I have found is that they were right. As bearing sulfide mineral in the tills appear to be the parent material, and reducing conditions can liberate As(V) sorbed to Fe(oxyhydr)oxides to waters. Over time I think what is happening is: the oxidative dissolution of As-bearing sulfides liberates As to waters and where this oxidative dissolution is incongruent some As is retained on the Fe(oxyhydr)oxide weathering product as sorbed and co-precipitated As. Arsenic sorbed to and co-precipitated with the oxidative weathering products can later be released by reducing conditions. The surprising discovery of my work is that both of these processes: the oxidation of As in sulfides and reduction of sorbed and co-precipitated As(V), appear to be occurring very close in time, very close in space, or both. I think the most interesting new direction that this work could take next is exploring the extent to which this may be reversible, in that low temperature and pressure reducing conditions with high As and high sulfate may lead to the precipitation of microcrystalline and cryptocrystalline daughter products.

This is not the dissertation I imagined writing in 2010. I expected to have identified a single, well-defined solid-phase source of arsenic and a single mechanism releasing it to waters. I thought I would have completed that part, and that I'd be moving into a regional predictive model by 2013, and I hoped to have it all wrapped up by 2014.

It is my hope that my work can be used to inform arsenic release and mitigation strategies for local governments, and guidelines for well drillers. For now, the best advice is still based on the 2005 work of Erickson and Barnes: wells with longer screens, farther from the confining layer, are less likely to have elevated As.

REFERENCES:

Akai, J., Izumi, K., Fukulara, H., Masuda, J , Nakano, S., Yoshimura, T., Ohjuki, H., Anarwarf, H.M., and Akai, K. (2004) Mineralogical and geomicrobiological investigations on groundwater arsenic enrichment in Bangladesh. *Applied Geochemistry*. 19,215-230.

Atlas R. M. (2004) *Handbook of Microbiological Media, Third Edition*., Taylor & Francis.

Ayotte J. D., Montgomery D. L., Flanagan S. M. and Robinson K. W. (2003) Arsenic in Groundwater in Eastern New England: Occurrence, Controls, and Human Health Implications. *Environ. Sci. Technol.* **37**, 2075–2083.

Bamburak, J.D. (2008) Cretaceous chemostratigraphic database and whole-rock and trace-element analyses for southwestern Manitoba (NTS 63F, G and H4); Manitoba Science, Technology, Energy and Mines, Manitoba Geological Survey, Data Repository Item DRI2008003, Microsoft® Excel® file.

Bannerjee, K, Amy, G.L., Prevost, M., Nour, S., Jekel, M., Gallagher, P.M., Blumenschein, C.D. (2008) Kinetic and thermodynamic aspects of adsorption of arsenic onto granular ferric hydroxide (GFO). *Water Research*. **42**, 3371-3378.

Bargar J. R., Tebo B. M., Villinski J. E. (2000) In situ characterization of Mn(II) oxidation by spores of the marine Bacillus sp. strain SG-1. *Geochim. Cosmochim. Acta.* **64**, 2775–2778.

Benner S. G., Polizzotto M. L., Kocar B. D., Ganguly S., Phan K., Ouch K., Sampson M. and Fendorf S. (2008) Groundwater flow in an arsenic-contaminated aquifer, Mekong Delta, Cambodia. *Appl. Geochem.* **23**, 3072–3087.

Bennett, B. and Dudas M.J. (2003) Release of arsenic and molybdenum by reductive dissolution of iron oxides in a soil with enriched levels of native arsenic. *Journal of Environmental Engineering Science.* **2**, 265-272.

Berg, J. A. (2006) Hydrogeology of Buried Aquifers *County Atlas Series, Atlas C-15, Geological Atlas of Pope County, Minnesota, Part B, Plate 7 of 9*. State of Minnesota, Department of Natural Resources, Division of Waters.

Berg, J. A. (2008) Hydrogeology of the surficial and buried aquifers *Regional Hydrogeological Assessment, Traverse-Grant Area, West-Central Minnesota, RHA-6, part B, Plates 3-6*. State of Minnesota, Department of Natural Resources, Division of Waters.

Bethke, C. (2008) *Geochemical and Biogeochemical Reaction Modeling.* Cambridge University Press, Cambridge. pp. 564.

Borch T., Kretzschmar R., Kappler A., Cappellen P. V., Ginder-Vogel M., Voegelin A. and Campbell K. (2010) Biogeochemical redox processes and their impact on contaminant dynamics. *Environ. Sci. Technol.* **44**, 15–23.

Borgaard, O.K. (1983) Effect of surface area and mineralogy of iron oxides on their surface charge and anion-adsorption properties. *Clays and Clay Minerals*. **31**(3), 230-232.

Briggs, P.H. and Meier A.L. (2002) The determination of forty-two elements in geological materials by inductively coupled plasma—mass spectrometry, Chapter 1 in Taggart, J.E., Jr., ed., *Analytical methods for chemical analysis of geologic and other materials,* U.S. Geological Survey: U.S. Geological Survey Open-File Report 02-0223, p. I1–I7. https://pubs.usgs.gov/of/2002/ofr-02-0223/

Bryndzia, L. and Kleppa, O.J. (1988) Standard molar enthalpies of formation of realgar (α-AsS) and orpiment (As_2S_3) by high-temperature direct-synthesis calorimetry. *The Journal of Chemical Thermodynamics*. **20**(6), 755-764.

Burgess W. G., Hoque M. A., Michael H. A., Voss C. I., Breit G. N. and Ahmed K. M. (2010) Vulnerability of deep groundwater in the Bengal Aquifer System to contamination by arsenic. *Nat. Geosci.* **3**, 83–87.

Chow, S.S. andTaillefert, M. (2009) Effect of arsenic concentration on microbial iron reduction and arsenic speciation in an iron-rich freshwater sediment. *Geochimica et Cosmochimica Acta.* **73**, 6008–6021.

Corkhill, C.L. and Vaughan, D.J. (2009) Arsenopyrite Oxidation – A review. *Applied Geochemistry*, **24**, 2342-2361.

Cramer, G. (1750) "Introduction à l'Analyses des Lignes Courbes algébriques". Geneva, Europeana pp 656-659.
Craw, D., Falconer, D. and Youngson, J.H. (2003) Environmental arsenopyrite stability and dissolution: theory, experiment, and field observations. *Chemical Geology*. **199**, 71–82.

Crock J. G., Lichte F. E. and Briggs P. H. (1983) Determination of Elements in National Bureau of Standards Geological Reference Materials SRM Obsidian and SRM Basalt by Inductively Coupled Argon Plasma -Atomic Emission Spectroscopy *Geostandards Newsletter*, **7**:2, 335-340.

Cullen, W. R. and Reimer, K. J. (1989) Arsenic speciation in the environment. *Chemical Reviews*. **89**, 713-764.

Cummings, D.E., F. Caccavo, S. Fendorf, R.F. Rosenweig, 1999. Arsenic mobilization by the dissimilatory Fe(III)-reducing bacterium Shaewanella alga BrY. Environmental Science and Technology 33:723-729.

D'haeseleer, P. (2005) How does gene expression clustering work? *Nature Biotechnology*. **23**(12), 1499-1501.

Eary, L.E. (1992) The solubility of amorphous As_2S_3 from 25 to 90ºC. *Geochimica et Cosmochimica Acta.* **56**:2267-2280.

Eisen, M.B., Spellman, P.T., Brown, P.O. and Botstein,D. (1998) Cluster analysis and display of genome-wide expression patterns. *Proc. Natl. Acad. Sci. USA*. **95**, 14863–14868.

Emerson D. and Merrill Floyd M. (2005) Enrichment and Isolation of Iron-Oxidizing Bacteria at Neutral pH. In *Methods in Enzymology* Academic Press. pp. 112–123.

Erbs, J.J., Berquo, T.S., Reinsch, B.C., Lowry, G.V., Banerjee, S.K. and Penn, R.L. (2010) Reductive dissolution of arsenic-bearing ferrihydrite. *Geochimica et Cosmochimica Acta.* **74**, 3382–3395

Erickson M. L. and Barnes R. J. 2004 Arsenic in Groundwater: Recent Research and Implications for Minnesota. *CURA Reporter*, **34**, 2, 1-7.

Erickson, M.L. 2005 Arsenic in Upper Midwest Ground Water: Occurrence and geochemical mobilization mechanisms. A dissertation submitted to the faculty of the graduate school of the University of Minnesota. Randall J. Barnes, advisor. 128pp.

Erickson, M. L. and Barnes, R. J. (2005a) Glacial sediment causing regional-scale elevated arsenic in drinking water. *Ground Water.* **43**, 796-805.

Erickson, M.L. and Barnes, R. J. (2005b) Well characteristics influencing As concentrations in ground water. *Water Research*. **39**, 4029-4039.

Erickson M. L. and Barnes R. J. (2006) Arsenic concentration variability in public water system wells in Minnesota, USA. *Appl. Geochem.* **21**, 305–317.

Foster, A.L., and C.S. Kim 2014 Arsenic Speciation in Solids Using X-ray Absorption Spectroscopy. Chapter 5 in *Arsenic: Environmental Geochemistry, Mineralogy, and Microbiology.* Robert J. Bowell, Charles N. Alpers, Heather E. Jamieson, D. Kirk Nordstrom, and Juraj Majzlan, editors. Mineralogical Society of America **79**, 257-370.

Friedman, J. and Alm, E.J. (2012) Inferring correlation networks from genomic survey data. Ed. Christian von Mering. *PLoS Computational Biology*. **8.9**, e1002687.

Gao, X., Wang, Y., Hu, Q. and Su, C. (2011) Effects of anion competitive adsorption on arsenic enrichment in groundwater. *Journal of Environmental Science and Health.* **46**, 1-9.

Goldberg, S., and Johnston, C.T. (2001) Mechanisms of arsenic adsorption on amorphous oxides evaluated using macroscopic measurements, vibrational spectroscopy, and surface complexation modeling. *Journal of Colloid and Interface Science.* **234,** 204–216.

Gotkowitz, M.B., Schreiber, M.E. and Simo, J.A. (2004) Effects of water use on arsenic release to well water in a confined aquifer. *Ground Water.* **42**(4),568-575.

Gowan, A.S. (2014) Quaternary Stratigraphy, County Atlas Series, Clay County. *Atlas C29 part A, Plate 4*. University of Minnesota, Minnesota Geological Survey.

Grosz, A. E., Grossman, J. N., Garrett, R., Friske, P., Smith, D. B., Darnley, A. G. and Vowinkel E. (2004) A preliminary geochemical map for arsenic in surficial materials of Canada and the United States. *Appl. Geochem.* **19**, 257–260.

Hansel C. M., Lentini C. J., Tang Y., Johnston D. T., Wankel S. D. and Jardine P. M. (2015) Dominance of sulfur-fueled iron oxide reduction in low-sulfate freshwater sediments. *ISME J.* **9**, 2400–2412.

Haque, S., Ji, J. and Johannesson, K. H. (2008) Evaluating mobilization and transport of arsenic in sediments and groundwaters of Aquia aquifer, Maryland, USA. *J. Contam. Hydrol.* **99**, 68–84.

Harris, K. L., Knaeble, A.R. and Berg, J. A. (1999) Quaternary Stratigraphy *Regional Hydrogeological Assessment, Ottertail Area, Minnesota MNRHA-6, part A, Plate 2*. University of Minnesota, Minnesota Geological Survey.

Harris, K. L. (2006) Surficial Geology *Regional Hydrogeological Assessment, Traverse-Grant Area, West-Central Minnesota, RHA-6, part A, Plate 1*. University of Minnesota, Minnesota Geological Survey.

Harris, K. L. and Berg, J. A. (2006) Quaternary Stratigraphy *Regional Hydrogeological Assessment, Traverse-Grant Area, West-Central Minnesota, RHA-6, part A, Plate 2*. University of Minnesota, Minnesota Geological Survey.

Harvey, C.F. Swartz, C.H., Badrussaman, A.B.M., Keon-Blute, N., Yu, W, Ali, M .A., Jay, J., Beckie, R. Niedan, V. Brander, D. Oates, P.M., Ashfaque, K.N., Islam, S. Hemond, H.F. and Ahmed M.F. (2002) Arsenic mobility and groundwater extraction in Bangladesh. *Science.* 298(5598), 1602-1606.

Harvey, C.F. and Beckie, R.D. (2005) Arsenic: Its biogeochemistry and transport in groundwater. In *Metal Ions in Biological Systems* (eds. A. Sigel, H, Sigel and R.K.O Sigel) Taylor and Francis, New York. pp. 145-169.

Hem, J.D., 1985. Study and interpretation of the chemical characteristics of natural water. USGS Water-Supply Paper 2254, Washington D.C. US Government Printing Office.

Hobbes, H.C. and A.S. Gowan (2014) Surficial Geology County Atlas Series, Clay County. *Atlas C29 part A, Plate 3*. University of Minnesota, Minnesota Geological Survey.

Hooyer T. S. and Iverson N. R. (2002) Flow mechanism of the Des Moines lobe of the Laurentide ice sheet. *J. Glaciol.* **48**, 575–586.

Hotelling, H. (1933) Analysis of a complex of statistical variables into principal components. *Journal of Educational Psychology* **24**:417-441.

Huerta-Diaz, M.A, and Morse, J.W. 1990 A quantitative method for determination of trace-metal concentrations in sedimnetary pyrite. *Marine Chemistry* 29, 2-3, 119-144. Hunter J. D. (2007) Matplotlib: A 2D Graphics Environment. *Computing in Science Engineering* **9**, 90–95.

IPCS (2001). Arsenic and arsenic compounds, 2nd ed. Geneva, World Health Organization, International Programme on Chemical Safety (Environmental Health Criteria 224; http://whqlibdoc.who.int/ehc/WHO_EHC_224.pdf).

Islam, F.S., R.L. Pederick, A.G. Gault, L.K. Adams, D.A. Polya, J.M. Charnock, J.R. Lloyd, 2005. Interactions between the Fe(III)-reducing bacterium Geobacter sulferreducens and arsenate, and capture of the metalloid by biogenic Fe(II). *Applied Environmental Microbiology*. 71:8642-8648.

Itai, T., Takahashi, Y., Seddique, A. A., Maruoka, T. and Mitamura, M. (2010) Variations in the redox state of As and Fe measured by X-ray absorption spectroscopy in aquifers of Bangladesh and their effect on As adsorption. *Appl. Geochem.* **25**, 34-47.

James, G., Witten, D., Hastie, T. and Tibshirni, R. (2014) *An Introduction to Statistical Learning with Applications in R.* Springer, New York, USA 426pp.

James, B.R. and Bartlett, R.J. (1999) Redox phenomena. In *Handbook of Soil Science*, (ed. M.E. Sumner) CRC Press, Boca Raton, Florida, USA.pp. 371-179.

Jennings C. E. (2006) Terrestrial ice streams—a view from the lobe. *Geomorphology* **75**, 100–124.

Jennings, C.E., Nicholas S.L., Gowan, A. S,, Adams, R.A. and Berg, J. A.(2015) Tracking arsenic up-ice from Minnesota. Geological Society of America North-Central Annual Meeting, Madison, WI, USA. #256113 (abstr.).

Jones, E., Oliphant, E., and Peterson, P. et al (2001-) SciPy: Open Source Scientific Tools for Python, http://www.scipy.org/

Kanivetsky, R. (2000) Arsenic in Minnesota Groundwater: Hydrogeochemical Modeling of the Quaternary Buried Artesian Aquifer and Cretaceous Aquifer Systems. St. Paul, Minnesota, Minnesota Geological Survey. Report of Investigation. 55pp.

Keon N. E., Swartz C. H., Brabander D. J., Harvey C. and Hemond H. F. (2001) Validation of an arsenic sequential extraction method for evaluating mobility in sediments. *Environ. Sci. Technol.* **35**, 2778–2784.

Kieft T. L., Fredrickson J. K., Onstott T. C., Gorby Y. A., Kostandarithes H. M., Bailey T. J., Kennedy D. W., Li S. W., Plymale A. E., Spadoni C. M. and Gray M. S. (1999) Dissimilatory reduction of Fe(III) and other electron acceptors by a Thermus isolate. *Appl. Environ. Microbiol.* **65**, 1214–1221.

Kocar B. D., Polizzotto M. L., Benner S. G., Ying S. C., Ung M., Ouch K., Samreth S., Suy B., Phan K., Sampson M. and Fendorf S. (2008) Integrated biogeochemical and hydrologic processes driving arsenic release from shallow sediments to groundwaters of the Mekong delta. *Appl. Geochem.* **23**, 3059–3071.

Kolker, A., Haack, S. K., Cannon, W. F., Westjohn, D. B., Kim, M.-J., Nriagu, J., and Woodruff, L. G. (2003) Arsenic in southeastern Michigan: in Welch, A. H., and Stollenwerk, K. G., eds., *Arsenic in Ground Water, Geochemistry and Occurrence*, Boston, Kluwer Academic Publishers, 488 p.

Lam, P.J., Ohnemus, D.C. and Marcus, M.A. (2012) The speciation of marine particulate iron adjacent to active and passive continental margins *Geochimica et Cosmochimica Acta*. **80**,108–124.

Langmuir, D., Mahoney, J. and Rowson, J. (2006) Solubility products of amorphous ferric arsenate and crystalline scorodite ($FeAsO4 *2H_2O$) and their application to arsenic behavior in buried mine tailings. *Geochimica et Cosmochimica Acta.* **70**, 2942-2956.

Liebniz, G.W. (1693) *Liebniz Series Three: Mathematical, Scientific, and Technical Correspondence 1672-1698.* Assembled and conserved by the Berlin-Brandenburg Academy of Sciences and the Academy of Sciences in Göttigen.

Lusardi B. A., Jennings C. E. and Harris K. L. (2011) Provenance of Des Moines lobe till records ice-stream catchment evolution during Laurentide deglaciation. *Boreas* **40**, 585–597.

Mai, N.T.H., Postma, D., Trang, P.T.K., Jessen, S., Viet, P.H. and Larsen, F. (2014) Adsorption and desorption of arsenic to aquifer sediment on the Red River floodplain at Nam Du, Vietnam. *Geochimica et cosmochimica acta.* 142,5587-600.

Malinowski, E. R., 1977. Determination of the number of factors and the experimental error in a data matrix. *Anal. Chem.* **49**, 612-617.

Malinowski, E. R., 1978. Theory of error for target factor analysis with applications to mass spectrometry and nuclear magnetic resonance spectrometry. *Anal. Chim. Acta* **103**, 339-354.

Manceau, A., Marcus, M. A. and Tamura, N. (2002) Quantitative speciation of heavy metals in soils and sediments by synchrotron x-ray techniques. In *Applications of synchrotron radiation in low-temperature geochemistry* (Eds. P.A. Fenter, M.L. Rivers, N.C. Sturchio, and S.R. Sutton) *Reviews in Geochemistry and Mineralogy*. 49, pp 579.

Marcus, M.A., Manceau, A. and Kersten, M. (2004) Mn, Fe, Zn and As speciation in a fast-growing ferromanganese marine nodule. *Geochimica et Cosmochimica Acta*, 68 (14) 3125–3136.

Marcus, M. A., MacDowell, A., Celestre, R., Manceau, A., Miller, T., Padmore, H. A. and Sublett, R. E. (2004) Beamline 10.3.2 at ALS: a hard X-ray microprobe for environmental and material sciences. *J. Synchrotron Rad.* **11**, 239-247.

Marcus, M.A. 2010. X-ray photon-in/photon-out methods for chemical imaging. *Trac-trends in analytical chemistry.* **29**(6), 508-517.

Marcus, M. A. and Lam P. J. (2014) Visualising Fe speciation diversity in ocean particulate samples by micro X-ray absorption near-edge spectroscopy. *Environ. Chem.* **11**, 10–17.

Mayhew L. E., Webb S. M. and Templeton A. S. (2011) Microscale Imaging and Identification of Fe Speciation and Distribution during Fluid–Mineral Reactions under Highly Reducing Conditions. *Environ. Sci. Technol.* **45**, 4468–4474.

McArthur, J.M., Banerjee, J.M. , Hudson-Edwards, K.A., Mishra, R., Purohit, R., P. Ravenscroft, Cronin, A., Howarth, R.J., Chatterjee, A., Talukder, T., Lowry, D., Houghton, S. and Chadha, D.K. (2004) Natural organic matter in sedimentary basins and its relation to arsenic in anoxic ground water: the example of West Bengal and its worldwide implications. *Applied Geochemistry*. **19**,1255–1293.

McMahon, P.B.(2001) Aquifer/aquitard interfaces: mixing zones that enhance biogeochemical reactions. *Hydrogeology Journal* **9**:34–43.

Meyer, G. N. (2015) County Atlas Series Atlas C-35 part A Meeker County plate 4 – Quaternary Stratigraphy. University of Minnesota, Minnesota Geological Survey.

Minnesota Department of Health (2001) *The Minnesota Arsenic Study (MARS)*. PB2001-101514. Cooperative Agreement and Grant Series. ATSDR Atlanta, GA, USA.

Minnesota Department of Health (2002) Public water supply water quality database. Data File.

Minnesota Geological Survey and Minnesota Department of Health (2004) Minnesota Computer Well Index. http://www.geo.umn.edu/mgs/cwi.htm

Minnesota Pollution Control Agency (1999) *Groundwater monitoring and assessment program GWMAPbaseline water quality of Minnesota's principal aquifers - Region 3, Northwest Minnesota*. Minnesota Pollution Control Agency, Environmental Outcomes Division, Environmental Monitoring and Analysis Section, Ground Water and Toxics Monitoring Unit. St. Paul, Minnesota. pp.66.

Nesbitt, H.W., Muir, I.J. and Pratt, A.R. (1995) Oxidation of arsenopyrite by air and air-saturated, distilled water, and implications for mechanism of oxidation. *Geochimica et Cosmochimica Acta,* **59**, 9 1773-1786.

Nesbitt, H.W. and Muir, I.J. (1998) Oxidation states and speciation of secondaryproducts on pyrite and arsenopyrite reacted with mine waste waters and air. *Mineralogy and Petrology* **62**:123-144.

Neumann, R., Ashfaque, H.N., A.B.M. Badrussamanm, M. Ashraf Ali, J.K. Shoemaker, C.F. Harvey, 2010. Anthropogenic influence on groundwater arsenic concentrations in Bangladesh. *Nature Geoscience* 3(1): 46-52.

O'Day, P.A., Vlassopoulos, D., Root, R., Rivera, N. and Turekian K.K. (2004). The influence of sulfur and iron on dissolved arsenic concentrations in the shallow subsurface under changing redox conditions. *Proceedings of the National Academy of Sciences of the United States of America.* **101**(38),13703-13708.

Oliphant T. E. (2007) Python for Scientific Computing. *Computing in Science Engineering* **9**, 10–20.

Ojakangas, R.W. and Matsch, C.L. (1982) *Minnesota's Geology*. University of Minnesota Press, Minneapolis, Minnesota, USA pp. 255.

Patterson, C.J. (1998) Laurentide glacial landscapes: The role of ice streams. *Geology.* 26(7),643-646.

Patterson, C.J., Knaeble, A.R., Setterholm and D. R. Berg, J.A. (1999) *Quaternary geology-upper Minnesota River basin, Minnesota [Part A].* Minnesota Geological Survey. Retrieved from the University of Minnesota Digital Conservancy, http://purl.umn.edu/59765.

Pearson, K. (1901) On lines and planes of closest fit to systems of points in space. *Philosophical Magazine* **2**(11):559-572.

Pickering I. J., Sneeden E. Y., Prince R. C., Block E., Harris H. H., Hirsch G. and George G. N. (2009) Localizing the chemical forms of sulfur in vivo using X-ray fluorescence spectroscopic imaging: application to onion (Allium cepa) tissues. *Biochemistry* **48**, 6846–6853.

Polizzotto, M. L., Harvey, C. F., Li, G. C., Badruzzman, B., Ali, A., Newville, M., Sutton, S. and Fendorf, S. (2006) Solid-phases and desorption processes of arsenic within Bangladesh sediments. *Chem. Geol.* **228**, 97-111.

Postgate J. R. (1984) *The sulphate-reducing bacteria*. 2nd ed., Cambridge University Press, Cambridge [Cambridgeshire] ; New York.
Prothero, D.R. and Schwab, F. (1996) *Sedimentary Geology: an introduction to sedimentary rocks and stratigraphy.* W.H. Freeman, New York. pp 557.

Quicksall A. N., Bostick B. C. and Sampson M. L. (2008) Linking organic matter deposition and iron mineral transformations to groundwater arsenic levels in the Mekong delta, Cambodia. *Appl. Geochem.* **23**, 3088–3098.

Richardson, S. and Vaughan, D. (1989) Arsenopyrite: a spectroscopic investigation of altered surfaces. *Mineralogical Magazine.* **53***,* 223-9.

Romero V., Costas-Mora I., Lavilla I. and Bendicho C. (2013) Insitu ultrasound-assisted synthesis of Fe3O4 nanoparticles with simultaneous ion co-precipitation for multielemental analysis of natural waters by total reflection X-ray fluorescence spectrometry. *J. Anal. At. Spectrom.* **28**, 923.

Root, R.A., Hayes, S. M., Hammond, C. M., Maier, R. M. and Chorover, J. (2015) Toxic metal(loid) speciation during weathering of iron sulfide mine tailings under semi-arid climate. *Applied Geochemistry.* DOI:10.1016/j.apgeochem.2015.01.005

Rossini, F.D., Wagman, D.D., Eavans W.H., Levine, S., Jaffe, I. (1952) Selected Values of Chemical Thermodynamic Properties, Circular of the National Bureau of Standards 500, U.S. Government Printing Office, Washington, DC.

Rowland, H.A.L., Pederick, R.L., Polya, D.A., Pancost, R.D., Van Dongem, B.E., Gault, A.G., Vaughan, D.J., Bryant, C., Anderson, B. and Lloyd, J.R. (2007) The control of organic matter on microbially mediated iron reduction and arsenic release in shallow alluvial aquifers, Cambodia. *Geobiology.* **5**, 281–292.

Rudnick R. L. and Gao S. (2003) Composition of the Continental Crust. *Treatise on Geochemistry* **3**, 659.

Saalfield S. L. and Bostick B. C. (2009) Changes in iron, sulfur, and arsenic speciation associated with bacterial sulfate reduction in ferrihydrite-rich systems. *Environ. Sci. Technol.* **43**, 8787–8793.

Schreiber, M.E and Rimstidt, J.D. (2013) Trace element source terms for mineral dissolution. *Applied Geochemistry*, **37**, 84-101.

Schreiber, M.E., Simo, J.A. and Freiberg, P.G. (2000) Stratigraphic and geochemical controls on naturally occurring arsenic in groundwater, eastern Wisconsin, USA. *Hydrogeology Journal.* **8**(2), 161-176.

Schwertmann, U. and Cornell, R.M. (1991) *Iron Oxides in the Laboratory: Preparation and Characterization*. John Wiley and Sons, New York 188pp.

Sims K. W. W., Newsom H. E. and Gladney E. S. (1990) Chemical fractionation during formation of the Earth's core and continental crust: clues from As, Sb, W, and Mo. In *Origin of the Earth* (Eds. H.E. Newsom and J.H. Jones) 291-317.

Smedley, P.L. and Kinniburgh, D.G. (2002) A review of the source,behaviour and distribution of arsenic in natural waters.*Applied Geochemistry.* **17**, 517–568.

Smith A. H., Hopenhayn-Rich C., Bates M. N., Goeden H. M., Hertz-Picciotto I., Duggan H. M., Wood R., Kosnett M. J. and Smith M. T. (1992) Cancer risks from arsenic in drinking water. *Environ. Health Perspect.* **97**, 259–267.

Slatt, R.M. and Eyles, N. 1981 Petrology of Glacial Sand: implications for origin and mechanical durability of lithic fragments. *Sedimentology*. **28**, 171-183.

Stuckey, J. W., Schaefer, M. V., Kocar, B. D., Dittmar, J., Pacheco, J. L., Benner, S. G. and Fendorf, S. (2015) Peat formation concentrates arsenic within sediment deposits of the Mekong Delta. *Geochim. Cosmochim. Acta* **149**, 190–205.

Stull, D. R., and Prophet, H., (1971) *JANAF Thermochemical Tables,* Second Edition, Nat. Stand. Ref. Data Ser., Nat. Bur. Stand. (U.S.), 37 (1971).

Taggart, Joseph E. (2002) *Analytical Methods for Chemical Analysis of Geologic and Other Materials, US Geological Survey*. US Department of the Interior, US Geological Survey. http://pubs.usgs.gov/of/2002/ofr-02-0223/

Taylor, S. R. and S. M. McLennan, 1985. The Continental Crust: its composition and evolution. Blackwell Scientific Publishers, Oxford; Taylor, S. R. and S. M. McLennan. 1995.

Tibshirani, R. (1996) Regression Shrinkage and Selection via the Lasso. *Journal of the Royal Statistical Society. Series B (Methodological)* 58:1 267-288.

Toner, B., Manceau, A., Webb, S. M., and Sposito, G., 2006. Zinc sorption to biogenic hexagonal-birnessite particles within a hydrated bacterial biofilm. *Geochim. Cosmochim. Acta* **70**, 27-43.

Toner, B.M., Nicholas, S.L., Briscoe, L.J., Knaeble, A.R., Berg, J.A. and Erickson, M.L. (2011) Natural sources of arsenic in Minnesota groundwater, *CURA Reporter.* **41**(3-4),3-10.

Toner, B.M., Marcus, M.A., Edwards, K.J., Rouxel, O. and German, C.R. (2012) Measuring the form of iron in hydrothermal plume particles. *Oceanography.* **25**, 209–212.

Toner, B. M., Nicholas, S. L., and Coleman Wasik, J. K. (2014) Scaling up: fulfilling the promise of X-ray microprobe for biogeochemical research. *Environmental Chemistry.* **11**, 4-9.

Toner, B. M., German, C. R., Dick, G. J. and Breier, J. A. (2016) Deciphering the Complex Chemistry of Deep-Ocean Particles Using Complementary Synchrotron X-ray Microscope and Microprobe Instruments. *Acc. Chem. Res.* **49**, 128–137.

Townshend, A. and Jackwerth, E. (1989) Precipitation of major constituents for trace preconcentration: potential and problems. *Pure&App/. Chem.* **61**, 1643–1656.

United States Natural Resources Conservation Service (2004) *Soil Survey Laboratory Methods Manual*. R. Burt Ed. United States Department of Agriculture Soil Survey Investigations Report No. 42.

van Geen, A., Bostick, B.C., Trang, P.T.K., Lan, V.M., Mai, N.N., Manh, P.D., Viet, P.H., Radloff, K, Aziz, Z., Mey, J.L., Stahl, M.O., Harvey, C.F., Oates, P., Weinman, B., Stengel, C., Frei, F., Kipfer, R. and Berg, M. (2013) Retardation of arsenic transport through a Pleistocene aquifer. *Nature.* **501** (7466), 204-207.

van 't Hoff, J.H. (1874) Sur les formules de structure dans l'espace. *Archives neerlandaises des sciences exactes et naturelles*. **9**,445-454.

Wagman, D.D., Evans, W.H., PArker, V.B., Schumm, R.H., Halow, I., Baily, S.M., Churney, K.L. and Nuttal, R.L. (1982) The NBS tables of chemical thermodynamic properties - selected values for inorganic and C-1 and C-2 organic substrances in SI units. *Journal of physical and chemical reference data.* **11.** http://www.nist.gov/data/PDFfiles/jpcrdS2Vol11.pdf

Walker, F.P., Schreiber, M.E. and Rimstidt, J.D. (2006) Kinetics of arsenopyrite oxidative dissolution by oxygen, *Geochimica et Cosmochimica Acta.* **70**, 1668-1676.

Webb, S. M., 2005. SIXPACK: A graphical user interface for XAS analysis using IFEFFIT. *Physica Scripta* **T115**, 1011-1014.

Weber, F.-A., Hofacker, A. F., Voegelin, A. and Kretzschmar, R. (2010) Temperature dependence and coupling of iron and arsenic reduction and release during flooding of a contaminated soil. *Environ Sci Technol.* **44**, 116-22.

Wedepohl K.H. (1995) The composition of the continental crust. *Geochim. Cosmochim. Acta* **59**, 1217–1232.

Welch, A.H., Westjohn , D.B., D.R. Helsel, D.R. and R.B. Wanty, R.B. (2000) Arsenic in ground water of the United States: occurrence and geochemistry. *Ground Water.* **38**(4), 589-604.

West, N., Schreiber, M. and Gotkowitz, M. (2012) Arsenic release from chlorine-promoted alteration of a sulfide cement horizon: evidence from batch studies on the St. Peter Sandstone, Wisconsin, USA . *Applied Geochemistry.* **27**(11), 2215-2224.

Wilkinson, L. and Friendly, M. (2009) The History of the Cluster Heat Map. *The American Statistician*, **63**(2), 179-184.

World Health Organization 2010 Exposure to Arsenic: a major public health concern. Geneva, Switzerland. http://www.who.int/ipcs/features/arsenic.pdf?ua=1.

Wright, H.E. (1972) Quaternary history of Minnesota. In Sims, P.K. and Morey G.B, *Geology of Minnesota, a centenial volume.* (Eds. P.K. Sims and G.B.Morey) St.Paul, Minnesota, USA. pp. 547-560.

Yu, Y., Zhu, Y., Gao, Z, Gammons, C.H. and Li, D. (2007) Rates of arsenopyrite oxidation by oxygen and Fe(III) at pH 1.8-12.6 and 15-45ºC. *Environ. Sci. Technol*. **41**, 6460-6464.

Zeng, T., Arnold, W. A., and Toner, B. M. (2013) Microscale characterization of sulfur speciation in lake sediments. *Environmental Science & Technology*. 47, 1287-1296.

APPENDIX 1: SEQUENTIAL EXTRACTIONS ON ARCHIVED TILL SAMPLES

Synopsis An aliquot of each of 7 samples of the archived tills (Chapter 2 Tables 2,3, and 4) was put through a sequential extraction of arsenic as an operational measurement of speciation within the context of plausible groundwater conditions in Minnesota.

1. Motivation

Sequential extractions are a wet-chemical method used to quantify speciation of a sample operationally. A single aliquot of a sample is reacted with a series of chemical reagents. Each reagent is intended to liberate an operational species of arsenic. An example of an operational species is "strongly sorbed arsenic". Phosphate is a competing anion with arsenate and arsenite for sorption sites on iron oxides (e.g. ligand exchange with ortho-phosphate) (Banerjee et al. 2008; Gao et al. 2011). The amount of arsenic liberated to solution by reaction with phosphate is the "strongly sorbed arsenic" fraction. At the end of a sequential extraction the sum of the extracted arsenic from all the extractions is compared with the total concentration of arsenic in the sample (measured separately). If the protocol included every type of arsenic and the procedure were done perfectly, the sum of the As in the extractants would equal the total concentration of the sample.

Advantages of sequential extraction are that a single aliquot of sample is used, so a small amount of sample is needed, and because the same sample is used there is less danger that splits of a sample may contain different amounts of the different types of As. A denser mineral (like As-pyrite) could end up more concentrated in some splits if careful

protocols are not followed. Disadvantages of sequential extraction are that some As species may be mobile outside their targeted reagent, and any sample loss in the repeated process of extracting, centrifuging, decanting, washing, centrifuging and decanting will be propagated through the rest of the extraction. If the operator drops a sample or a tube breaks then the entire extraction has to be re-done, it is not possible to repeat just that step. To minimize the risk from sample loss the samples were extracted in duplicate.

There are also non-sequential extraction methods, called parallel extractions, in which separate aliquots of the same sample are extracted once, with one reagent each. Parallel extractions share with sequential extractions the disadvantage that some As species may be mobilized outside the targeted reagent. The sum of a parallel extraction usually exceeds the total As concentration of the sample. An advantage of a non-sequential extraction is that sample loss through handling error is not propagated, and a single extraction can be repeated if a sample is lost. Irregular splits are a greater danger for a non-sequential extraction, and much more sample is required. For this study, for most samples around 100 g of clean, unground sample was available after removing material that had been in contact with the drilling apparatus. This is roughly 250 times as much sample as was used in the extraction, 0.4 g. In most cases enough material was available to do a parallel extraction. However, to limit the danger of metal contamination of the sample, each aliquot for extraction (and for X-ray Absorption Spectroscopy) was ground to 150 μm by hand using ceramic, agate and corundum mortars. It would have been

extremely difficult to process enough sample for a parallel extraction using these methods.

2. Methods

An As sequential extraction method modified from Keon et al. 2001 was used for the archived tills (see Table A.1.1). For safety reasons the Keon et al. methods were modified by substituting a sodium dithionite and citrate solution (U.S. Natural Resources Conservation Service, 2004) for the titanium(III)-citrate and EDTA-bicarbonate" step as a strong reducing agent to liberate the operational species "As co-precipitated in amorphous Fe oxyhydroxides". The Keon et al. hydrofluoric acid step was removed entirely, without substitution, both for safety reasons and because As bound in silicate minerals is unlikely to be labile to natural waters. Their methods were further modified in that the samples were centrifuged longer but at slower speed, and I used a dilute NaCl solution instead of water to clear persistent suspended flocs in the post-$MgCl_2$ water washes.

Samples were prepared as described in Chapter 2 (Chapter 2, 3.4 Sample Processing). Outer parts of the core that had been in contact with the core barrel and drilling water were removed from the core and retained separately. In the case of aquifer materials that did not retain a regular shape, the portion for processing was collected from the innermost part in the core bag. The inner portion of the core was disaggregated in a ceramic mortar and pestle, and sieved to remove pebbles greater than 2 mm. The > 2 mm pebble fraction was retained separately. The < 2 mm fraction was then split and an aliquot of the sample (~ 50 g) was ground to < 150 μm using a corundum mortar and

pestle. The remaining split of the < 2 mm fraction was retained separately and subsequent splits of this < 2 mm fraction were subjected to sediment dissolution chemistry. The < 150 μm fraction was split into aliquots for dissolution chemistry, sequential extraction, and X-ray absorption spectroscopy.

Ground samples were weighed into 45 ml acid-washed Teflon centrifuge tubes. Attempts to use falcon tubes failed because the tubes did not survive centrifugation. Attempts to use LDPE centrifuge tubes failed because the snap-on lids snapped off in the vacuum of the airlock.

All glass, plastic, and Teflon was acid washed in 10% HNO_3. No metal was used. Reagents were introduced into the Teflon vials using serological pipettes.

All extractions were performed at room temperature except for EPA 3050B which was done at 95°C. Steps through the dithionite were undertaken in a Coy H_2N_2 anaerobic chamber with palladium-oxide O_2 scavenging plates mounted on recirculating fan boxes. The dithionite (strong reducing agent) was pipetted into the sample tubes in the glove box and then the samples were passed out of the anaerobic chamber and the dithionite tumble-shaking and all subsequent steps were done in ambient air. In general steps followed each other immediately with no down time, but during the interval between the room-temperature HNO_3 and the hot HNO_3 the sealed Teflon tubes were held overnight in the refrigerator.

Reagents for the anaerobic steps were mixed in the anaerobic chamber using N_2 sparged MilliQ water. Pre-weighed water for each reagent was sparged using an acid-washed sparging jig in pyrex autoclave bottles. Reagents were pre-weighed in small autoclave bottles, passed into the glove bag, uncapped and allowed to equilibrate with the H_2N_2 atmosphere.

Twenty-six samples and two blanks were extracted. Samples were 0.4 g of ground glacial sediment weighed and processed (shaken, centrifuged, decanted) in 40 mL of extractant solution as described above. The blanks contained no sample, these were Teflon tubes identical to those containing the sample, filled, shaken, centrifuged and decanted along with the sample-bearing tubes. Twelve of the samples run were duplicates of OTT3_73. A large volume of OTT3_73 was ground and homogenized to be used as a standard for several extractions. Six other samples were run in duplicate. One each of the OTT3_73, OTT3_74 and UMRB2_175 samples were dropped, burst, or otherwise lost during the extraction.

Extracted solutions were analyzed via ICP-MS in the Aqueous Geochemistry Laboratory by Rick Knurr, Department of Earth Sciences, University of Minnesota-Twin Cities, on a Thermo Scientific XSERIES 2 ICP-MS w/ ESI PC3 Peltier cooled spray chamber, SC-FAST injection loop, and SC-4 autosampler. Samples were diluted appropriately and 20 ppb of Y internal standard was added. All elements except Li, B, P were analyzed using He/H2 collision-reaction mode.

3. Results

3.1 Proportions of As operational species as measured by sequential extraction

Table A.1.2 is a summary table showing the mean As concentration of each sample with each extractant solution. The 16 complete tables of all results from these extractions are appended as excel files with this document for the committee, and at the time of submission to the graduate school will be added to the UMN data depository. These tables are:

Nicholas seq extr MgCl2 (1) - trace stnd add – 010312

Nicholas seq extr MgCl2 (2) - trace stnd add – 010312

Nicholas seq extr MgCl2 (ww) - trace stnd add – 010312

Nicholas seq extr HCl(1) - trace stnd add – 122911

Nicholas seq extr HCl(ww) - trace stnd add – 122911

Nicholas seq extr NaH2PHO4(1) - trace stnd add – 122911

Nicholas seq extr NaH2PHO4(2) - trace stnd add – 122911

Nicholas seq extr NaH2PHO4(ww) - trace stnd add – 122911

Nicholas seq extr oxalate oxalic acid - trace stnd add – 123011

Nicholas seq extr oxalate oxalic acid (ww) - trace stnd add – 123011

Nicholas seq extr - NaDithionate citrate - trace stnd add – 123011

Nicholas seq extr NaDithionate citrate (ww) - trace stnd add – 123011

Nicholas seq extr HNO3 (1) - trace stnd add – 123011

Nicholas seq extr HNO3 (2) - trace stnd add – 123011

Nicholas seq extr - HNO3 (ww) - trace stnd add – 010312

Nicholas seq extr EPA 3050B - trace stnd add - 122911

Figures A.1.1-7 have the same axes so that differences in overall concentration of As in the samples can be seen as well as relative abundance of different operationally defined As species. Relative proportions of As liberated in in the extracted solutions are similar among most of the samples. In general, the largest amount of As released in the samples came from the room temperature nitric acid extractions, followed by nearly equal amounts of As released by the HCl and EPA 3060B (hot nitric acid) steps. Arsenic displaced by phosphate anion competition (strongly sorbed As) tended to make a more significant contribution in till samples than in outwash samples. Two of the three glacial aquifer samples (OTT3_73 and OTT3_75) had a more significant contribution of As from the ammonium oxalate step (As co-precipitated with amorphous Fe oxyhydroxides) than did till samples. The dithionite extraction liberated the least As in all samples. Arsenic displaced by $MgCl_2$ was proportionate (~ 10 %) to the overall As concentration in all samples. Arsenic concentration of the process blanks was low (Table A.1.1).

Some of the water washes had higher As concentrations than were measured in the extractant solutions. Arsenic concentrations in the phosphate water wash and the room temperature nitric acid water wash were often higher than the second extraction of the reagent. The As concentrations of the dithionite water wash were as high or higher than that of the extractant.

3.2 *Comparison of As concentration as measured by sequential extraction with As concentration determined by sediment dissolution*

Table A.1.4 is a comparison of the total As concentration in the samples as measured by the sum of the As liberated by sequential extraction, As as measured by hydride generation atomic absorption (HG-AA) at the USGS contract lab, As measured by 4 acid digestion and ICP-MS at the USGS contract lab, and As measured by acid digestion at the UMN Earth Sciences ICP-MS lab (Rick Knurr).

Total As concentrations from the sequential extractions were higher than the total concentrations of arsenic measured by USGS or by UMN. This difference is particularly striking in OTT3_73, the working standard. Eleven separate aliquots of < 150 μm OTT3_73 were extracted and analyzed by ICP-MS at UMN (n=11, stdev=1.1). Three separate aliquots of < 150 μm OTT3-73 were digested and analyzed by ICP-MS at UMN (n=3, stdev=0.32), and one aliquot of < 2 mm OTT3-73 was digested and analyzed using HG-AA and ICP-MS at the USGS contract lab.

3.3 Comparison of As speciation as measured by sequential extraction with As speciation measured via As speciation mapping

There are As speciation maps for two of the extracted samples: OTT3-73 (glacial stream sediment, aquifer) and OTT3-74 (contact till, aquitard). Figures A.1.8 and 9 and Figures A.1.10 and 11 show the fractions of operationally defined As based on the sequential extraction and the As species measured directly via XAS As speciation mapping. Colors were chosen to match groups where the direct measurement speciation and operational speciation would tend to agree. The HCl extraction step was not matched to a direct measurement because it is designed to target many operational categories of As: As co-precipitated with acid volatile sulfides, carbonates, manganese oxides, and very amorphous Fe oxyhydroxides (Keon et al. 2001).

In both OTT3_73 and OTT3_74, the As(III) fraction as defined by As speciation mapping is larger than the operationally defined ionically bound As (As liberated by $MgCl_2$). As-sulfide as defined by As speciation mapping is approximately the same fraction as the combined As liberated by HNO_3 and EPA3050b in OTT3_73. The combined HNO_3 and EPA3050b fraction is somewhat less than the As sulfide fraction as defined by As speciation mapping in OTT3_74. In both OTT3_73 and OTT3_74 the combined phosphate, ammonium oxalate, and citrate-dithionite labile fraction is very close to the fraction of As(V) as defined by As speciation mapping.

4. Discussion

The source of the difference in measured As concentration between the sum of the sequential extraction and the 4-acid sediment dissolution by the USGS and UMN labs is difficult to diagnose. Arsenic concentrations in blanks was low (Table A.1.2), so reagent contamination does not appear to be the cause of the difference between the extraction concentrations and the sediment dissolution concentrations. We would expect that a sequential extraction would have less total As than a complete digestion because of the potential for loss of As in the process of reacting and decanting in 16 different solutions. Reagent carryover in the sediment pellet could cause double counting of a small amount of As at each step within the series. This potential carryover could be calculated by estimating the porewater volume of the sediment pellet.

The difference is greatest between the sequential extractions and the USGS lab numbers (Table A.1.2). The simplest explanation for this is that the sequential extractions and the UMN ICP-MS samples were run on < 150 μm ground samples, the USGS lab worked on the < 2 mm size fraction. It is possible that some As was protected from the 4-acid digestion within large grains. The difference between the USGS and sequential extraction numbers is greatest on two of the outwash samples OTT3_73 and OTT3_75. Samples for sequential extraction and the UMN digestion were homogenized by rolling on paper before aliquots were split. The < 2 mm fraction for USGS was also homogenized by rolling and then split but the entire sample was not used. Small-mass

samples of homogenized coarse material have a greater potential to be different from each other than the same mass samples of homogenized finely ground material.

The final step of the sequential extractions is EPA 3050B, a day-long refluxing digestion in hot peroxide and nitric acid. If we subtract the As extracted in 3050B from the sum of the sequential extractions then the total As concentration from the sequential extraction is closer to the UMN digestion numbers. Both the USGS method (Taggart; Briggs and Meier 2002) and the UMN digestion include a hot nitric acid step but the quantity of nitric acid is low and the length of the digestion in shorter (minutes rather than hours). The USGS and UMN digestion both include a hydrofluoric acid step which was excluded from the sequential extraction method.

Concentrations were more similar between the USGS and UMN digestion results but the UMN results were higher overall, and closer to the concentrations from the summed sequential extractions.

Analytical Challenges

Originally it was intended that that the sequential extractions would be a high-throughput method for looking at As speciation in the samples, and that we would select samples for spectroscopy based on results of sequential extractions. A new atomic absorption spectrometer with a hydride-generator inlet was purchased for these analyses. However, we could not get replicable measurements over the course of a two-hour run with the inlet

as it was installed by the manufacturer. Absorption peaks flattened, delayed and extended past the analytical window of the instrument after the first few standards had been run. This was because liquid sample was getting into the inlet downstream of the gas-liquid separator. The reaction vessel of the gas-liquid separator was not always able to contain droplets produced by the reaction and these were carried into the inlet. Ed Nater advised and showed me how to build a deeper, narrower gas-liquid separator out of Teflon parts. After building the Ed model and adjusting the sample timing for the different volume the problem occurred less frequently. Chilling the $NaBH_4$ reductant and the HCl carrier to 4° C also lowered the incidence of droplets entering the gas-inlet line and improved results somewhat but over the course of a run caused leaking in the switching valve, because of thermal contraction of the fitted parts and O-rings. Somewhat better results (fewer droplets but no leaking) were achieved by chilling the $NaBH_4$ but leaving the HCl at room T, but we could not get consistent results on standards over the course of a run.

Only after Toner lab technician Michael Ottman worked on the AA for several weeks and installed an inline sample drier could we get replicable results for the course of a run. During this we also discovered that several of the sequential extraction reagents had matrix incompatibilities with the hydride generator. Some of the extractants could not be pre-reduced using the method of the manufacturer (no reaction occurred) and others produced a precipitate that could not be run through the instrument.

During the struggle with the AA, which carried on over a period of months, XAS spectroscopy moved forward on the samples using sediment dissolution chemistry results (Chapter 2 Tables 2,3,4, Chapter 3 Table 1) to inform sample selection.

Table 19 Glacial sediment sequential extraction samples.

Sample Name	Sample Description	Depth (m)	[a]As mg/kg	[b]Fe %	[b]S %	Fe/S
OTT3-73	outwash sand and gravel (aquifer)	22.3	3.9	1.83	0.43	4
OTT3-74	Upper Goose Formation contact till (aquitard)	22.6	7.8	2.79	0.44	6
OTT3-75	outwash sand and gravel (aquifer)	22.9	3.1	1.31	0.21	6
OTT3-184	James River till (aquitard)	56.1	7.9	1.98	0.59	3
TG3-149	Gervaise formation till (aquitard)	45.4	8.4	2.87	0.53	5
UMRB2-175	sand and gravel (aquifer)	53.3	6.6	1.7	0.55	3
UMRB2-176	unnamed till (aquitard)	53.6	7.8	1.88	0.52	4

Table 20 Sequential extraction procedure

Target Operational Species	Reagent	Extraction Procedure
Ionically bound arsenic (salts)	2M $MgCl_2$	In H_2N_2 anaerobic chamber 1)Tumble-shake 2 hours, centrifuge[a], decant 2) Tumble-shake 2 hours, centrifuge[a], decant 3) MilliQ water wash[b]
Strongly adsorbed As	0.1 M NaH_2PO_4	In H_2N_2 anaerobic chamber 1) Tumble-shake 16 hours, centrifuge[a], decant 2) Tumble-shake 24 hours, centrifuge[a], decant 3)0.1% NaCl wash[b]
Arsenic co-precipitated with acid volatile sulfides, carbonates, manganese oxides, and very poorly crystaline Fe oxyhydroxides	1N HCl	In H_2N_2 anaerobic chamber 1) Tumble-shake 1 hour, centrifuge[a], decant 2) 0.1% NaCl wash[b]
Arsenic co-precipitated with poorly crystaline Fe oxyhydroxides	0.2 M ammonium oxalate/oxalic acid, pH 3	In H_2N_2 anaerobic chamber Dark extraction (tubes covered in foil) 1) Tumble-shake 2 hours, centrifuge[a], decant 2) 0.1% NaCl wash[b]
As co-precipitated with crystalline Fe oxyhydroxides.	sodium dithionate, sodium citrate	In fume hood 1) Tumble-shake overnight, centrifuge[a], decant 2) 0.1% NaCl wash[b]
Arsenic co-precipitated with pyrite and amorphous As_2S_3	16N HNO_3	In fume hood 1)Tumble-shake 2 hours, centrifuge[a], decant 2)Tumble-shake 2 hours, centrifuge[a], decant 3) 0.1% NaCl wash[b]
Orpiment and remaining recalcitrant As minerals	Hot 30% H_2O_2 16N HNO_3	In wash-down fume hood (Yoo lab) EPA method 3050 B: hot hydrogen peroxide and nitric acid. Samples are digested with alternating hydrogen peroxide and nitric acid at 95°C and refluxed with watch-glass covers in glass test-tubes in a heater block

a: samples were sealed tightly in their Teflon tubes and airlocked out of the glove bag for centrifugation. They were kept sealed through centrifugation, and passed back into the glove bag for decanting.
b: Milli-Q water washes and 0.1% NaCl washes were 30 minutes of tumble-shaking followed by centrifugation and decanting.

Table 21 As concentration of extractants

Reagent	Mean OTT3-73 standard (11) outwash	standard deviation	Mean OTT3-74 contact till	Mean OTT3 75 (2) outwash	Mean OTT3-184 (2) till	Mean UMRB2-175 outwash	Mean UMRB2-176 (2) contact till	Mean TG3-149 (2) till	Mean vial 13 Blank	Mean vial 14 Blank
As extracted in MgCl2(1)µg/kg	438	46	533	323	605	433	592	678	1.2	1.5
As in MgCl2 [2]µg/kg	263	70	331	243	296	151	347	286	1.47	1.31
As in MgCl2 wash µg/kg	17	4	22	11	14	19	25	35	0.0	0.0
sum of As extracted in MgCl2 µg/kg	**718**	**98**	**886**	**577**	**916**	**602**	**964**	**999**	**2.7**	**2.8**
As in NaH2PO4 (16hr) µg/kg	788	73	201	456	1090	848	981	1380	0.7	0.6
As in NaH2PO4 (24hr) µg/kg	176	17	206	133	223	175	199	263	0.7	0.8
As extracted in H2PO4 wash µg/kg	249	52		148	87	123	192	333	0.2	0.9
sum of As extracted in NaH2PO4 µg/kg	**1213**	**108**	**407**	**736**	**1400**	**1146**	**1372**	**1976**	**1.6**	**2.3**
As in HCl µg/kg	1421	199	1776	1033	1858	1406	1875	1944	1.9	1.5
As in HCl wash µg/kg	93	10	115	73	92	81	90	195	0.0	0.0
sum of As extracted in HCl µg/kg	**1514**	**204**	**1890**	**1106**	**1950**	**1487**	**1965**	**2139**	**1.9**	**1.6**
As in Am/Ox µg/kg	930	103	1893	841	509	682	528	1244	0.4	0.3
As extracted in oxalic acid wash µg/kg	357	46	456	364	294	338	313	472	1.6	1.7

Reagent	Mean OTT3-73 standard (11) outwash	standard deviation	Mean OTT3-74 contact till	Mean OTT3 75 (2) outwash	Mean OTT3-184 (2) till	Mean UMRB2-175 outwash	Mean UMRB2-176 (2) contact till	Mean TG3-149 (2) till	Mean vial 13 Blank	Mean vial 14 Blank
sum of As extracted in Am/Ox µg/kg	**1287**	**123**	**2349**	**1205**	**803**	**1020**	**841**	**1716**	**2.0**	**2.0**
As Na citrate dithionite µg/kg	251	33	234	219	288	306	202	300	1.5	1.4
As extracted in dithionite wash µg/kg	194	33	220	184	210	226	246	287	0.9	1.8
sum of As extracted in citrate dithionite µg/kg	**445**	**55**	**454**	**402**	**497**	**532**	**448**	**588**	**2.4**	**3.2**
As in HNO3 25C (1)µg/kg	972	285	1116	987	1997	1328	2135	1994	0.4	0.4
As in HNO3(2) µg/kg	253	51	425	273	466	312	454	402	0.3	0.3
As in HNO3 (wash) µg/kg	270	59	419	194	485	227	581	485	0.1	0.0
sum of As extracted in HNO3 µg/kg	**1496**	**359**	**1960**	**1454**	**2948**	**1867**	**3171**	**2881**	**1**	**1**
As extracted with EPA 3050B µg/kg	**1319**	**163**	**2077**	**801**	**1749**	**1383**	**2026**	**2481**	**0.5**	**0.3**
sum of extracted arsenic ug/kg	**7993**	**1110**	**10023**	**6282**	**10263**	**8038**	**10787**	**12779**	**11.8**	**13.0**
sum of extracted arsenic mg/kg	**8.0**	**1.1**	**10.0**	**6.3**	**10.3**	**8.0**	**10.8**	**12.8**	**0.01**	**0.01**

Table 22

Sample Name (number of replicates)	Glacial Sediment Type	Sum of Sequential Extraction mg As/kg	HG-AA from USGS mg As/kg	ICP-MS from USGS mg As/kg	ICP-MS UMN mg As/kg
OTT3_73 standard (11)	outwash	8.0	3.9	5	6.3
OTT3 74	contact till	10.0	7.8	9	9.1
OTT3 75 (2)	outwash	6.3	3.1	5	3.7
OTT3-184 (2)	till	10.3	7.9	8	8.6
UMRB2 - 175	outwash	8.0	6.6	6	6.3
UMRB2-176 (2)	contact till	10.8	7.8	7	6.3
TG3-149 (2)	till	12.8	8.4	10	9.6

Comparison of the total As concentration in the samples as measured by the sum of the As liberated by sequential extraction, As measured via hydride generation atomic absorption (HG-AA) at the USGS contract lab, As measured via 4 acid digestion and ICP-MS at the USGS contract lab, and As measured via ICP-MS after acid digestion in the University of Minnesota Department of Earth Sciences Aqueous Geochemistry Laboratory.

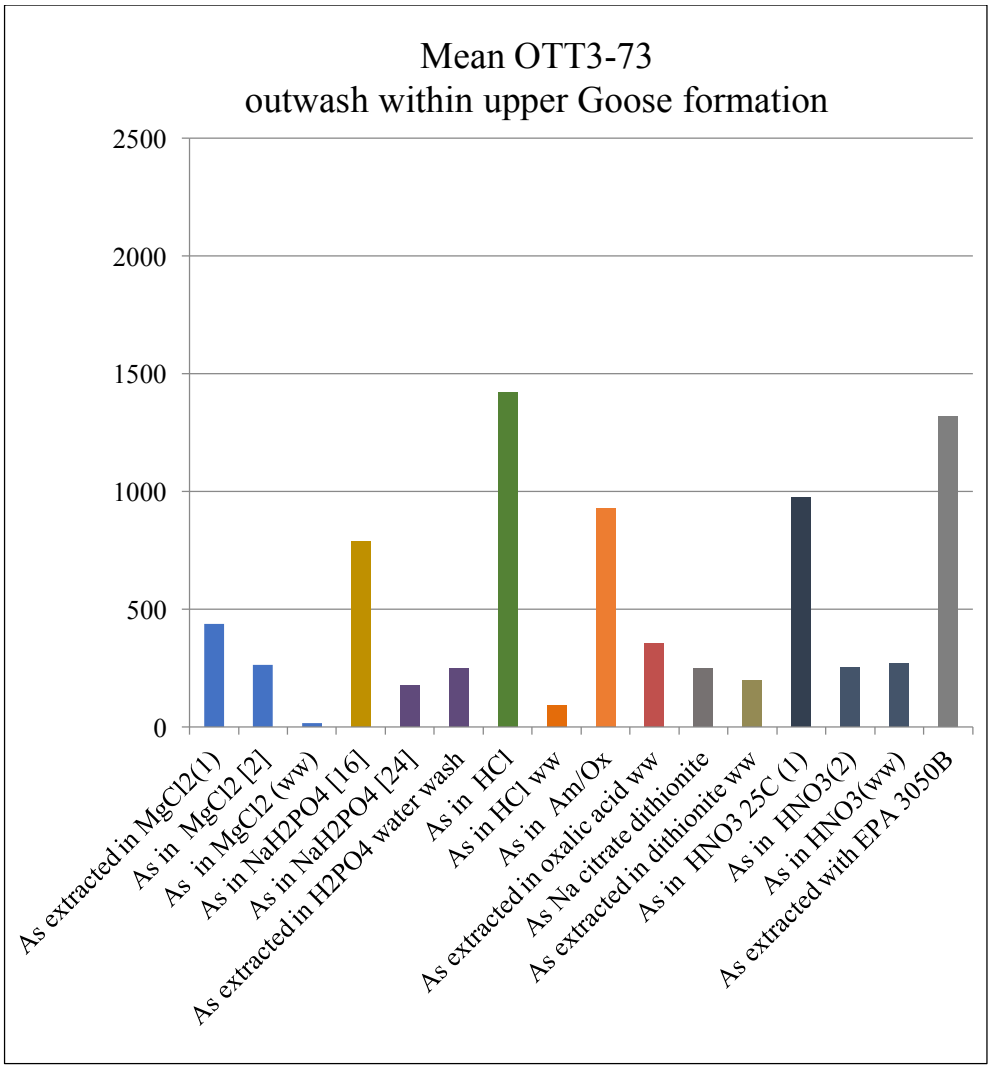

Figure 26 Results of sequential extraction OTT3-73

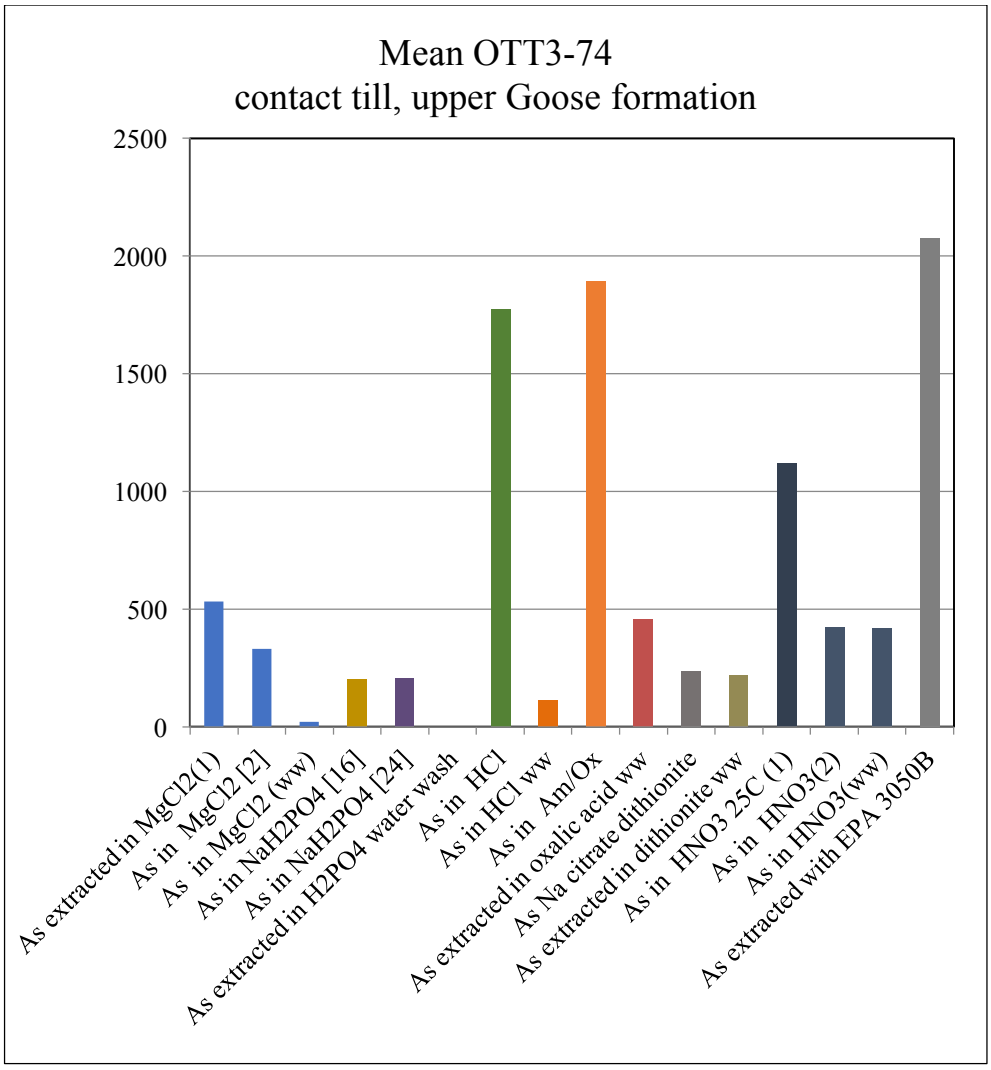

Figure 27 Results of sequential extraction OTT3-74. This sample was used as an internal standard and results here are the mean of 11 duplicate measurements.

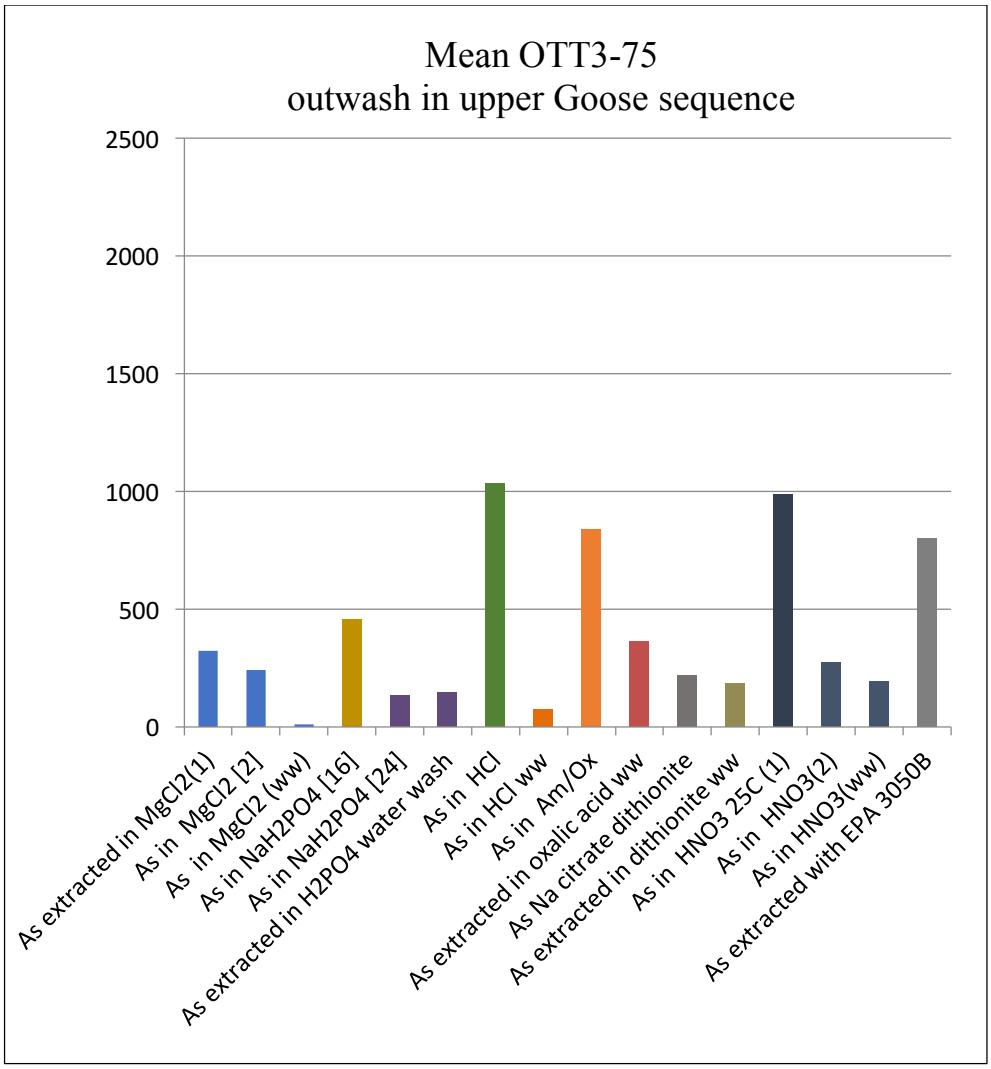

Figure 28 Results of sequential extraction OTT3-75

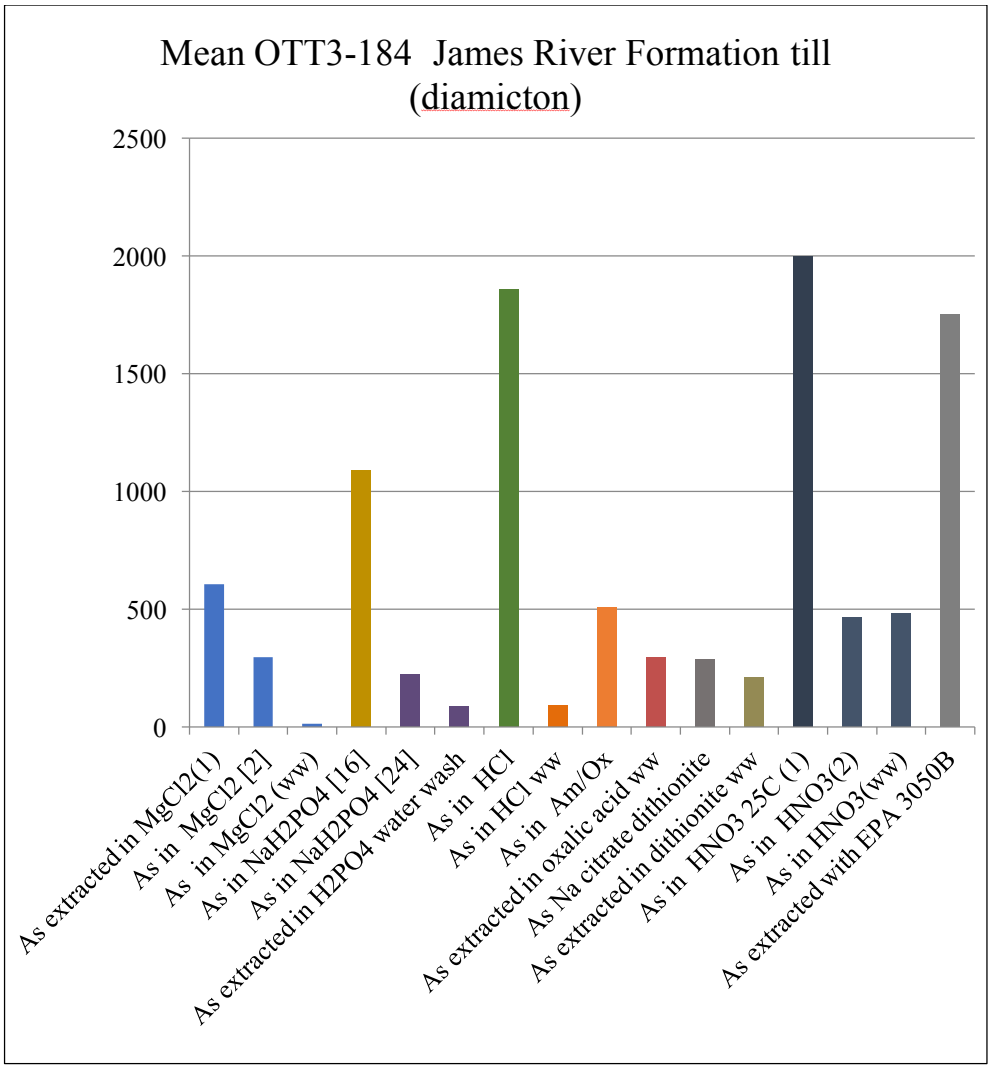

Figure 29 Results of sequential extraction OTT3-184

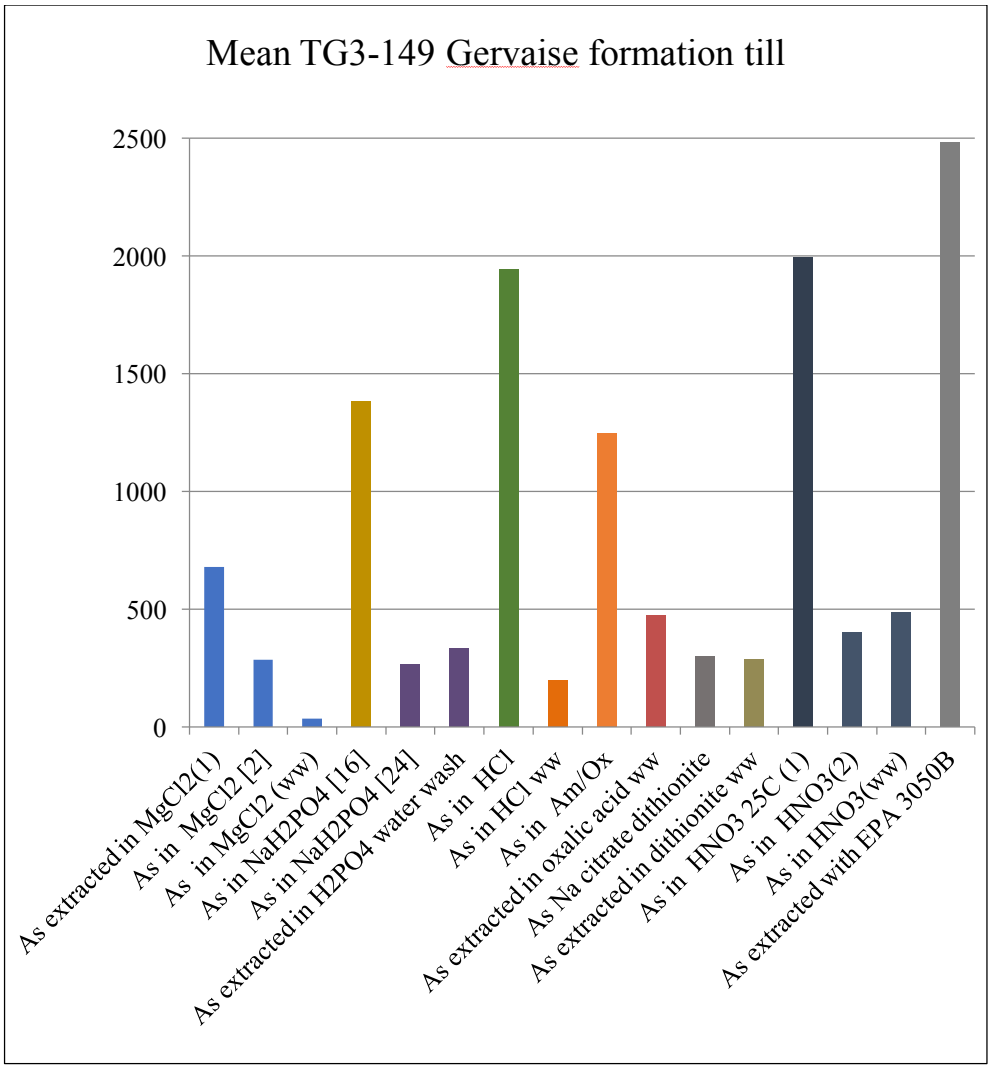

Figure 30 Results of sequential extraction TG3-149

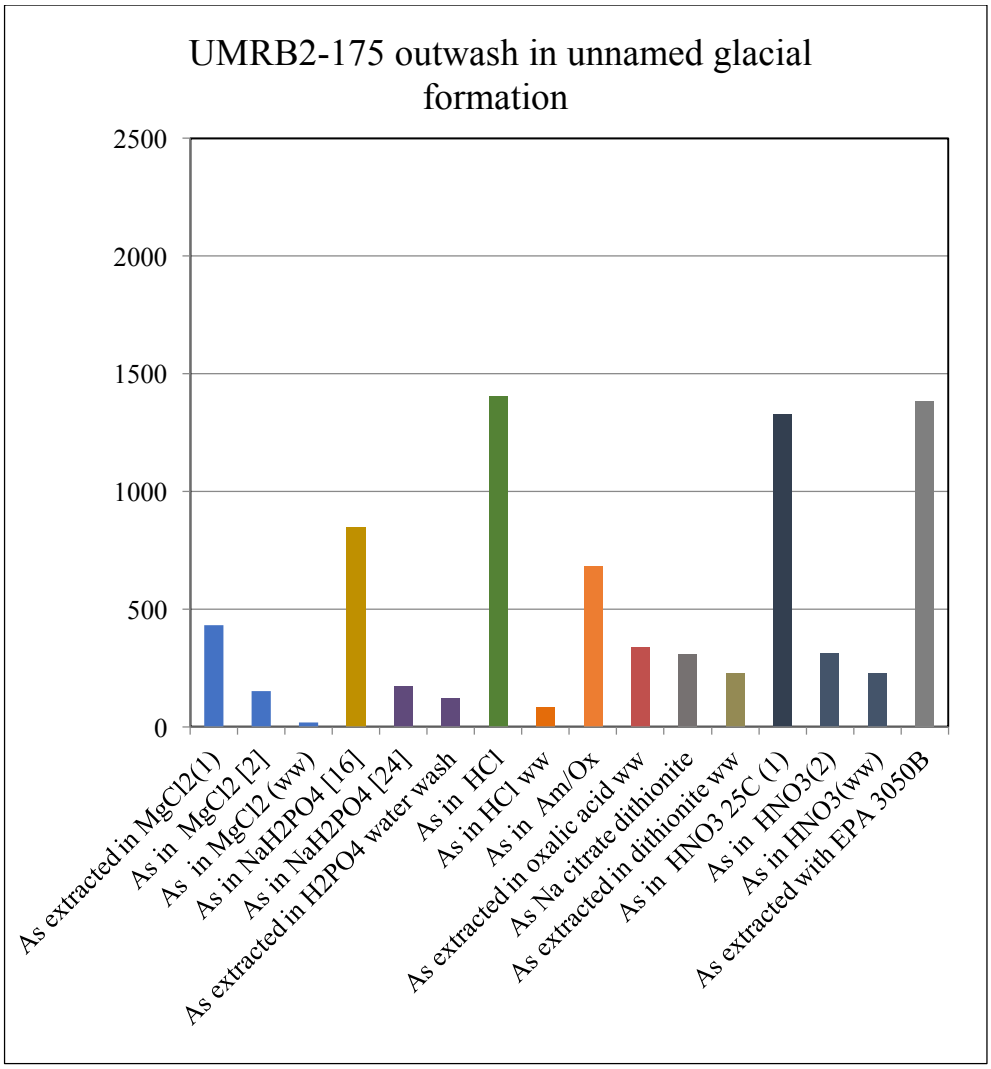

Figure 31 Results of sequential extraction UMRB2-175

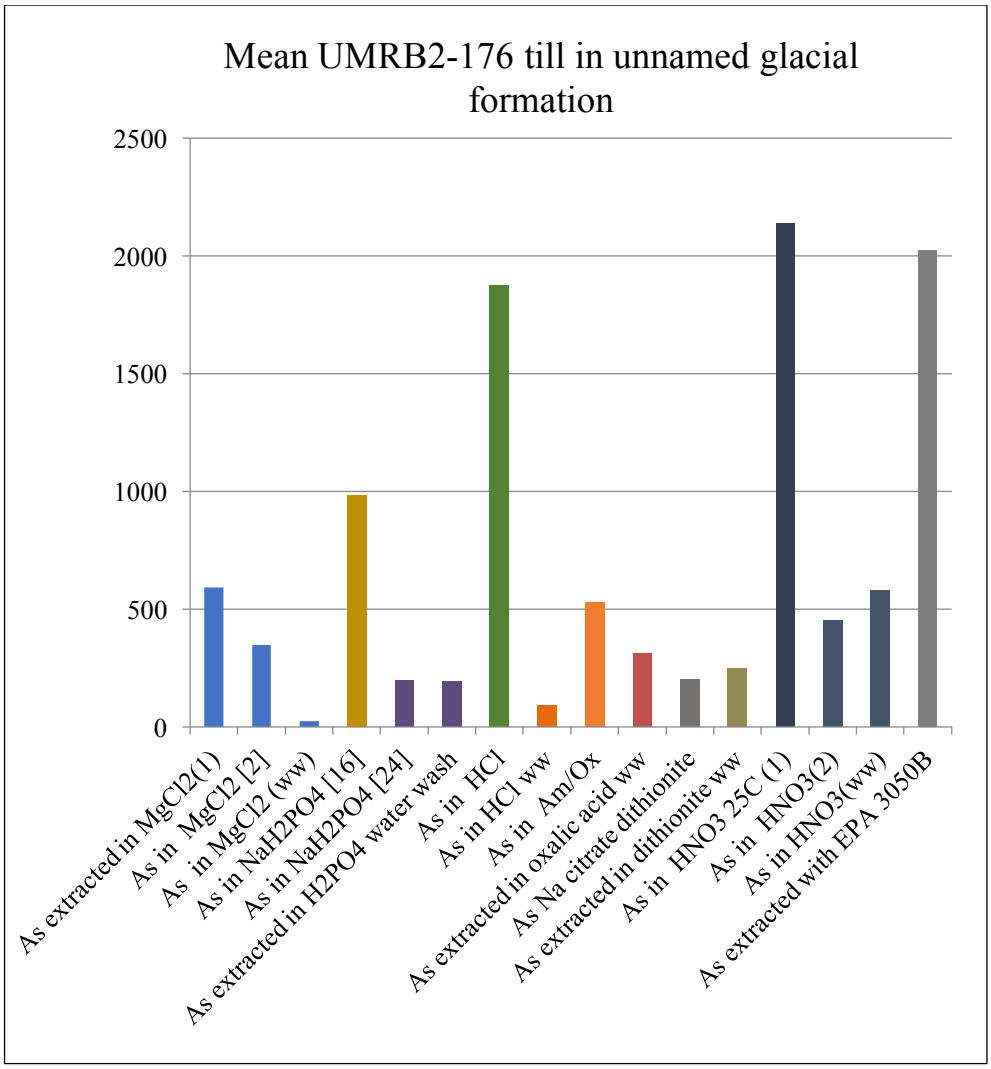

Figure 32 Results of sequential extraction UMRB2-176

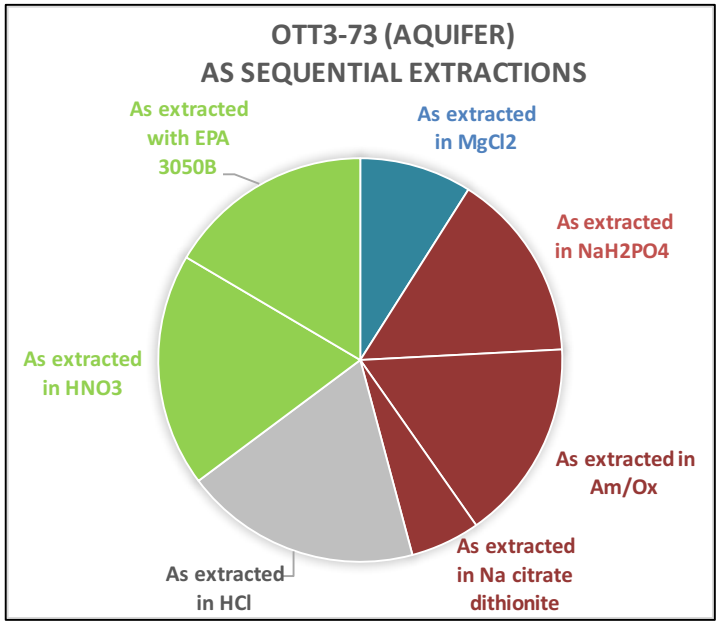

Figure 33 As speciation of OTT3-73 as defined operationally by sequential extraction

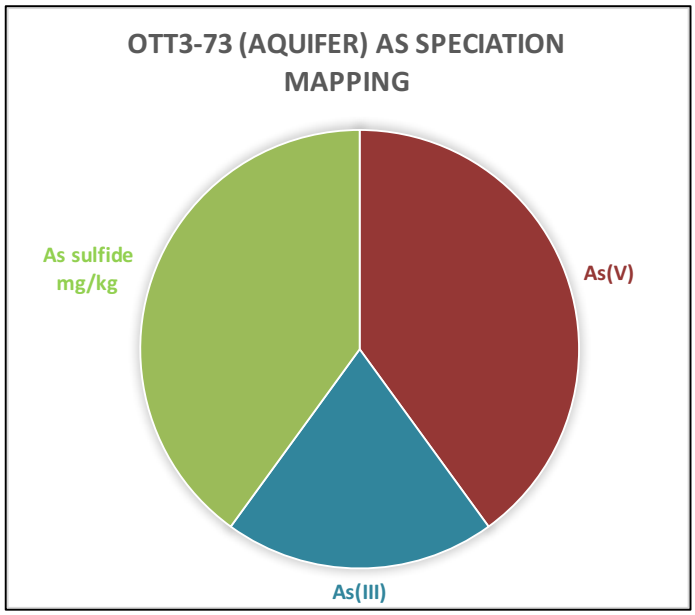

Figure 34 As speciation of OTT3 73 based on As speciation mapping

Colors were chosen to match groups where the direct measurement speciation and operational speciation would tend to agree. The HCl extraction step was not matched to a direct measurement because it is designed to target many operational categories of As: As co-precipitated with acid volatile sulfides, carbonates, manganese oxides, and very amorphous Fe oxyhydroxides (Keon et al. 2001).

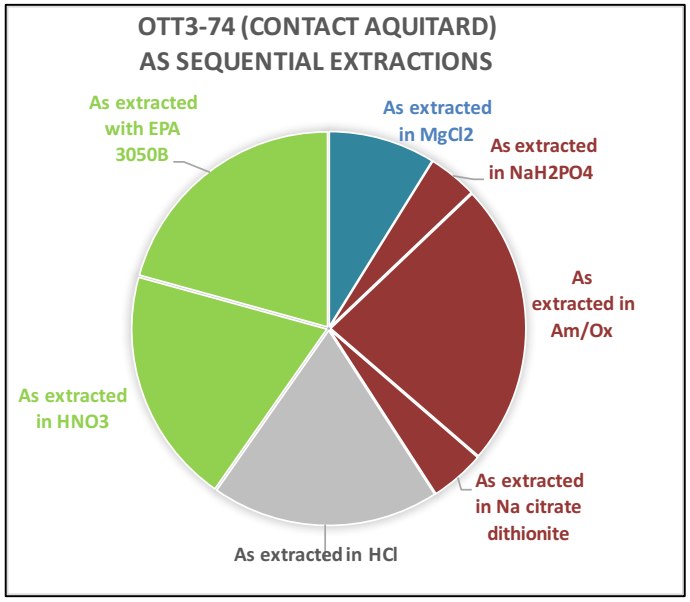

Figure 35 As speciation of OTT3-74 as defined operationally by sequential extraction

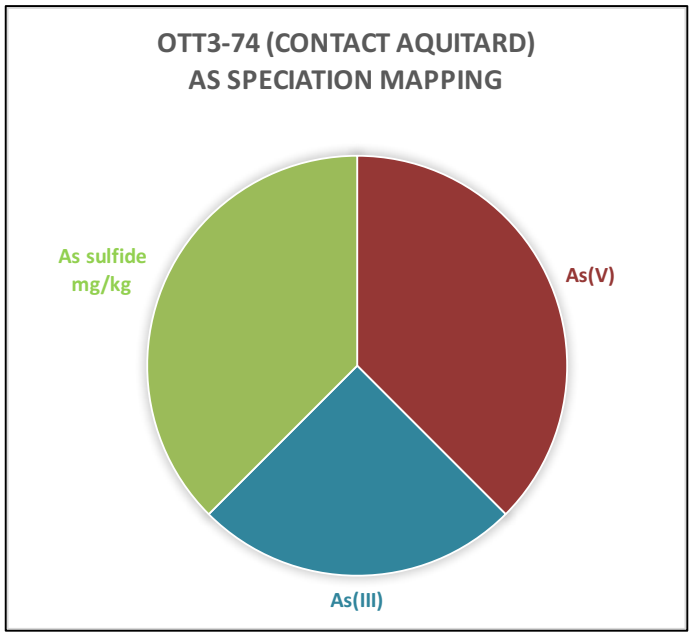

Figure 36 As speciation of OTT3-74 based on As speciation mapping

Colors were chosen to match groups where the direct measurement speciation and operational speciation would tend to agree. The HCl extraction step was not matched to a direct measurement because it is designed to target many operational categories of As: As co-precipitated with acid volatile sulfides, carbonates, manganese oxides, and very amorphous Fe oxyhydroxides (Keon et al. 2001).

APPENDIX 2: MEEKER COUNTY CORE MS-6 ENRICHMENT EXPERIMENT

Introduction: Professor Toner and I had been interested in doing an enrichment experiment to look at microbially-mediated As release from the glacial sediments. In an enrichment experiment an aliquot of a sample is introduced to media that is intended to encourage particular microbial metabolisms. This is often the earliest microbial experiment done with a set of samples because it allows some important disprovable questions like: are there microbial processes, as stimulated by experimental conditions, that change the form of As, S, or Fe?

We had been interested in doing this for some time because of the spectroscopy and dissolution chemistry results from the archived tills (Chapter 2) and the Clay County studies (Chapter 3), but we had to wait for a suitable core or go drill one ourselves. This is because the inoculation of microbes comes from the sample itself, so the microbes need to be:

1) alive

2) alone, which is to say uncontaminated with microbes from the surface.

The ideal way to do this would be to bring the prepared media to the drilling site and to spoon the sample directly into the media using sterile technique.

The Minnesota Geological Survey was planning on drilling several cores in Meeker County, which is an area with several high-As wells. The area for the M6 core (44.98, -

94.64) was close to one, known, elevated-As well and three wells of similar depth for which we had no water chemistry data.

Microbial metabolisms addressed: The main solid phase sources of As to groundwater are arsenic sorbed to or co-precipitated with iron oxides, and As-bearing sulfides. For the enrichment experiment we were interested in four metabolisms that could liberate As from solids to water: Fe oxidizers, Fe reducers, sulfate reducers, and elemental sulfur oxidizers. We did not attempt to address a direct arsenic metabolism.

(1) The **Fe-oxidizer** enrichment solution was Mohr's salt (ammonium iron sulfate, $(NH_4)_2Fe(SO_4)_2 \cdot 6H_2O$) (modified from Emerson and Floyd 2005). These reagents were prepared and samples were handled in an $N_2H_2CO_2$ atmosphere. The Fe(II) in the Mohr's salt dissociates to an aquo complex and is intended to be oxidized to Fe(III) by Fe oxidizing microorganisms.

(2) The **Fe-reducer** enrichment solution (after Kieft et al. 1999) was an aliquot of FeIII suspension with lactate, acetate and pyruvate as the organic substrates for Fe-reducing microbes. These reagents were prepared and samples were handled in an $N_2H_2CO_2$ atmosphere glove box. The Fe(III) precipitate was made by Brandi Cron-Kammermans following the FeOOH method of Schwertmann and Cornell (1991), and washed twice. The final suspension was autoclaved just before being added to the FeIII-reducer enrichment media.

(3) The **sulfate-reducer** enrichment solution (after Postgate et al. 1984) was calcium sulfate and magnesium sulfate with lactate, acetate and pyruvate as the organic substrates for sulfate-reducing microbes. These reagents were prepared and samples were handled in $N_2H_2CO_2$ atmosphere glove box.

(4) The **sulfur-oxidizer** enrichment solution (after Atlas et al. 1993) was a sodium thiosulfate and iron chloride solution, which formed a precipitate of elemental sulfur (S_0). The elemental sulfur was intended to be oxidized to sulfate by an S_0 oxidizing microorganism. This was prepared and sampled in the laminar-flow hood.

Groundwater for media.

Initially we attempted to make an artificial groundwater for making the incubation media, and for the control samples. Well and groundwater in Meeker County and much of Minnesota are saturated for carbonate minerals at the surface. At depth they are below saturation because of the greater partial pressure of CO_2 at depth. To make a similar groundwater we had to mix it with MilliQ water and sparge the solution with gaseous CO_2 to bring carbonates below saturation. Rebecca Sims (Toner lab research fellow) and I made some test volumes and found that they were not very stable; carbonates precipitated overnight. They were also too high in Na and K (frequent cations for the trace-grade anions we were using).

There is a capped well on public land about 1500m north of core MS-6. This is a former schoolhouse site, and the schoolhouse well had been capped. The staff at the Meeker County Courthouse were able to put me in touch with some of the neighbors who were very helpful and confirmed that the well was there and that the cap was accessible. However, in the end we decided against trying to get permission and equipment to re-open and pump this well for incubation water.

Fortunately, I had a large database of well-waters chemistry in Minnesota. Staff at the city of Litchfield very kindly offered to let me have municipal well water upstream of their fluoridation and chlorination plant. Unfortunately, Litchfield city water is very close to the EPA MCL for arsenic and I was concerned that this would overwhelm the amount of arsenic that might be liberated from the samples.

Water wells in eastern central Minnesota (the metro) had similar major ion concentrations to those of the As-affected wells in Meeker County (carbonate, sulfate, Cl-, Na, Ca, Mg) but without the arsenic. I asked Scott Alexander (Earth Sciences, University of Minnesota) about possibly pumping one of the test-wells on campus and he suggested the well in the Wildlife Biology Fisheries Lab at UMN. As it turns out there is a large, indoor, freshwater-fish rearing lab on the St. Paul campus. Fisheries staff were very generous with their well water and I filter-sterilized it and used it to mix the media and the blanks. The pH of the well water for open-air incubations was adjusted by sparging with an N_2-CO_2 mix. Well water for the anaerobic incubations was sparged with N_2 for

an hour per liter, then the pH was adjusted by sparging with the N_2-CO_2 mix.

Methods: I had a few weeks between hearing of the planned coring and the day the core was recovered in which to plan and test the media and to track down materials. We decided to incubate at the in-situ temperature of the cores which we thought would be around 10°C. No incubators were available to borrow at that time so we bought a wine-fridge for this purpose (normal household refrigerators do not come up to 10°C).

Core MS-6 was recovered by the Minnesota Geological Survey. The supervising geologist was Gary N. Meyer and the coring contractor was Traut Wells. The temperature of the core at 30, 60, and 90m depth was 12°C. Core sections were brought to the surface and extruded into plastic tubes. I took 1 m sections of interest about 60 m away from the drill truck, cut through the plastic tubing and used a sterile spatula to open the core. A second sterile spoon was used to remove the the sediment sample from the inside of the core and to place it into a sterile Whirl-Pak.

Collected samples were kept in a cooler to prevent freezing and were brought back to UMN and kept in the 12°C incubator until they were dispersed into the enrichment media. Separate sub-samples for major and trace-element chemistry were collected for sediment dissolution analysis at the USGS contract lab.

Six samples were incubated with 6 growth media and included three duplicates, one of which was poisoned with sodium azide (NaN_3) as an abiotic control sample. Each of the enrichment media had a blank and a poisoned blank. In total this was 120 incubations.

Each of the six strata had these:

- 2 Fe oxidizers 1 Fe oxidizer with Na azide
- 2 Fe reducers and 1 Fe reducer with Na azide
- 2 SO_4 reducer and 1 SO_4 reducer with Na azide
- 2 S_0 oxidizers and 1 S_0 oxidizer with Na azide
- 2 anerobic groundwater and 1 anaerobic groundwater with azide
- 2 aerobic groundwater and 1 aerobic groundwater with azide

Each of the enrichment media had these blanks (media without inoculation)

- 1 Fe oxidizer and 1 Fe oxidizer with Na azide
- 1 Fe reducer and 1 Fe reducer with Na azide
- 1 SO_4 reducer and 1 SO_4 reducer with Na azide
- 1 S_0 oxidizer and 1 S_0 oxidizer with Na azide
- 1 anaerobic groundwater and 1 anaerobic groundwater with Na azide
- 1 aerobic groundwater and 1 aerobic groundwater with Na azide

***Strata chosen for incubation*:**

Strata from core MS-6 for incubation were chosen as paired aquifer-aquitard samples and named based on the core, the depth, and the type of stratum sampled. Gary Meyer's descriptive core log illustration of MS-6 is appended as **Figure 1**. Because the full sample names were very long and quite similar, each sampled stratum was also given a nickname to make it easier to read the hundreds of incubation bottles, syringes, filters, and subsample vials. Each of these was labelled with both the full sample name and the nickname. The descriptions and formation names in italics are directly quoted from Meyer (2015) and can be seen labelling these strata in Figure 1.

- MS6 100 ft aquitard "Alan" *Grey loamy till, Sauk Center Member of the Lake Henry Formation*
- MS6 100.5 ft aquifer "Gary" *Grayish-yellow, medium-grained sand, gravelly sand, and sand and very fine- to fine-grained gravel; abrupt lower contact; Lake Henry Formation*
- MS6 106 ft aquifer "Angie" *Grayish-yellow, medium-grained sand, gravelly sand, and sand and very fine- to fine-grained gravel; abrupt lower contact; Lake Henry Formation*
- MS6 106 ft aquitard "Barb" *Greenish-gray, sandy till; gray at 108'; Meyer Lake Member, Lake Henry Formation*
- MS6 323 ft aquitard "Harvey" *Greenish-gray, very fine-grained sandy silt;*

calcareous; grades to yellowish-gray by 322.5' with increasing organics; gray to olive-black below 323'; few laminae of silty, very fine-grained sand; interglacial

- MS6 323 ft aquifer "Carrie" *Gray, fine- to medium-grained sand interbedded with yellowish-gray to olive-black, silty clay with shells; very small pebbles in sand and clay; interglacial*

Sediment dissolution chemistry: Aliquots of the solid sample for trace and major element chemistry were collected along with the incubation aliquots. Because the inoculation had to take place very shortly after the samples were recovered from the core, the concentration of As, Fe and S in the samples was not known until several months after the last subsamples had been drawn from the incubations. Sediment chemistry was measured at the USGS contract lab after the method by Taggart (2002) which is described in more detail in Chapter 2. Table X is a complete table of trace and major element chemistry for the Meeker County core M-6 samples.

Table 23 Strata for incubation

Sample name	Depth (m)	As (hydride) $mgkg^{-1}$	Fe %	S %
MS6 100ft aquitard "Alan"	30.5	2.7	1.4	0.02
MS6 100.5ft aquifer "Gary"	30.6	3	0.81	0.08
MS6 106ft aquifer "Angie"	32.3	1.9	0.73	0.02
MS6 106ft aquitard "Barb"	32.3	2.1	1.49	0.02
MS6 323ft aquitard "Harvey"	98.5	14.7	1.4	0.45
MS6 323ft aquifer "Carrie"	98.5	9.8	1.16	0.24

***Inoculations*:** Initial inoculations took place over four days, April 5-6 and April 8-9 2013. The geological samples for inoculations were dispersed in filter-sterilized anaerobic groundwater inside the $H_2N_2CO_2$ anaerobic chamber, in pre-weighed, autoclaved beakers with stir-bars. (Beakers and stir bars were weighed together, then wrapped in foil and autoclaved.) The autoclaved bundles were put into the anaerobic chamber when cool, the sample aliquot was dispersed in the beakers with a fixed volume of filter-sterilized anaerobic groundwater.

The innoculants for the anaerobic media were pipetted out of the beaker during vigorous stirring to keep the sediments suspended and added to the pre-prepared anaerobic incubation media in the incubation bottles. The bottles were sealed inside the anaerobic chamber. Each inoculation was 5ml of sample suspension.

Then the sample beakers were brought out of the anaerobic chamber and put into the laminar flow hood where the samples were pipetted into the prepared aerobic sample media and sealed.

Incubation bottles were incubated at 12°C and shaken every day.
Incubations were sub-sampled at the time of inoculation (time 0) and at 1 week (time 1), 2 weeks (time 2), 1 month (time 3), and three month intervals (time 4).

Anaerobic samples were sub-sampled in the $H_2N_2CO_2$ glove box, and aerobic samples were sub-sampled in the laminar flow hood.

Samples were removed by syringe, then the needle was discarded and replaced with a filter, and the sample was filtered into a 15ml falcon tube, and acidified to 1% HCl. A second needle was placed in the septum during sampling to make up the pressure difference and to introduce fresh air or gas mixture into the samples. For sampling times 0 to 3, 3 ml of solution was removed, for sample time 4 (final sampling) 10 ml of solution was removed.

Before sampling, incubation bottle septa were flame-sterilized with ethanol. For anaerobic samples the septa were covered with flame-sterilized foil caps and brought into the anaerobic chamber for sampling.

Filters for Fe oxidizers and reducers were rinsed with 3 ml 0.1M $NaPO_4$ to dislodge As that might have sorbed to solids in the filter. The phosphate rinses were retained and acidified as were the samples. All filters were retained and frozen.

Concentration of inoculations: 5 ml aliquots of suspension were also dispersed into pre-weighed boats to determine how much solid sample had been in the aliquots. These were put into a drying oven and weighed the following week. 5 ml of suspended aquitard samples contained approximately 0.3 mg of solid sample. 5 ml of suspended aquifer

samples contained about 0.25 mg of solid sample. I had expected that the solid concentration of the aliquots would be much higher.

The range of As concentrations in the incubated strata was from 1.9 to 14.7 $mgkg^{-1}$ (Table 1). Each inoculation of 5 ml of dispersed sample contained approximately 0.3 g of solid sample, and these were diluted in 100 ml of sample media. If all of that arsenic were liberated into the incubation media (which is unlikely) the concentration of As in the media could range from 5.7 to 44.1 μgL^{-1}. Expected concentrations of inoculated media are one to two orders of magnitude lower.

***Measurement via AA*:** The intended method of measurement for these was atomic absorption spectrophotometery via hydride generation (HG-AAS). All the abiotic samples with the Na-azide, and all the sulfate samples produced a precipitate during the pre-reduction step that that precluded running the samples via HG-AAS. Mike Ottman, Reba Van Beusekom, Brandi Cron-Kammermans and I worked on this method during 2014-2015 and concluded that although there may be a way to overcome the azide precipitate problem by using a different pre-reducing agent, the simpler course would be to use a different lethal agent like mercury chloride for the abiotic samples.

Michael Ottman and Brandi Cron-Kammermans continued to work on the Meeker County samples, including some As standard additions to the Fe(III) suspension. They found that the added arsenic did not make it through the filtering step necessary for

measuring the samples by HG-AAS and concluded that the As was binding to the Fe solids in the suspension and subsequently getting trapped in the filter. For either ICP or HG-AA these samples would have to be digested, unfiltered, to measure arsenic and it would be difficult to distinguish between As liberated from the sediments via this digestion and As liberated from the added Fe oxide solids.

Michael Ottman did further work on these reagents and on alternative reagents, the following are Mike's comments, written by Mike.

> *"Additional barriers to a working method were the presence of S-containing compounds (SO_4) that were rapidly reduced to H_2S in the presence of $NaBH_4$; this caused interference in the analysis of the As hydride. Finally, the high concentrations of Fe present in the enrichment media posed two specific issues. First, FeIII oxides are known to strongly bind As from solution. Secondly, the reduction of FeIII to FeII is more favourable than the reduction of AsV to AsIII, meaning that a 'scavenging' of reductant by FeIII in solution could take place. In order to circumvent these problems, we employed the use of two matrix modifiers that served to eliminate the issues affiliated with the high Fe concentrations. 1,10 phenanthroline, an organic molecule containing amine groups that coordinate with Fe, was experimented with as an Fe complexer that would dissolve and then passivate the resultant solution phase Fe in order to prevent reductant scavenging and As sorption. Further experiments were also carried out with L-cysteine, an amino acid containing a thiol group that is implicated in metal complexing. The addition of L-cysteine was meant to serve a dual purpose, as the molecule has been used as both a matrix modifier and a pre-reductant in As hydride generation work.*
> *However, difficulties were encountered with both approaches. L-cysteine failed to function as a reductant and did not result in the generation of a sufficient As signal. 1,10 phenanthroline did successfully complex Fe, but"* was still unworkable for HG-AAS. Michael Ottman pers. com 2016.

***Measurement via ICP*:** Analysing these samples via ICP-MS would probably circumvent some of the matrix effects in preparing the samples for AA but it would not solve the problem of As binding to Fe oxides during the filtration step. Analysing 120 samples over 5 sample events is 600 analyses. It would be more than 800 if we add the

phosphate rinses. Unless this were being done "in house" as was the intention with the HG-AA, this would be very expensive.

Considerations for future work: If I were to undertake this kind of experiment again I think it would be important to test the matrix effects of the media with the measurement method before starting.

More solid sample could be introduced by homogenizing the solid sample, and then spooning it directly into a pre-weighed prepared bottle of prepared media. On the other hand this could increase the risk of contamination of the solid sample with ambient microbes.

I would probably elect to run a smaller sample because sampling 120 media bottles in and out of a glove bag takes 4 days. Although the wine fridge kept its temperature very nicely, an incubator that could keep the samples moving would probably be better than swirling them once a day.

We might consider using a gas manifold rather than a glove bag for sampling the anaerobic samples (instead of a needle open to the glove-box atmosphere, the compensating needle is plumbed into the supply gas at low pressure.) In this way the anaerobic samples could be sub-sampled in the laminar flow hood, which is less

cumbersome and cleaner (to avoid microbial contamination of the samples) than the glove-bag.

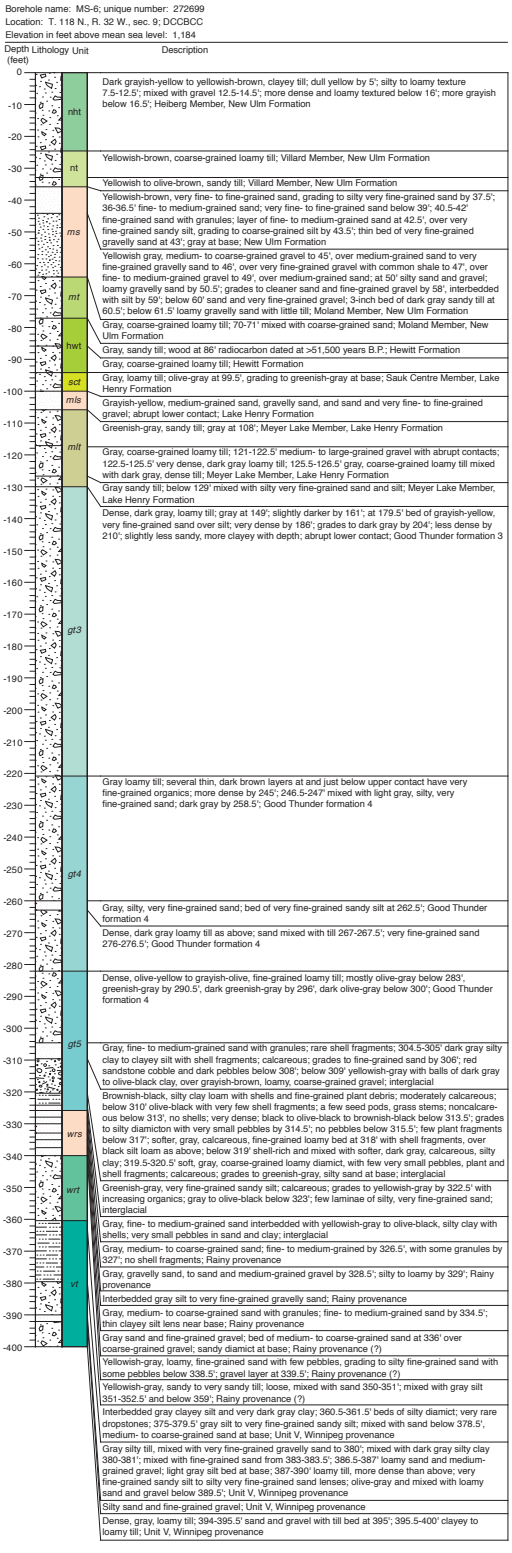

Figure 37 Meyer 2015 Descriptive log of core MS-6